Classification and Content Based Retrieval of Digital Mammograms and Placental Sonograms

Thesis submitted to Cochin University of Science and Technology in partial fulfillment for the award of the Degree of

DOCTOR OF PHILOSOPHY

Under the Faculty of Technology

By

SIMILY JOSEPH
(Reg.No. 3846)

Under the guidance of
Dr. B. KANNAN

Department of Computer Applications
Cochin University of Science and Technology
Cochin - 6820 22, Kerala, India

August 2013

Dr. B. Kannan (Supervising Guide)
Associate Professor
Dept. of Computer Applications
Cochin University of Science and Technology

Certificate

Certified that the thesis entitled "**Classification and Content Based Retrieval of Digital Mammograms and Placental Sonograms"** is a bonafide record of research carried out by **Simily Joseph** under my guidance in the Department of Computer Applications, Cochin University of Science and Technology, Kochi-22. The work does not form part of any dissertation submitted for the award of any degree, diploma, associateship, or any other title or recognition from any University.

Kochi-22

Date: **Dr. B. Kannan**

Dr. B. Kannan (Supervising Guide)
Associate Professor
Dept. of Computer Applications
Cochin University of Science and Technology

Certificate

This is to certify that all the relevant corrections and modifications suggested by the audience during the Pre-synopsis seminar and recommended by the Doctoral Committee of the candidate have been incorporated in the thesis.

Kochi-22

Date: **Dr. B. Kannan**

Declaration

I hereby declare that the thesis entitled **"Classification and Content Based Retrieval of Digital Mammograms and Placental Sonograms"** is the outcome of the original work done by me under the guidance of Dr. B. Kannan, Associate Professor, Department of Computer Applications, Cochin University of Science and Technology, Kochi-22. The work does not form part of any dissertation submitted for the award of any degree, diploma, associateship, or any other title or recognition from any University.

Kochi-22 **Simily Joseph**

Date:

Acknowledgement

First and foremost, I thank God Almighty for the wisdom and perseverance he has bestowed upon me during this research period, and indeed, throughout my life.

I take this oppurtunity to express my heartfelt gratitude to my supervising guide Dr. B. Kannan, Associate Professor, Department of Computer Applications, Cochin University of Science and Technology for accepting me as a research scholar. His kind advice, constant encouragement and affectionate support are greatly appreciated. Whenever I struggled, his valuable guidance helped me to become forward-thinking and self-sufficient.

I am greatly thankful to Dr. K.V. Pramod for his generous support and inspiration throughout my research. The mentoring I have received from him has spanned well beyond academic research.

I am grateful to Dr. Reji Rajan Varghese, Head, Dept. of Biomedical Engineering, Cochin Medical College, Kochi for introducing me to the problem domain of placental maturity analysis and for his continuous support.

My sincere acknowledgement goes to Dr. M.R. Balachandran Nair, consultant radiologist, Ernakulam Scan Center for his valuable suggestions and providing the required data for my research. I am thankful to all the staff at Ernakulam Scan Center and technicians of Siemens.

I acknowledge Dr. Agnes Jacob, for her kind advice and suggestions. I thank Prof. Thomas Varghese, Rebecca Thomas and Annie Joseph for their valuable and timely help.

I sincerely thank DST and Cochin University, for providing financial assistance during the period of my research. I acknowledge Dr. M. Jathavedan, Dr. A. Sreekumar, S. Malathi and M.B. Santhoshkumar of Cochin University of Science and Technology.

My sincere thanks to all non teaching staff of my department for their cordial relation, sincere co-operation and valuable help. Thanks to M/s MindMine Brand Communications and M/s Thadathil Electronics for their technical support.

I thank all the research scholars of my department especially Bino Sebastian, Binu V.P., Jessy George, Jomy John, Murukesh M., Ramkumar R., Remya A.R. and Sindhumol S. for their valuable ideas and suggestions.

It is beyond words to express my gratitude to my siblings and loving parents, P.T. Joseph and Aleykutty Joseph for their prayers and blessings. I thank my father in law, Antony Jacob and mother in law Prof. Pauline Rose Matthai for their support throughout my research period.

I dedicate my accomplishment to my husband, Jacob Antony for the inspiration, motivation and everlasting support he has rendered for my research and life.

Simily Joseph

Contents

List of Figures

List of Tables

List of Abbreviations

ANN	Artificial Neural network
BDA	Biased Discriminant Analysis
BIRADS	Breast Imaging Reporting and Data Systems
BWT	Binary Wavelet Transform
CAD	Computer Aided Diagnosis
CBIR	Content Based Image Retrieval
CBMIR	Content Based Medical Image Retrieval
CC	Craniocaudal
CLAHE	Contrast Limited Adaptive Histogram Equalization
CT	Computed Tomography
DCIS	Ductal Carcinoma In Situ
DPF	Dynamic Partial Distance Function
DWT	Discrete Wavelet Transform
ELM	Extreme Learning Machine
FCM	Fuzzy C-Means
FFDM	Full Field Digital Mammography
FWT	Fast Wavelet Transform
GA	Genetic Algorithm
GLDS	Grey Level Difference Statistics
ICMR	Indian Council for Medical Research
IDC	Invasive Ductal Carcinoma
ILC	Invasive Lobular Carcinoma
IUGR	Intrauterine Growth Restriction
IBC	Inflammatory Breast Carcinoma
KNN	K-Nearest Neighbour
LBP	Local Binary Pattern
LCIS	Lobular Carcinoma In Situ
LDA	Linear Discriminant Analysis
LRM	Local Range Modification
LTP	Local Ternary Pattern
LPQ	Local Phase Quantization
MIAS	Mammographic Image Analysis Society

MLP	Multi Layer Perceptrons
MLO	Mediolateral Oblique
MQSA	Mammography Quality Standards Act
MRI	Magnetic Resonance Imaging
mRMR	Minimum Redundancy Maximum Relevance
MRMD	Multi Resolution Manifold Distance
MRS	Magnetic Resonance Spectroscopy
MSE	Mean Squared Error
NGTDM	Neighbourhood Grey-Tone-Difference Matrix
NTF	Negative Tensor Factorization
PACS	Picture Archiving and Communication Systems
PCA	Principal Component Analysis
PDE	Partial Differential Equation
PET	Positron Emission Tomography
PSNR	Peak Signal to Noise Ratio
Ref	Reference
ROC	Receiver Operator Characteristic
ROI	Region of Interest
RMSE	Root Mean Squared Error
RST	Rough Set Theory
SCG	Scaled Conjugate Gradient
SFM	Statistical Feature Matrix
SGLDM	Spatial Grey-Level-Dependence Matrix
SMMS	Symmetric Maximized Minimal Distance
SMO	Sequential Minimal Optimization
SLFN	Single Hidden Layer Feedforward Neural Network
SNR	Signal to Noise Ratio
SSIN	Structural Similarity Index
STFT	Short-Term Fourier Transform
SVM	Support Vector Machine
SVR	Support Vector Regression
UQI	Universal Quality Index

Preface

Image processing has been a challenging and multidisciplinary research area since decades with continuing improvements in its various branches especially Medical Imaging. The healthcare industry was very much benefited with the advances in Image Processing techniques for the efficient management of large volumes of clinical data. The popularity and growth of Image Processing field attracts researchers from many disciplines including Computer Science and Medical Science due to its applicability to the real world. In the meantime, Computer Science is becoming an important driving force for the further development of Medical Sciences.

The objective of this study is to make use of the basic concepts in Medical Image Processing and develop methods and tools for clinicians' assistance. This work is motivated from clinical applications of digital mammograms and placental sonograms, and uses real medical images for proposing a method intended to assist radiologists in the diagnostic process. The study consists of two domains of Pattern recognition, Classification and Content Based Retrieval. Mammogram images of breast cancer patients and placental images are used for this study.

Cancer is a disaster to human race. The accuracy in characterizing images using simplified user friendly Computer Aided Diagnosis techniques helps radiologists in detecting cancers at an early stage. Breast cancer which accounts for the major cause of cancer death in women can be fully cured if detected at an early stage. Studies relating to placental characteristics and abnormalities are important in foetal monitoring. The diagnostic variability in sonographic examination of placenta can be overlooked by detailed placental

texture analysis by focusing on placental grading. The work aims on early breast cancer detection and placental maturity analysis. This dissertation is a stepping stone in combing various application domains of healthcare and technology.

Chapter 1: Introduction describes the work presented in this thesis. The motivation of the work, significance, objectives and major contributions are outlined.

Chapter 2: Digital Mammograms and Placental Sonograms - An Overview of the Background discusses the basics of cancer, diagnosis measures, importance of digital mammography and need of automation. Also a brief description of the significance of placental grading and the importance of automated grading are given.

Chapter 3: Literature Review presents survey of the related work done in the classification and retrieval of digital mammograms and placental sonograms. The first part lists major works reported in the classification of mammogram images and placental images preceeded by the historical developments in each area. The second part briefs developments in CBIR techniques.

Chapter 4: Preprocessing and Feature Extraction chapter begins with the description of databases used in this study. The major preprocessing techniques used to improve the quality of both mammogram and placenta images are described and a new algorithm is proposed for removing the speckle noise in ultrasound images. Finally, the feature extraction techniques used in this study are explained.

Chapter 5: Classification Using Supervised Learning Algorithms discusses the use of four machine learning classifiers and the use of ensembles for performance improvement. The novelty in the classification process is the use of ELM for classifying placental images and the identification of best suited feature set combination. The use of Principal Component Analysis helps to reduce the dimensionality of feature set.

Chapter 6: Multiple Image Query System for Medical Image Retrieval presents the basic theory of CBIR technologies. An algorithm based on multiple image queries is proposed herewith for CBIR systems. This chapter evaluates the retrieval performance of mammogram and sonogram images using single image queries and multiple image queries.

Chapter 7: Conclusion and Future Works summarizes the thesis and mentions the possible extensions of the current work.

List of Publications

- Simily Joseph, M.R. Balachandran Nair, Reji Rajan Varghese, Kannan Balakrishnan , “Ultrasound Image Despeckling using Local Binary Pattern Weighted Linear Filtering”, **International Journal of Information Technology and Computer Science**, MECS, **2013, 06, 1-9 .**
- Simily Joseph, Reji Rajan Varghese, Kannan Balakrishnan, “Content Based Image Retrieval of Placental Sonogram”, **IEEE International Conference** on **Communication and Signal Processing - ICCSP'13**, April 2013, Chennai.
- Simily Joseph, Kannan Balakrishnan, “Multi query Content Based Image Retrieval system with Applications to Mammogram Images”, **International Journal of Advanced Research in Computer Science,** vol. 3, No. 3, May-June 2012.
- Simily Joseph, Kannan Balakrishnan, “Multi-Query Content Based Image Retrieval System using Local Binary Patterns”, **International Journal of Computer Applications**, vol. 17, No. 7, pp. 1-5, 2011.
- Simily Joseph, Kannan Balakrishnan, “Local Binary Patterns, Haar Wavelet Features and Haralick Texture Features for Mammogram Image Classification Using Artificial Neural Networks”, ACITY 2011, July 15-17, Chennai. **Proceedings published by Springer-Advances in Computing and Information Technology**, 2011, vol.198, part 1, 107-114.
- Simily Joseph, Jomy John, Kannan Balakrishnan, Pramod K. Vijayaraghavan, "Content based image retrieval system for

Malayalam handwritten characters", **Proceedings of IEEE International Conference** on Electronics Computer Technology (ICECT), 2011, pp. 386-390.

- Simily Joseph, Anoop K.S, Remya M.R, Kannan Balakrishnan, “Design of a Multi-Image Query Sytem for Content Based Medical Image Retrieval”, ICMCBIR 2010, 21-23, July, PESIT, Banglore.
- Simily Joseph, Kannan Balakrishnan, “Comparison of MLP, SVM, J48 Classifiers for Mammogram Image Classification”, ICACC, May 3-4, 2010, Amal Jyothi College of Engineering, Kanjirappilly.
- Simily Joseph, Kannan Balakrishnan, “Automated Classification of Mammogram Abnormalities using J48 Decision Tree Classifier”, NCSC, January 20-22, 2010, Marian College, Kuttikkanam.

Chapter 1
INTRODUCTION

Recent developments in Information Technology modernize many disciplines of health care especially Biomedicine. Sophisticated methods have been proposed to automatically extract, useful information from radiology images leading to the discovery of new knowledge. The accuracy of any diagnosis method using medical imaging technologies depends on the quality of medical images and expertise of radiologist [1]. Computer Aided Diagnosis (CAD) aims the identification and localization of abnormalities at an early stage, which prevents the further spread of abnormality with the help of proper clinical management. The work in this dissertation consists of two phases, phase 1- the classification of mammogram and placental images, phase 2- their retrieval. These two phases are preceded by preprocessing and feature extraction methods. The architecture is given in Fig.1.1. This study is a novel approach in placental grading and the contributions in digital mammogram analysis, having scope for further research. This chapter gives an introduction of the problem domain, challenges, motivation, significance and major contributions of the work.

Breast cancer is the second major cause of cancer death in women [2]. It affects the health and lives of millions and millions of women world over. In recent years we notice a rapid growth in the number of breast cancer

patients in all countries irrespective of development. Recent study by ICMR (Indian Council for Medical Research) says that one in 22 women in India is at the risk of breast cancer. The number of breast cancer cases reported increases by one in every 2 minutes [3]. Most of the breast cancer cases are detected only at advanced stages. In the rural areas of the developing and under developed countries women are unaware of the fact that breast cancer is fully curable if detected at an initial stage. Use of Computer Aided Diagnosis (CAD) helps in early detection of breast cancer. This study aims at the automated detection of breast cancer using techniques in Machine Learning and image retrieval.

This study also focuses on the classification and retrieval of similar grade placental images. Placenta connects the growing foetus to the uterine wall and allows nutrient intake, waste elimination, and gas exchange via mother's blood supply [4]. The normal degenerative processes in placenta result in many subtle changes. One such change is the presence of calcification. Placental development begins by around 4 to 5 weeks of gestation. According to Grannum et al. [5] placenta can be grouped into 4 grades, grade 0 to grade 3. The different grades are observed from late first trimester to 39 weeks of gestational period. This work also analyses the characteristics of placenta during this gestational period. As the accuracy of manual grading depends on several subjective factors, automated grading becomes important.

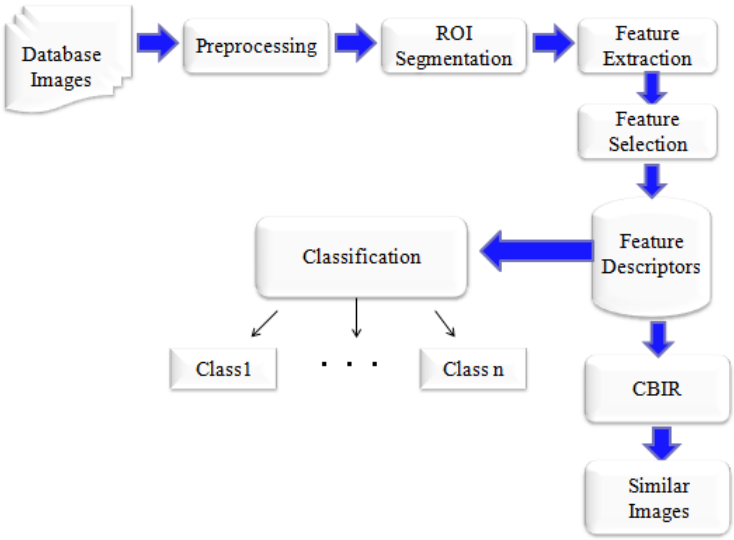

Figure 1.1 An overview of the proposed system

1.1. Challenges

- Medical images cannot be precisely segmented due to their low contrast and high noise content.
- Image cross sections of objects lack clear shape and boundary.
- Biovariability exist for most of the anatomical parts.
- Not many techniques are available to deal with the semantic gap and sensory gap [6].
  - ❖ Semantic gap: is the lack of coincidence between the information that one can extract from the visual data and the interpretation that the same data have for a user in a given situation [7].
  - ❖ Sensory gap- is the gap between the object in the world and the information in a (computational) description derived from a recording of that scene.

1.2. Motivation of the Work

Recently, in Medical Imaging, many development oriented studies have been made by scientists to assist radiologists. Early detection of cancerous lesions play a vital role in the diagnostic process and is important for the complete cure of breast cancer [2]. Prevention of breast cancer is difficult, but if detected at an initial stage it can save the life of thousands of patients. The different methods that exist for diagnosing breast cancer are mammogram, ultrasound, Magnetic Resonance Imaging (MRI) and Positron Emission Tomography (PET). Cost effectiveness, minimum and optimum radiation, early identification of abnormalities are the reasons for the wide usage of mammogram in breast cancer screening. The recent decrease in mortality rate shows the importance of early detection techniques. Factors like difficulty in identifying suspicious region, position of cancer tissue, the large volume of mammograms given to each radiologist and the repeated nature of work adversely affect the correct interpretation of mammograms. In certain cases, superimposed tissues cause obscure cancerous lesions. To overcome these problems Computer Aided Diagnosis (CAD) techniques can be used [8].

The advances in healthcare over decades have resulted in the development of various computerized methods and tools to support foetal monitoring. Ultrasound is the ideal and most widely used tool by clinicians to capture foetal images. Obstetrics ultrasound examination analyses the anatomy, growth, lung maturity and placental maturity of the foetus. If growth parameters are less compared to gestational age, and if placental maturity is more it indicates an increased probability of IUGR (Intrauterine Growth Restriction). Placental grading can diagnose intrauterine growth restriction. Also grading is an alternate way to predict gestational age and

lung maturity [9]. Placenta appears to be different when the overlapping tissues are more. This makes the manual grading difficult. Moreover the diagnosis result varies among examiners [10]. As the accuracy of manual grading depends on several subjective factors, automated grading is important. This study also focuses the automated classification of placenta into different grades and their retrieval.

The possibility for assisted diagnosis, interpretation and decision making is motivated by factors such as time constraints on readers, disparities between readers based on perceptual errors, lack of training and fatigue. Considerable inter-observer variation has been documented in number of studies [11]. This distinction results partly from the complexity of processing the immense collection of knowledge needed to interpret image findings. Access to appropriate information is a basic necessity in medical field especially in diagnosis. The rapid growth in the quantity, easy availability and accessibility of medical records motivate research into automated image retrieval. However, apart from conventional algorithms used in image retrieval process, the proposed work retrieves required images with the help of multiple image queries using logical operators, AND, OR and NOT.

1.3. Significance of the Work

- Automated classification of abnormalities helps radiologists for quick decision making.
- Screening and early detection, together with improved therapy have resulted in a striking improvement in survival.

- Identification of cancerous lesions which may be missed due to limitations in human eye/brain visual system and the occurrence of vast number of normal cases in screening programs.
- In placental sonograms, diagnostic results vary with different examiners and machine conditions. It is very important to overcome the variability in manual grading to arrive at correct conclusions.
- Repeated scanning during pregnancy increases the volume of data, which highlights the need for automation.
- Content Based Image Retrieval (CBIR) system overcomes difficulties such as manual annotation, subjectivity, language dependency and incompleteness that exist in traditional text based search engines.
- CBMIR (Content Based Medical Image Retrieval) systems assist radiologists in diagnosis, by learning from prior known cases.
- Easy analysis of disease specific information among patients using different modalities is possible.

1.4. Objectives of the Work

The primary focus of this research work is to design and develop methods and algorithms for improving the performance of classification and content based retrieval of digital mammograms and placental sonograms. The following objectives are set to accomplish this.

- Explore the use of classical as well as new Machine Learning techniques in the study of breast cancer and placental maturity.
- Identify the major challenges in the automated analysis of digital mammograms and placental sonograms and solve these issues.

- Develop new preprocessing techniques for improving the quality of digital mammograms and placental sonograms.
- Identification and extraction of relevant features for improving the accuracy in classification and retrieval.
- Overcome difficulties in manual grading of placental sonogram through automated grading.
- Develop new techniques in Content Based Medical Image Retrieval.

1.5 Contributions

1.5.1 Technical contributions

- Development of a new linear filter based on local binary pattern for removing speckle noises in ultrasound images.
- Collected ultrasound images of placenta and developed database using it.
- Use of hybrid feature extraction methods for the study of mammogram & placental images gives good result in classification and retrieval.
- Automated classification of placental images helps to overcome the variability in manual grading.
- Introduction of a new classifier, Extreme Learning Machines for the classification of placental sonograms.
- Design of multiple image query system for expressing the user's requirement in a better way in retrieving similar images.
- Use of Content Based Image Retrieval techniques for retrieving similar grade placenta images.

1.5.2 Social Contributions

- The proposed work is a contribution in the health care especially in the growth of a healthy foetus and for the general health and well being of women.
- The contribution of the study helps in foetal monitoring and provides medical assistance if required.
- Computer Aided Diagnosis using new algorithms avoids inter/intra variability in diagnosis, and helps the radiologists to improve the accuracy and reliability of their diagnosis.
- A Primary mammogram screening can be conducted in rural areas. An automated system can easily screen the huge volume of data which can be send for further diagnosis if required.

1.6. Chapter Summary

This work is an integration of Computer Science and Medical Science, and highly contributes to the specified problem domains. This chapter gives a gist about the thesis, system framework, challenges faced, motivation for this work and major contributions. In the coming chapters more detailed technical explanation and experimental analysis are given.

Chapter 2

DIGITAL MAMMOGRAMS AND PLACENTAL SONOGRAMS – AN OVERVIEW OF THE BACKGROUND

2.1 Introduction

Recent developments in computer technology have tremendous impact on medical imaging. Modern radiological modalities perform well when integrated with computers. The recent improvements in breast cancer screening and foetal monitoring result from the developments in modern imaging technology. There has been a significant increase in the area of Computer Aided Diagnosis of both breast cancer and placental maturity analysis. This chapter gives a concise background of the problem under study.

2.2 Digital Mammogram for Breast Cancer Detection

Rapid and uncontrolled growth of abnormal cells results in cancer. The division and proliferation of cells lead to the formation of tumor. Depending on the biological behavior of a tumor it can be classified into benign or malignant. If the tumor does not invade to surrounding tissue it is called benign and if it invades and metastasis to surrounding, it is a malignant tumor [12]. The four predominant types of cancer are Carcinomas, Sarcomas, Leukemias and Lymphomas. Breast cancer is a type of Carcinoma. According to 2013 statistics of American Cancer Society [13], approximately 2,32,340 new cases of invasive breast cancer 64,640 non invasive breast cancer and 39,620 breast cancer deaths are expected to occur in U.S. women. In 2011 the statistics were 2,30,480,

57,650 and 39,520 respectively [14]. In 2005, 211,240 new cancer cases and 40,410 cancer death are reported [15] and in 1999, it was 175,300 and 43,300 respectively [16]. According to the breast cancer statistics in INDIA, 144,937 women were newly detected with breast cancer and 70,218 women died of breast cancer in 2012. In 2008, the numbers were 115,251 and 53,592 respectively [17]. These statistics alarm the urgency in early detection of breast cancer. In this section a brief view of risk factors, symptoms, diagnosis, treatment of breast cancer, importance of digital mammography and need of computer aided diagnosis of breast cancer are discussed.

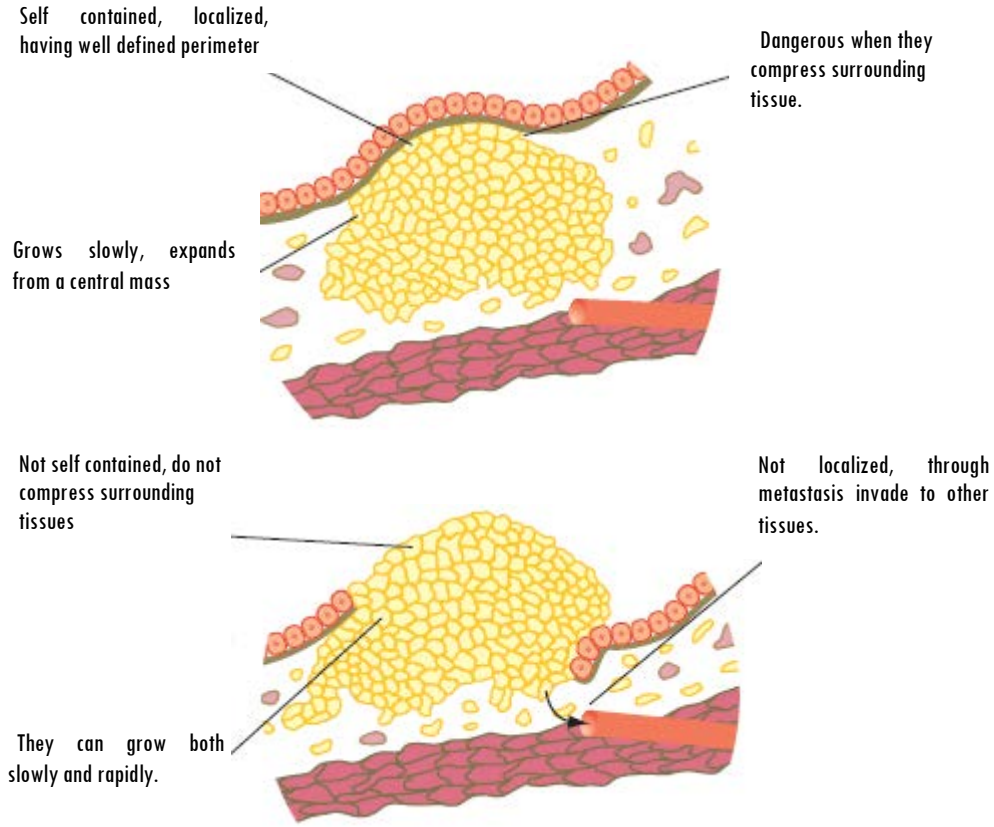

(Source: Almeida et al. Cancer: basic science and clinical aspects: Wiley-Blackwell,2011)

Figure 2.1 Characteristics of benign and malignant tumors

2.2.1 Breast anatomy

Anatomically breast is located within the superficial fascia of the anterior thoracic wall. It overlay the pectoral muscle and extends from the level of second and third rib to the intra mammary fold, which is at the level of sixth or seventh rib of human rib cage. Each breast has fifteen to twenty lobes of glandular tissues that radiate and open at the nipple. The lobules that are present in the small chamber of lobes contain clusters of alveolar glands that produce milk. The alveolar gland passes milk to lactiferous duct. The breast anatomy is given in Fig. 2.2. Breast cancer can arise in different areas of breast like duct and lobules. The epithelial cells present in the lactiferous ducts or lobules can easily develop to malignant tumor. According to the involvement of different tissues and the severity, breast cancer is classified into ductal carcinoma in situ (DCIS), invasive ductal carcinoma (IDC), lobular carcinoma in situ (LCIS), invasive lobular carcinoma (ILC) and inflammatory breast carcinoma (IBC).

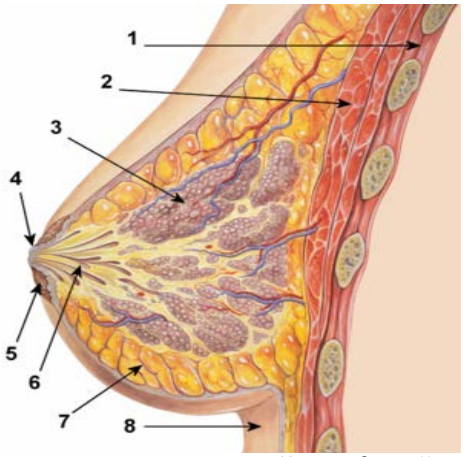

1.Chest
2.Pectoralis muscles
3.Lobules
4.Nipple
5.Areola
6.Milk duct
7.Fatty tissue
8.Skin

(Source: https://en.wikipedia.org/wiki/Breast)

Figure 2.2 Breast anatomy

2.2.2 Breast cancer risk factors and symptoms

In the current decade rapid improvement has occurred in understanding the cause and diagnosis of breast cancer [18]. Gender and age are the strongest risk factors. Family history with genetic mutation in BRCA1 and BRCA2 increases the chance of developing breast cancer. Reproductive functionalities such as nulliparity, late age at first pregnancy, early menarche and late menopause are also shown to increase risk. Breast density is a powerful risk factor for diverse subtypes of breast cancer. Environmental causes like exposure to radiation, use of pills and hormone replacement therapy, life style, alcohol consumption, high intake of fat and animal protein, smoking and obesity are also some established risk factors of breast cancer. Maintaining a healthy life style by balancing the weight, increasing physical activity, avoiding alcohol and smoking and the like can reduce breast cancer risk. Any change in the size or shape of breast, change in armpit, change in nipple, thickening or presence of lump in the breast and puckering appearance of the skin are some of the common symptoms of breast cancer.

2.2.3 Diagnosis methods

Advancing the frontiers of medical imaging requires the knowledge and use of latest imaging technologies. Diagnosis techniques should be able to characterize the tumor. It should be able to identify and map the structural and morphological differences in tumor like solid mass, calcium deposits, breast asymmetries, architectural distortion and angiogenesis. Above all, the diagnosis methods should be practical, inexpensive and harmless. Mammography, MRI, Ultrasound, PET are the commonly available methods used for breast cancer diagnosis [19].

Mammography

Mammography allows intervention at an early stage of cancer progression. Early detection of lesions using mammogram reduces disease specific mortality. Mammogram findings vary depending on the physical, mechanical and biological characteristics of tissue under examination. The principles and use of mammography are detailed in section 2.2.6.

MRI

Magnetic Resonance Imaging (MRI) provides excellent identification of structural abnormalities in breast. Compared with ultrasound and mammogram, MRI offers improved visualization of multi focal and multi-centric lesions, high sensitivity, and determination of chest wall invasion which leads to excellent staging of breast cancer. The cost of MRI is high compared to other diagnostic methods.

PET

Positron Emission Tomography (PET) uses a radioactive material to produce 3-D image of the functional characteristics of the body. Computerized reconstruction of the image provides better recognition. It performs excellent in neo-adjuant chemotherapy (change in metabolism) compared to other diagnostic methods. Anatomic and metabolic functions of the organ can be obtained by combining PET with MRI and CT.

Ultrasound

Ultrasound imaging is used as an adjuant to mammography. In case of a doubt lesion, after mammogram, ultrasound can be used to detect whether the lesion is a cyst or solid mass. According to the nature of the tissue, the

response of the ultrasound varies. The use of 3D ultrasound imaging permits proper localization of tumor and measurement of tumor volume.

Other Common Systems

Scintimammography is a nuclear medicine approach that relies on the emission of radioactive substances from tracers that are injected into the body. The effect of tracers is more pronounced in cancerous tissue than in normal tissue. Therefore malignant tissues can be easily distinguished from benign tissues. Following are some of the techniques that are under active investigation. Magnetic Resonance Spectroscopy (MRS), Thermography, Electrical Impedance Imaging, Electronic Palpation and Full Field Digital Mammography (FFDM).

2.2.4 Treatment and prevention

Depending on the stage and biological characteristic of the tissue, the physician will recommend the type of treatment best suited for the patient. The patient's age, preference of treatment, general health, size of tumor, involvement of lymph node and presence of hormone receptors play a vital role in physician's decision making. The main treatments are surgery, radiotherapy, chemotherapy, hormone therapy and targeted therapy. Either one of these or a combination of more than one can be applied for immediate cure.

2.2.5 Importance of digital mammography

- Small, safe dose of radiation is used.
- Less Expensive.
- Can identify breast cancer when it is very small - 2 to 3 years before you can feel it.

2.2.6 Principles of digital mammography

Mammogram provides information about breast morphology, normal anatomy and gross pathology. Mammographic unit use X-rays to produce images of the breast. Mammographic system includes an X-ray generator, an X-ray tube and gantry, and a recording Medium [20]. The X-ray generator modifies received voltage to supply the X-ray tube with the power required to generate an X-ray beam. Low energy X-rays are generated by the X-ray tube when a stream of electrons, step up to high velocities by a high-voltage supply from the X-ray generator, bump with the tube's target anode. The cathode includes a wire filament that, when heated, produces the electron source. The target anode is struck by the impinging electrons. X-rays leave the tube through a port window of beryllium. The filters in the pathway of X-ray beam adjust the X-ray spectrum. The incoming X-rays are shaped by either a collimator or cone apertures and then passed through the breast. Fig. 2.3 explains the basic principle of mammogram image formation.

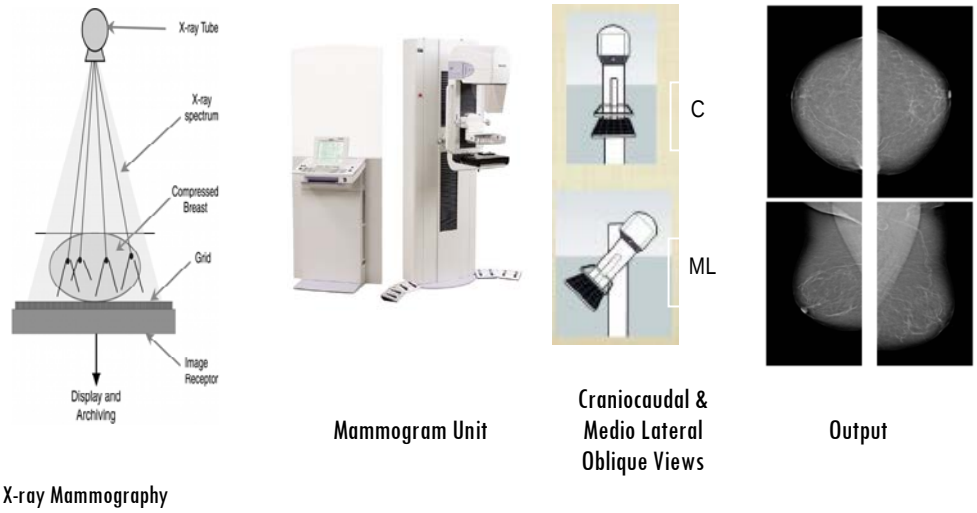

Figure 2.3 Mammogram image formation

2.2.7 Breast abnormality detection using digital mammograms

Early screening using X-ray mammography could reduce death rate due to breast cancer by detecting and treating when cancers are very small [21]. Mammographic examination generally consists of two views; Craniocaudal (CC) and Mediolateral Oblique (MLO) as in Fig. 2.3. Mammography interpretation involves screening for abnormal tissues and diagnosis of the detected abnormalities. According to Breast Imaging Reporting and Data Systems (BIRADS), the major signs in X-ray mammogram are masses, microcalcification clusters, architectural distortions and bilateral asymmetry. In diagnostic mammogram the morphology of benign and malignant tissues is different. It is depicted in Fig. 2.4. In the examination of mammogram images, the following abnormalities are taken care of:

1. Soft tissue density especially if borders are not well defined.
2. Clustered microcalcification in specific areas.
3. Calcification within or closely associated with a soft tissue density.
4. Asymmetric density or parenchymal distortions.

Breast cancers are radiodense which appears as bright spots in mammogram and fat is radiolucent that appear in colour ranging from dark grey to black. Dense fibroglandular fat tissue can obscure small cancers. The proportion of fat to fibroglandular tissue is called breast density. Women with dense breast have a higher percentage of fibroglandular tissue than fat tissue. The mammographic breast composition defined by BIRADS [22], which is a quality assurance tool, designed to standardize mammographic reporting is as follows.

Type 1: The breast is entirely fat.

Type 2: Scattered fibroglandular densities, 25 % to 50%.

Type 3: Heterogeneously dense breast tissue, 51 % to 75%.

Type 4: Extremely dense, > 75 % glandular.

Mass

Mass is a space occupying lesion seen at least in two different mammographic projections. Mass is called an asymmetric density when seen only in a single projection. Mass can be mainly divided into the following three categories.

1. Spiculated Mass

It is an indication of invasive breast cancer characterized by radiating spicules from a central soft tissue.

2. Circumscribed Mass

It is an indication of a benign condition with well defined or sharply defined margin. Features such as number, margin and density need to be carefully analysed.

3. Non specific soft tissue densities

This is the main reason for small cancers. These appear in some specific areas.

In general, masses with irregular shape and ill defined or speculated margin are more likely to be malignant and masses with circumscribed oval shape are usually benign.

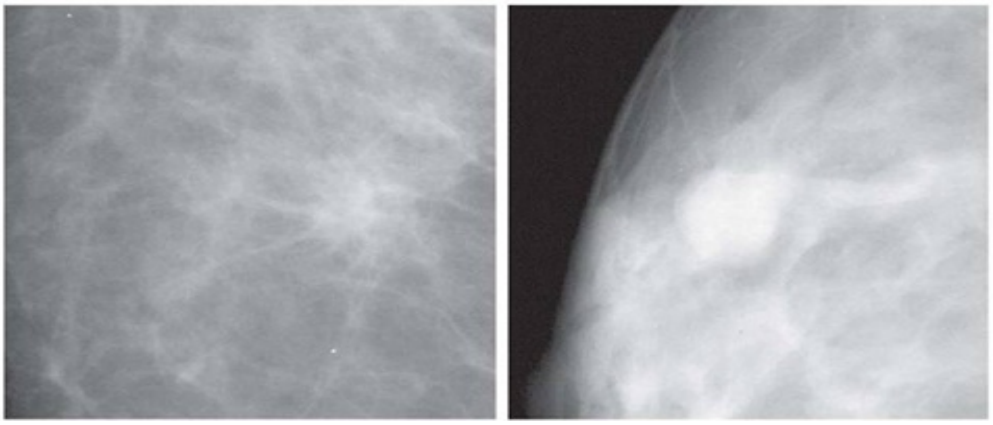

Malignant Benign

(Source: Rodney et al., Contemporary Issues in Cancer Imaging.)

Figure 2.4 Sample mammogram images of malignant and benign masses

Microcalcifications

These are tiny flecks of Calcium, which show up as bright white spots on mammogram [23]. Microcalcifications are characterized by their distribution, that is, they appear either isolated or in clusters. The morphology of malignant microcalcification and benign microcalcification is different. Size of an individual microcalcification varies from 0.1 to 10 mm with an average diameter of about 0.5 mm. The presence of three or more microcalcifications within 1 cm^2 defines a cluster. The size, shape, contrast and distribution of location of microcalcification in a cluster are used for characterizing the individual and cluster regions of microcalcification. The characteristics of malignant microcalcification are, they are numerous in number, more densely packed, small, varying in size and orientation [1]. Benign calcifications are larger, more rounded, smaller in number, less densely packed and more homogeneous in size and shape as in Fig.2.5.

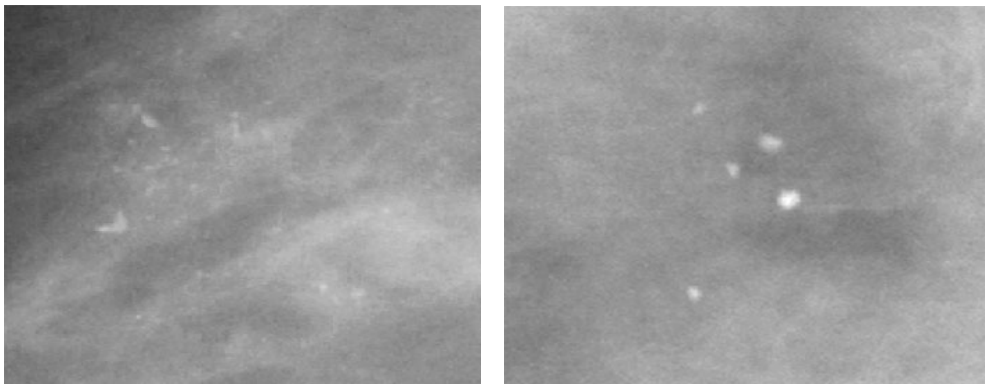

Malignant Benign

(Source: T. M. Deserno, *Biomedical image processing*: Springerverlag Berlin Heidelberg, 2011)

Figure 2.5 Sample images of malignant and benign microcalcification clusters in mammograms

Architectural Distortion

The normal architecture is distorted with spiculations radiating from a point and focal retraction or distortion of the edges of the parenchyma.

Focal Asymmetry

Focal asymmetry and global asymmetry are the two types of bilateral asymmetries present in mammogram images. Focal asymmetry is difficult to describe as it lacks borders and conspicuity of a true mass. When the amount of fibroglandular tissue in one breast is high compared to the other in the same area, it leads to global asymmetry [24].

In general the presence of defined margin around suspicious area indicates a benign lesion [25]. Usually malignant lesions may not have defined margin. The benign tumor is relatively slow in growing and does not invade to surrounding tissue. In contrast malignant tumors have rapid growth and are able to metastasis.

Limitations of Mammography

- Normal breast structures may obscure cancerous lesions particularly in dense breast with high composition of fibroglandular tissues.
- Superimposed tissue can cause unnecessary recall after diagnosis.
- Complex structures can mask abnormality.
- Inter-intra observer variability is high.
- Low positive predictive value for biopsy recommendations.
- Chances of misinterpretation leading to high false positive and false negative.
- Wrong interpretations may sometimes lead to over diagnosis and over treatment.

2.2.8 Computer Aided Diagnosis (CAD) in breast cancer screening

Computerized image analysis has been used over the past twenty years in order to achieve good results in diagnosis. Generally CAD systems are of two types: Computerized Aided Detection (CADe) and Computerized Aided Diagnosis (CADx) [1]. Both CAD schemes are useful for better localization and characterization of abnormalities. CADe schemes are used in screening mammography and CADx schemes are used in diagnostic mammography. CAD involves selection of different cases, interpretation of cases using computer algorithms, validation of algorithm, case performance evaluation by radiologist and final performance evaluation by clinical trials. Different steps like thresholding, Region of Interest (ROI) extraction, calculation of intelligible features to discriminate the segmented structures and

classification of lesions using extracted features can be done with high precision using CAD systems [26].

Advantages of CAD

- CAD can reduce the oversight of suspicious lesions.
- It can provide additional information for making biopsy recommendation.
- It improves radiologist's detection accuracy.
- CAD provides a second opinion by overcoming the limitations posed by human visual system.
- It helps in correct decision making even at the presence of overlapping tissue parenchyma.
- Assist radiologists in the interpretation of radiology images and directs their attention to the ROI.
- The results are reproducible and realistic.
- It can easily identify signs of pathology which the radiologist can further review.
- It reduces cost of double reading by improving the accuracy of individual reading.

2.3. Placental Sonograms

In this section we discuss the principles of ultrasound imaging, use of ultrasound imaging in obstetrics, relevance of placental grading and need of automated grading of placental sonograms.

2.3.1 Principles of ultrasound imaging

Ultrasound imaging uses [27] sound waves of frequency in the range 1 to 15 MHz. Compared with existing medical imaging modalities, it is real time, inexpensive, non ionizing and safe. Parameters that are described by ultrasound are pressure, density, propagation direction, wavelength and particle displacement. Ultrasound is a kind of sinusoidal pressure wave. In ultrasound machines, the images of the biological tissues are constructed by transmitting focused beam of sound waves into the human body using a transducer. The sound waves that are reflected back determine the structure of the tissue being imaged. Fig. 2.6 explains the process of ultrasound image formation [28].

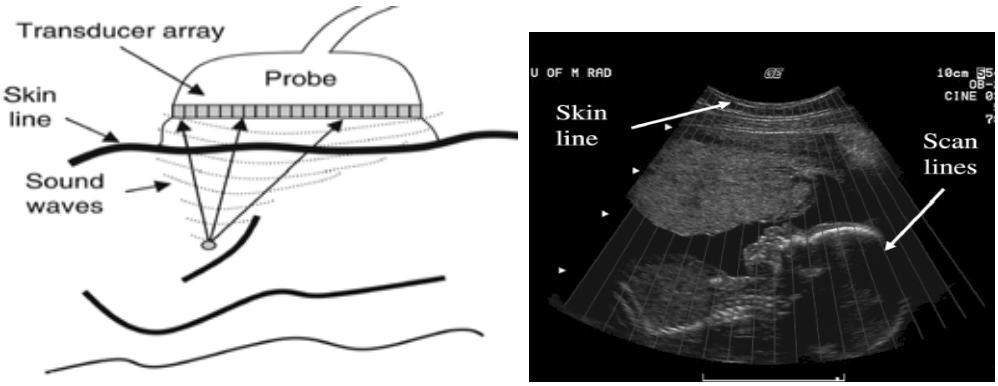

Figure 2.6 Ultrasound image formation

The transmit voltage applied to the transducer generates acoustic pressure at the phases of the transducer. A fraction of the waves from the propagated sound waves are reflected back on reaching the tissue surface depending on the acoustic impedance of the tissue along the path of the beam. The echo signals that are reflected back are converted to electrical signals. These signals are amplified and processed to produce ultrasound

images. The brightness of the formed image depends on the reflected echoes. The delay between pulse transmission and pulse reception, and the speed of propagation can be used for calculating the depth of the feature.

Ultrasound has two modes. A - mode (Amplitude mode) and B - mode (Brightness mode). The uses of A - mode are detection of eye tumor, liver cirrhosis and myocardial infraction whereas B - mode is used to produce 2-D Tomographic images by sweeping the beam repeatedly back and forth through the anatomical structure. Example:- Foetal monitoring.

2.3.2 Ultrasound in obstetrics

Ultrasound imaging has been actively applied to abdominal, breast, heart, blood vessel, and foetus imaging. It provides correct visualization of the internal parts of the body, measures blood flow and elasticity. The advances in healthcare over decades have resulted in the development of various computerized methods and tools to support foetal monitoring. Ultrasound is the ideal imaging technique for foetal monitoring. Structural anomalies of the foetus are best seen on ultrasound scan and therefore clinicians suggest that all mothers should be offered at least one thorough ultrasound scan at around 18-20 weeks or earlier [29]. Foetus's growth pattern is well explained in ultrasound. Prenatal diagnosis is very important as it can identify an early gestation abnormality.

2.3.3 The Placenta

Placenta is a foetomaternal organ that is in close contact with mothers body [30]. Development of placenta begins as soon as the foetal membrane establishes close and stable contact with uterine mucosa, that is, as soon as the blastocyst implants [31]. Placenta helps to exchange respiratory gases,

nourishments, extracts waste between mother and foetus. It starts functioning close to the fourth gestational week like an endocrine organ and provides necessary support for the development of a healthy foetus [32].

Human placenta appears as a disk like thickening of the membranous sac formed by chorionic plate and basal plate [33]. Pathology of human placenta is shown in Fig.2.7. Both the sheets enclose intervillous spaces. The intervillos space contains maternal blood which circulates around the placental villi. The villi are complex tree like projections of the chorionic plate into the intervillous space. The foetal vessels present inside the villi are attached to the circulatory system via chorionic plate and umbilical chord. The chorionic plate and basal plate are combined to each other at the placental margin and forms chorion leaves.

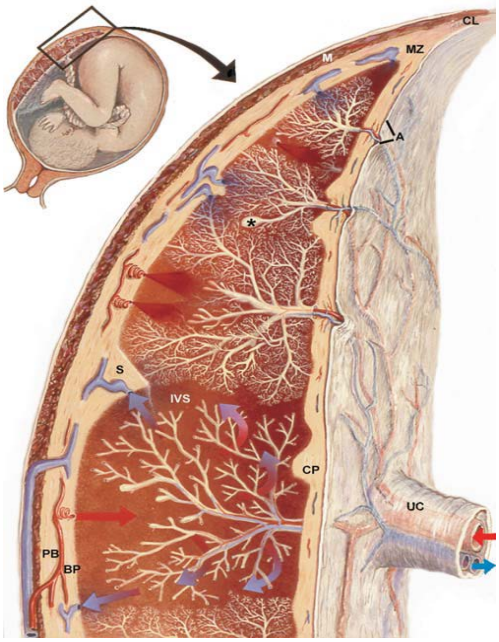

CP	:	Chorionic Plate
BP	:	Basal Plate
IVS	:	Intervillous Space
M	:	Myometrium
CL	:	Chorion Laeve
A	:	Amnion
MZ	:	Marginal Zone
UC	:	Umbilical Chord

(Source: Benirschke et al., Pathology of the human placenta, Springer, 2006)

Figure 2.7 Placental pathology

Major Functions of Placenta

- Foetal oxygenation.
- Endocrinological functions.
- Protein synthesis.
- Protective functions.
- Catabolic and resorptive functions.
- Synthetic and secretary functions of liver.
- Hematopoiesis of the bone marrow during first trimester.
- Heat transfer of the skin.
- Immunological functions.

2.3.4 Placental grading

Calcification is a normal degenerative process in placenta that increases with gestational age (age between conception and birth) and appears as irregularly distributed. According to the difference in texture patterns and appearance of placental body Grannum et al. [5] grouped placenta into different grades. The characteristics during different gestational period and corresponding grades are given in Table 2.1.

Table 2.1 Characteristics of different grades of placental images

Grade	Gestational period	Characteristics
Zero	Late first trimester – Early second trimester	Smooth chorionic plate with no indentations, homogeneous appearance of placental body.
One	Mid second trimester- Early third	Subtle indentations in chorionic plate, presence of echogenic densities, size and number of calcification increases.
Two	Late third	Marked indentations in chorionic plates, size and number of calcification increases.
Three	29 weeks – post date	Complete indentations and irregular calcifications

2.3.5 Importance of grading

Sonographic appearances and texture characteristics provide useful information regarding placental maturity [31]. Premature calcification can cause Intera Uterine Growth Restriction (IUGR), placental dysfunction, preeclampsia, hypertension and foetal distress in labor. Infants with IUGR show two patterns of growth, asymmetric and symmetric IUGR. The reason behind asymmetric IUGR is uteroplacental insufficiency. Sonographic assessment of the placenta should be done to find the presence of abnormal conditions such as placenta praevia, vasa praevia, placenta accrete, abruptio placenta, placental bed infraction [34]. These abnormal conditions are due to abnormal implantation of placenta, abnormal adherence of the placenta to the uterus, premature separation of the implanted placenta and so on. Therefore the examinations of morphology, anatomy, location, size and implantation, texture analysis of placenta are important. The vascular lesions in the placenta are some indications of abnormalities in complicated pregnancy. Placenta abruption is one of the main causes of perinatal morbidity and mortality.

Relevance of Grading

- If growth parameters are less compared to gestational age and if placental maturity is more it indicates an increased probability of IUGR [35].
- It helps in the diagnosis of IUGR [36].
- There exists a correlation between gestational age and placental grading.

2.3.6 Need of automated grading

- Each radiologist may have different evaluations of the same placenta, ie. high inter observer variability [30].
- Poor evaluation reproducibility.
- High subjectivity in evaluation.

2.4 Chapter Summary

In this chapter an overview of the problem domains are detailed. In the first part, the cause and effects of breast cancer, major treatment options, reason for selecting digital mammography and the importance of CAD systems are discussed. The second part discusses the use and principles of sonography in obstetrics, placental grading and need for automation.

Chapter 3
LITERATURE REVIEW

3.1 Introduction

We have witnessed great interest and advances in Computer Aided Diagnosis technologies. The last decade paved way for a large number of new techniques and systems. In this chapter, we survey the key theoretical contributions made in classification and content based retrieval and also investigate potential methods to improve the accuracy of classification and retrieval systems. This chapter is mainly divided into 3 parts, which review classification of digital mammogram, classification of placental sonogram and Content Based Medical Image Retrieval.

3.2 Review on Computer Aided Diagnosis of Digital Mammograms

Mammography is the best available technique for early detection of breast cancer. Lesions in mammograms are defined by large number of features and sometimes these can be easily misinterpreted by radiologists [24]. Screening programs have contributed to a significant fall in mortality rates through early detection of the disease. But the difficulty involved in the interpretation and the high volume of cases given to radiologist can sometimes result in wrong conclusion. Computer Aided Detection/Diagnosis is an affordable solution to all such problems [37]. CAD helps radiologists in the accurate screening and diagnosis. This section presents an overview of

digital image processing and soft computing techniques used to address quite a lot of areas in CAD of breast cancer, including: noise reduction, contrast enhancement, segmentation, detection and analysis of calcifications, masses and other abnormalities. Section 3.2.1 briefs the historical development of CAD system for breast cancer analysis.

3.2.1 Historical development

The discovery of X-ray by Roentgen in 1894 paved way for next generation of clinical diagnosis [19]. Eventhough the use of X-ray imaging for the detection of breast cancer was first recommended in the beginning of 19^{th} century, mammography was accepted as a technology only during 1960s, after a series of technical advances that produced higher quality images. In 1930 Albert Salomon, a famous pathologist in Berlin created images of 3,000 gross mastectomy specimens, examining black spots at the centres of breast carcinomas which were merely microcalcifications. Robert Egan and Anderson, TX, in 1960 used high resolution industrial film for mammography, capable of producing simple and reproducible mammograms with better image detail. He screened 2,000 nonsymptomatic women and found out 53 "occult carcinomas." In 1963 the result from the first randomized, controlled trial of screening by the Health Insurance Plan of New York, reports that, mammography could reduce the 5 year breast cancer mortality rate by 30 percent.

Owing to the urgency and importance of early and accurate diagnosis of breast cancer, a lot of efforts have been taken to enhance the clinical diagnosis in the last three decades. It was Lee Lusted, in 1955 [38] who mentioned about automated diagnosis of radiographers by computer. In 1967 Winsberg et al. [39] published a paper describing a CADx system in which

computers are used to characterize the lesions on a mammogram as benign or malignant. This work was not successful since the Computer Vision techniques at those times were limited. From 1970 onwards, commercial mammographic unit has been developed by various companies like Siemens, Philips, and Picker [19]. In mid eighties, there were two studies, the first work reported by Getty et al. proposed a CAD system which was not automated [40]. The second work by Chan et al. [41] propose an automated CADx system. These works paved way to many of the new approaches in CADe and CADx schemes. In1990 International Breast Cancer Screening Network (IBSN) formed to assess Mammography Quality Standards Act screening programs and in 1992 Mammography Quality Standards Act (MQSA) has been passed [19].

3.2.2 Contrast enhancement techniques

One of the main problems with mammography is that images are having low contrast. This makes it difficult for radiologists to interpret the results. Contrast enhancement methods are motivated by the fact that microcalcifications and masses tend to be brighter or different than their surroundings [42]. The basic idea here is to employ image enhancement methods to improve the contrast of suspicious areas, so that they can be easily separated from their surroundings. Conventional enhancement techniques are classified into global and local processing. Global enhancement techniques are effective in enhancing the entire image having very low contrast. This technique reassigns the intensity values of pixels and forms a new distribution different from the original. Contrast stretching, convolution mask, histogram equalization and histogram matching are examples for global enhancement. In many cases global enhancement fails to

enhance fine details and sometimes it works only for images having single object. Therefore local processing is used for enhancing small objects.

Gordon and Rangayyan [43] used "fixed neighbourhood method" to enhance the mammogram. Noise and other unwanted background information are also enhanced which leads to difficulty in microcalcification detection. Use of contrast-ratio adaptive neighbourhood operation loses some characteristics of microcalcification, therefore both the false positive rate and false negative rate are high. The use of an optimal adaptive enhancement method reduces this effect considerably [44]. Kim *et al.* [45] proposed an adaptive image enhancement method based on the first derivative and local statistics. The artifacts that could be misread as microcalcifications were removed, and the significant features of the mammographic image were enhanced by adding the adaptively weighted gradient images. Linear transformation enhancement filter proposed by Kom et al. [46] use a mass pattern dependent enhancement approach. This approach does not depend on the original contrast and background properties. The lesions in the resultant image will be clearer, leading to higher performance in further analysis. The use of iris filter to enhance the suspicious regions in mammogram can be found in Ref. [47]. Those structures having values above a minimum size are enhanced and those below that size are suppressed. The suspicious areas are then segmented by thresholding and morphological operations. Romualdo [48] uses Anscombe transformation, which is a variance-stabilizing transformation used to convert a random variable with a Poisson distribution into a variable with an approximately additive, signal-independent Gaussian distribution. To enhance the contrast, a filter based on the modulation transfer function of the imaging system is applied.

Use of fuzzy image preprocessing can increase the contrast of the mammogram images [49]. Fuzzy image processing system is a rule based system that uses fuzzy logic to reason about image data. Fuzzy Histogram Hyperbolization algorithm (FHH) is applied to improve the contrast of the image. The enhancement algorithm consists of four phases. Parameter initialization phase, fuzzification phase in which membership values are assigned to different grey level sets, the grey-level adjustment phase and finally making of new grey levels. Adaptive fuzzy logic contrast enhancement [50], combined approach of fuzzy logic and structure tensor [51] are other major works in this area.

In wavelet based enhancement, [52, 53, 54], wavelet filters are used for transforming the image from spatial domain to spatial frequency domain. Laine et al. [55] propose the first work using wavelet enhancement techniques for mammographic image enhancement. Original image is decomposed into multiscale representation. Using a non linear mapping the coefficients of each sub band is modified. Three multiscale representations, namely the dyadic wavelet transform, the φ-transform and the hexagonal transform are studied. Scharcanski and Jung [56] presented a wavelet-based method to perform noise reduction and image enhancement, using noise equalization, wavelet shrinkage and scale-space analysis. The proposed method only used two detail images (horizontal and vertical) instead of three detail images (horizontal, vertical, and diagonal). Use of wavelet shrinkage helps to preserve edges that were persistent over several scales and removes residual noise. Mencattini et al. [57] presented an adaptive tuning of enhancement degree at different wavelet scales for enhancing microcalcifications. For enhancing masses they have combined both dyadic wavelet information and mathematical morphology.

Morphological top-hat [58], homomorphic filtering [52], CLAHE (Contrast Limited adaptive Histogram Equalization) [54] and LRM (Local Range Modification) [59] are some of the techniques proposed for contrast enhancement of mammogram images.

3.2.3 Segmentation

Segmentation plays an important role in image analysis. Segmentation identifies the region of interest depending upon the problem. When segmentation is applied on mammogram images, the image gets partitioned into several non-overlapping regions such that the suspicious regions with abnormalities are separated from the background parenchyma. Segmentation mainly depends on two properties of image intensity: similarity and discontinuity [60]. The high radiographic density of abnormal region than other regions makes segmentation easy. Compared to the segmentation of microcalcifications, the segmentation of masses has added difficulty because of their fuzzy nature and highly irregular contours and their low contrast. Region based and boundary based are the major kinds of segmentation methods that are commonly used in medical image segmentation. Other commonly used methods for mass and microcalcification segmentation such as threshold based, wavelet based, mathematical morphology based, Fuzzy- C means clustering based and fractals based are also discussed here.

Threshold based segmentation methods are of two types - global thresholding and local thresholding. Global thresholding [61, 62] techniques are based on the global information. Since the abnormalities are brighter than the surrounding tissues, it makes thresholding a practical method for segmentation. The abnormal areas form extra peaks on histogram while a healthy region has

only a single peak. After getting global threshold value, the objects can be separated from the background. Dominguez and Nandi [63] performed segmentation of regions via conversion of greyscale images to binary images at multiple threshold levels. Global thresholding methods are weak in identifying ROIs (Region of Interest) [64]. Therefore to refine the result of global thresholding, local thresholding is used. Threshold value is determined locally for each pixel, based on the intensity values of the neighbouring pixels. Region based processing is based on the fact that pixels inside same region share similar characteristics. Region growing, a kind of region based segmentation [64, 65, 66] initially selects a seed point and then groups the pixels having similar properties as that of seed pixel. In conventional region growing, there is no restriction for the shape of the region. Therefore the formed region can sometimes move into adjacent structures resulting in erroneous partitions. Therefore Rojas Dominguez et al. [67] propose a method that segments two sets of breast mass counter of both benign and malignant lesion using dynamic programming and constraint region growing methods. The knowledge of geometrical information about the general shapes of the objects to be segmented is considered as a constraint function. Dynamic programming based boundary tracing is applied to segment mass counter. Docusse et al. [68] propose a method for characterizing the border of microcalcification. Wavelet transform is applied, and using region growing algorithm on the reconstructed image microcalcifications are identified.

Unlike region based segmentation, boundary based segmentation algorithms are characterized by change in intensity value. Edges, deformable models, active contours and level set are examples in this class. Wirth et al. [69] use active contours to extract breast contour, based on the gradient information

at the breast-air interface. The general idea of dynamic contour models is to approximate the boundary of a mass by minimizing the energy function of a closed contour consisting of connected line segments [70]. Since active contours are good in curve approximation it is well suited for breast contour extraction. Brake et al. [71] proposed a discrete dynamic contour model that was initialized with a circular contour of a fixed size. In the case of level set approaches, a contour is represented as the zero level of a higher dimensional scalar function. The surface is designed such that its intersection with the *xy*-plane matches the represented contour. Unlike traditional active contour model, level set model can easily handle topological changes like splitting or merging of parts of the contour. Shi et al. [72] proposed a level set approach for mass segmentation with an initial contour obtained by K-means clustering. A level set approach using a contour obtained using the radial gradient index approach is proposed by Yuan et al. [73]

Wavelet transform, which spatially localizes high frequency components, is an attractive alternative for the detection of high spatial frequency components. Due to the small size and high degree of localization, microcalcifications represent high-spatial frequencies in the image. Therefore, wavelet transform is widely used for the segmentation of microcalcifications [74-78]. The general idea of these approaches is to decompose a ROI into its subbands using the wavelet transformation and to weight the coefficients of the subbands so that microcalcifications are enhanced. The background tissue as well as the noise are suppressed once the inverse wavelet transform is applied to the data. Microcalcification segmentation with the use of continuous wavelet transform is proposed by Arikidis et al. [79].

Morphological operations are good in dealing with geometrical aspects of image analysis problems. Zhao et al. [80] developed a method to identify suspicious calcifications based on morphological adaptive threshold and morphological skeleton information. Morphological Component Analysis [81] can be used for decomposing mammogram image into piecewise smooth component and texture component. The characteristics of morphological component analysis are, it maintains the local contrast of the original mammogram, conserves the margin properties, suppresses noise and unwanted materials and the like. Wroblewska et al. [82], segmented areas with microcalcification using opening by reconstruction with the help of top hat techniques.

Fuzzy C-Means clustering (FCM), which is an extension of K-means clustering is also widely used for intensity based segmentation of mammogram abnormalities [58, 83]. In FCM a fuzzy membership function is used to associate each different structure in image to every cluster. Selection of initial seed point is the important task in FCM based approaches. An extension to this is, sub segmentation using probabilistic fuzzy c-means (PFCM) [84]. It involves segmentation within the cluster, that is, looking for less representative data inside the cluster. Fractal models are also used for the segmentation of mammogram abnormality [85,86]. Mammogram structures are having high similarity with high local self-similarity which is the basic property of fractal object. The disadvantage is that, it consumes too much computation time.

3.2.4 Pectoral muscle removal

Several methods have been used for the removal of pectoral muscle. It is an important step in Computer Aided Detection of breast cancer. The removal of pectoral muscle reduces bias of mammographic density estimation and enables region based processing in abnormality detection algorithms [87]. In most of the works reported, pectoral muscle is approximated using a straight line and the refinement of those edge pixels results in the identification of pectoral muscle [88]. Multiple-linked self organizing neural network [89], threshold based [90], Hough transform [91, 92, 93], Radon transform [94] are some of the major works in this regard. Domingues et al. [95] use Support Vector Regression (SVR) for the identification of pectoral muscle in mammograms. SVR model is used for predicting the end points at top and bottom row of the image using grey scale values. The shortest path between the end points corresponds to pectoral muscle. Sultana et al. [96] explore the use of mean shift algorithm followed by region growing for the identification of pectoral muscle. Camilus et al. [97] presented graph cut based segmentation algorithm for removing pectoral muscle. Using Bezier curve the rugged edges of pectoral muscle are smoothed.

3.2.5 Feature extraction

Another important step of CAD of breast cancer is the feature extraction process and selection of optimal features. The general guidelines to select significant features principally consist of four considerations: Discrimination, Reliability, Independence, and Optimality [98]. In this stage the features that characterize specific properties of the tissues are identified and the most important features are selected for the classification (benign or malignant) [24]. Table 3.1 reports the major features reported in the literature,

which are used for the detection and classification of breast abnormalities. Later a survey of recently developed feature extraction techniques is given.

Table 3.1 List of Feature extraction methods used for the detection and classification of mammogram abnormalities

Type of features	Feature description	Authors
Intensity features	Contrast measure of ROIs, average grey level of ROIs, standard deviation inside ROIs or variance, skewness of ROIs, kurtosis etc.	Tarassenko et al.[1995] [99] Huo et al.[1998] [100] Christoyianni et al.[2000] [101]
Shape	Individual microcalcification features	Davies et al.[1990] [102] Nishikawa et al.[1992] [103] Woods et al.[1993] [104] Jiang et al.[1996] [105] Zheng et al.[1996] [106] Yu et al.[2000] [107]
	Margin speculation, margin sharpness, area, circularity, convexity, rectangularity, perimeter, perimeter to area ratio etc.	Huo et al.[1998,2001] [100,108] Petrick et al.[1999] [109] Li et al.[2001] [98]
	Geometrical shape features Moment invariants, Fourier descriptors	Fauci et al.[2004] [110] Faramawy et al.[1996] [111]
Texture	Co occurrence features Grey level run length (GLRL) features SGLD features:	Daponte et al.[1997] [112] Dhawan et al.[1996] [113] Kim et al.[1999] [114] Petrick et al.[1999] [109] Li et al.[2001] [98] Sahiner et al.[1998,2001] [115, 116]
	GLDS features	Weszka et al.[1976] [117] Hardin et al.[1994] [118] Sahiner et al.[1996] [119]
	RLS features	Sahiner et al.[1998] [115]
BIRADS descriptors	Spiculation feature and circumscribed margin feature.	Sahiner et al.[2008] [120]
Wavelet features	Energy, entropy, and norm extracted from the wavelet transform sub-images.	Strickland et al.[1996] [75] Dhawan et al.[1996] [113] Yu et al.[2000] [107]
Scale space features	Features extracted from the image processed by Laplacian of Gaussian filter.	Netsch et al.[1999] [121]
Fractal dimension	Features used to describe the distribution of the microcalcification, cluster area, and number of microcalcifications in an area.	Daponte et al.[1991][112] Bothorel et al.[1997] [122]

Sameti et al. [123] uses photometric features from two independent regions in the mammogram. Photometric features are characterized by the absolute intensity, its distribution and optical density level of object. The

different texture features used are discrete texture feature, Markovian Texture Features, non Markovian Texture Features, run length texture features and fractal texture features. Braz Junior et al. [124] performed spatial texture analysis of mammogram images for classifying images into normal-abnormal and benign-malignant. Geostatistical texture measures such as Moran's index and Geary's coefficient are used. Morans index and Geary's coefficient describes the strength of associations between responses as a function of distance and direction. Moayedi et al. [125] propose the use of contourlet features, co occurrence matrix features and geometrical features. Contourlet transform is applied after removing the pectoral muscle and segmenting the ROI. Contourlet transform exploits multi scale and time frequency localization properties of wavelets. It offers a high degree of directionality and anisotropic structured basis function. Buciu et al. [126] use directional features for automatic tumor classification. Patches of abnormal areas are manually extracted and decomposed using Gabor wavelet. Gabor functions possess different orientation properties which are easily tuned by modifying the Gaussian parameters. Directional features at different orientations and frequency are extracted. Nanni et al. [127] perform a comparative analysis of Local Ternary Pattern (LTP), and Local phase Quantization (LPQ) and uniform bins of LTP. In LTP, from the histogram of the local binary patterns, bins with highest variance are selected. LPQ uses the local phase information extracted from the 2-D Short Term Fourier Transform (STFT) computed over a rectangular neighbourhood at each pixel position of the image. The concept of "bag of primitive texture patterns" are used for recognizing architectural distortions in mammogram [128]. Initially a compact representation of the anisotropic, irregular, aperiodic but directionally oriented textures are observed from mammogram images.

Fundamental patterns are learned using expectation maximization. Fractals based texture analysis is widely used in the recognition and classification of mammogram abnormalities [129, 130, 131]. The different methods that are used for measuring the fractal dimension are Reticular cell counting method, Differential box counting method, Blanket method, Fourier power spectrum method, Fractional Brownian motion model etc. , details can be found in [132] .

3.2.6 Feature selection

Feature selection is the method of picking up of optimum subset of features from the massive collection of features available in a given problem domain. Feature selection process consists of four basic steps, namely subset generation, subset evaluation, stopping criterion, and result validation [133]. Subset generation is a search procedure that generates candidate feature subsets for evaluation based on a specific searching strategy. Each candidate subset is evaluated and compared with the previous best subsets according to a certain evaluation criterion. If new subsets turn out to be better, they substitute the previous ones. This process is repeated until a given stopping criterion is satisfied. Commonly used feature selection methods are Genetic algorithm [134, 135, 136], Principle Component Analysis [137],[126], Discriminant Analysis [123] and the like. Genetic Algorithms (GAs), are adaptive heuristic search algorithms based on the principles of Darwinian evolution. In GA based algorithms the possible solutions of the problem are represented as chromosomes. The GA then creates a population of solutions based on the chromosomes and evolves the solutions by applying genetic operators such as mutation and crossover to find best solution based on the predefined fitness function [138]. Principal Component Analysis isolates the principal components of the dataset and eliminates those components that

contribute the least to the variation in the data set. Discriminant analysis uses training data to estimate the parameters of discriminant functions of the predictor variables. Discriminant functions determine boundaries in predictor space between various classes.

Mohanty et al.[139] propose a method that combines both fast branch and bound technique and genetic algorithm. Use of online feature selection method which can pick up the necessary features that can do the underlying task is also reported [140]. Multiobjective genetic algorithm [141], Particle Swarm Optimization [142], Rough Set Theory (RST) [143] and correlation based [144] are some of the other works reported.

3.2.7 Classification and detection of mammogram abnormalities using soft computing techniques

3.2.7.1 Detection and classification of microcalcifications

The presence of microcalcification clusters is a vital sign for the detection of early breast carcinoma. A timely sign of 30–50% of breast cancer identified mammographically is the appearance of clusters of fine, granular microcalcification. The strong association between the appearance of the microcalcification clusters and the diseases show that the automated detection/classification of microcalcifications can be very useful to manage breast cancer.

In 2003, Cheng et al. [42] give a detailed survey of Computer Aided Detection and classification of microcalcifications in mammogram images. The authors have surveyed different approaches used in various stages of automated detection such as contrast enhancement, segmentation, feature extraction and classification. Pal et al. [140] propose a multi-stage neural network aided system

for detection of microcalcifications in digitized mammograms. Ren et al. [145] use balanced learning to overcome bias associated with the distribution of data. The proposed learning algorithm with neural network is used for the recognition of microcalcifications. Karahaliou et al. [146] perform the analysis of texture of tissue surrounding microcalcification. Grey level texture features and wavelet coefficients are used for the analysis. A probabilistic neural network is used for characterizing malignant tissues from benign ones. Dheeba et al. [147] propose swarm optimized neural network system for classification of microcalcification in mammograms. Table 3.2 gives a report of major work done using soft computing techniques in the classification and detection of microcalcification.

Table 3.2 List of soft computing techniques used for the detection and classification of microcalcifications in mammogram images

Author Name	Classifier	Results
Woods et al.[1993] [104]	KNN	Area under ROC: 0.929
Dhawan et al.[1993] [148]	ANN	Accuracy: 74 %
Bankman et al.[1993] [149]	Bayesian classifier	Accuracy: 100 %
Zheng et al.[1996] [106]	ANN	TPF: 90% , FP: 0.77%
Dhawan et al.[1996] [113]	ANN	Accuracy : 74 %
Wroblewska et al.[2003] [82]	ANN	Accuracy : 90 %
Bothorel et al.[1997] [122]	Fuzzy decision tree	Specificity : 92% Sensitivity of 96%
Kramer et al.[1998] [150]	KNN	Accuracy: 100
Kim et al.[1999] [114]	ANN	Area under ROC : 0.88
Ferrari et al.[1999] [151]	ANN	Accuracy : 88%
Verma et al.[2001] [152]	ANN	Accuracy : 88.9%
Soltanian-Zadeh et al.[2001] [153]	KNN	Area under ROC :0.82

3.2.7.2 Detection and classification of masses

Detection of mass is quite difficult than detection of microcalcification. Masses are quite subtle, and usually seen in the dense areas of the breast tissue, have smoother boundaries than microcalcifications and appears in different

shapes such as circumscribed, speculated, lobulated or ill-defined. Table 3.3 reports the major papers published regarding the detection of masses.

In 2005 Sampat et al. [154] made an attempt to give an overview of Computer Aided Detection and Diagnosis in mammography. They have analysed the various techniques specifically suited for identification and classification of masses and microcalcifications. Different researchers have focused on particular subset of masses. Pixel based and region based methods were excellent in detecting speculated masses. Later in 2006 [138], Cheng et al. have discussed the various approaches used for the automated detection and classification of masses in mammograms. Preprocessing approaches such as global histogram modification, local processing, multiscale processing are discussed. They have discussed the four different types of segmentation techniques used: classical techniques, fuzzy techniques, bilateral image subtraction and multiscale techniques. Features showing image characteristics of intensity, texture and shape are commonly used in mass detection. Step wise feature selection and genetic algorithm are the commonly used feature selection methods. The use of linear discriminant analysis, artificial neural network with different algorithms, Bayesian network, binary decision trees and use of combined classifiers are also summarized.

In 2008 Verma et al. [155] propose a novel network architecture and learning algorithm for the classification of mass abnormalities in digitized mammograms. The new learning algorithm can increase the memorization ability without affecting the generalization capacity of the network. For this purpose they have introduced additional neurons in the hidden layer for each class. Mammographic mass detection using wavelets as input to neural networks is proposed in [156].

Classification using ELM with Wavelet features, GLSDM, Gabor filter based features reports 94 % accuracy [157]. Three different activation functions namely, unipolar, bipolar, and Gaussian are used. Maximum efficiency is reported for Bipolar activation function with 28 hidden neurons for GLSDM based feature vector, Bipolar activation function with 30 hidden neurons for Gabor filter based features and Gaussian activation function with 30 hidden neurons for Wavelet based features.

Subashini et al. [158] propose a method to assess breast density in digital mammogram. Histogram based thresholding is used to separate image from background. Using SVM classifier the proposed work classifies mammogram tissues into fatty, glandular and dense. Borges Sampaio et al. [159] present a computational methodology that assists specialists to detect breast masses in mammogram images. Using cellular neural networks, suspected regions are segmented. Shape descriptors are used for the classification with SVM.

Zhang et al. [160] build an ensemble system for mass classification using mass contour and mass shape features. Luo et al. [161] using forward and backward feature selection, showed that breast density is an irrelevant feature for the diagnosis of breast masses in mammogram. The use of SVM with Sequential Minimal Optimization (SMO) and its ensembles give good result. Leod et al. [162] use Variable Hidden Neuron based ensemble technique for mass classification in digital mammogram. The method is based on the concept that, the internal architecture of neural network and data distribution are changed, different classifiers that represent knowledge in different way can be built. They have also proposed neural network ensemble for mammogram mass detection [163]. West et al. [164] investigated the result of classifier diversity that is, the number of different classifiers in

ensemble, on the generalization accuracy capability of the ensemble. Their results established that most of the improvement occurred with ensembles formed from 3-5 different classifiers.

Table 3.3 List of soft computing techniques used for the detection and classification of masses in mammogram images

Author Name	Classifier	Results
Sahiner et al.[2001] [165]	LDA	Area under ROC: 0.89
Bovis et al.[2000] [134]	ANN	Area under ROC: 0.72
Li et al.[1995] [166]	Fuzzy Decision Tree	TP : 93 %, FP : 3.1 %
Arikidis et al.[2008] [79]	Genetic Programming	Accuracy : 98%
Campanini et al.[2004] [167]	SVM	TP : 80% FP: 1.1 %
Wei et al.[2005] [168]	LDA classifier	TP : 90% , FP : 1.82 %
Sahiner et al.[1996] [119]	Convolution neural network	Area under ROC: 0.87
Braz Junior et al.[2009] [124]	SVM	Accuracy: 92.89 %, Area under ROC: 0.91
Moayedi et al.[2010] [83]	SVM Family	SEL weighted SVM- Accuracy : 96.6% SVFNN- Accuracy : 91.5% kernel SVM- Accuracy: 82.1%
Sameti et al.[2009] [123]	Jackknifed classification	Accuracy: 72 %
Fraschini et al.[2011] [169]	ANN	Area under ROC : 0.91 Sensitivity: 94.4%, Specificity: 84.6%.
Nanni et al.[1971] [86]	SVM	Area under ROC : 0.97.

3.2.7.3 Detection and classification of other abnormalities

Verma et al. [170] propose a novel soft cluster neural network technique for the classification of suspicious areas in digital mammogram. During the training phase soft clusters of features are created by removing weak clusters/neurons and keeping strong clusters. They have also proposed soft clustered based direct learning classifier for the classification of abnormal patterns in mammogram [171]. Ren et al. [172] compare the performance of

ANN and SVM with imbalanced data. To learn effectively from imbalanced data set, a new learning strategy with optimized decision making has been proposed. The results show that, the performance of both classifiers improves when used with the new learning algorithm. Wang et al. [173] use structured SVM (sSVM) to classify ROI into normal or cancerous. The basic idea of nonlinear s-SVM is to transform data vectors from the input space to high dimensional feature space by a nonlinear mapping and then discover data structures via kernalized agglomerative hierarchical clustering. Yoon et al. [174] propose Minimum Redundancy Maximum Relevance (mRMR) score based approach for classifying abnormalities into masses and microcalcifications. Bagui et al. [175] propose a classification method based on rank nearest neighbour classification rules. Classification using KNN based on this approach reports 98.1 % accuracy for multivariate data analysis of breast cancer. Meselhy Eltoukhy et al. [176] perform a comparative analysis of wavelet and curvelet decomposition. Euclidian distance based classification categorizes mammogram image into benign, malignant and normal. As curvelet transform is able to capture multidimensional features in wedges as opposed to points in wavelets, curvelets give better result for breast cancer detection. Fuzzy Rough Set's hybrid scheme [49], GA based neuro fuzzy techniques [177], expert system based on neuro fuzzy rules [178], self adaptive resource allocation network classifier for mammogram image [179] are some of the major works reported in the detection and diagnosis of breast abnormalities.

Architectural distortion

Architectural distortion is the most commonly missed abnormality in false negative cases. According to Perry et al. [180], progress in the detection

of architectural distortion could direct to a successful improvement in the diagnosis of breast cancer. Ayres et al. [181] explore the use of phase portraits using Gabor filters for the detection of architectural distortion. Zwiggelaar et al. [182] proposed a technique to identify irregular patterns of linear structures by detecting the radiating spicules and/or the central mass likely to occur with spiculated lesions. Guo et al. [132] propose the use of Hausdorff fractal dimension and an SVM classifier to characterize ROIs with architectural distortion and those with normal mammographic patterns. Matsubara et al. [183] use fractal dimension to differentiate between normal and architectural distortion patterns in mammographic ROIs. The area under the ROC curve achieved was 0.89. The use of mathematical morphology to detect architectural distortion around the skin line and a concentration index to detect architectural distortion in the mammary gland has been explored by Ichikawa et al. [184]. Sensitivity rates of 94% with 2.3 false positives per image and 84% with 2.4 false positives per image respectively, were reported.

Bilateral Asymmetry

The asymmetry between the left and right mammograms of a given subject is a significant indication of breast cancer [144]. The BI-RADS [122] definition of asymmetry indicates the presence of a greater volume or density of breast tissue without distinct mass or more prominent ducts, in one breast as compared to the corresponding area in the other breast. Analysis of asymmetry is important as it can provide information regarding the development and growth of new masses, parenchymal distortion, and small asymmetric dense regions. Miller and Astley [185] detects bilateral asymmetry using a semi automated texture based method and measures of shape, topology, and distribution of brightness in the fibroglandular disk [186].

3.2.8 Commercial systems for mammogram image classification

Image Checker by R2 technology was the first commercial mammographic system approved by FDA [187]. This system can digitize screen-film mammograms, automatically detect suspicious regions, and display those detections to a radiologist. Intelligent Systems Software, Inc developed MammoReader capable of detecting primary signs of breast cancer. iCAD's new Second Look Digital CAD technology , MagView mammography reporting software are some of the commercially available CAD systems used for breast cancer screening.

3.3 Classification of Placental Sonograms

3.3.1 Historical development

In 1940s, Theodore Dussik, a neurologist from the University of Vienna used ultrasound in first, as a diagnostic tool to locate brain tumors and the cerebral ventricles [188]. Professor Ian Donald of Scotland [189] developed practical technology and applications for ultrasound in the 1950s. It was Ian Donald in 1955 who first put into practice using two metal flow detectors to scan specimens of fibroid and ovarian cysts. Later in 1958 he published a paper titled “investigation of abdominal masses by pulsed ultrasound”, which entirely dealt with the use of ultrasound in clinical obstetrics and gynecology. Accurate location of the placenta was the holy grail of antenatal diagnosis in the early 1960s. Placenta praevia was the cause of significant maternal mortality due to severe haemorrhage in late gestation [190]. In early 1960s placenta praevia had been identified as the major cause of maternal mortality due to severe haemorrhage in late gestation. Therefore identification of the location of placenta was a dreadful task at those times. Studies conducted failed to define the lower

placental edge. In 1966 Ken Gottesfeld and the Denver group published the first paper on ultrasound placentography. In 1968 Donald Usama Addulla was able to define placenta in all orientations. Studies related to foetal biometry and IUGR has been proposed in Ref. [191]. Later developments and studies are oriented towards the identification of different measures such as Thoracic Circumference (TC), Biparietal Diameter (BPD), Abdominal Circumference (AC) and foetal abnormalities [4]. Real time scanners were introduced in early to mid 1970s. The advances in the technology of integrated circuit helped the development of small, movable and inexpensive ultrasound machines. The first commercial linear array real time scanner was the ADR, a small company founded by Martin Wilcox. In 1985 colour doppler imaging was incorporated into real time scanning. Harmonic imaging was introduced by the end of 1990s and studies and discussion regarding the importance of 3-D and 4-D imaging in obstetrics and gynecology had begun. By 2000, the latest, real time scanning machine with high resolution transducer, colour and power doppler facilities with 3-D/4-D option was developed.

3.3.2 Ultrasound of the placenta

According to Abramowicz et al. [34], sonographic examination of placenta is important for foetal monitoring. The examination should include: location, assessment of size, thickness, volume, implantation, morphology, anatomy and search for any abnormal condition. Placenta praevia and vasa praevia are the anomalies related to the location of placenta [192]. The abnormal implantation of placenta leads to placenta praevia. Sonographic examination can identify the different types of placental praevia. If the foetal vessel runs through the membrane, unprotected by placental covering, it can cause membrane

rupture leading to high risk of foetal exsanguinations and death. This condition is called vasa praevia [193]. Studies conducted by Baulies et al. [194] suggest that ultrasound examination of vasa praevia is having high detection rate. Placenta accrete, abruption placenta, placenta bed infarction and hematomas are the anomalies reported with implantation. Placenta accreta is defined as the abnormal observance of the placental body inside the uterus due to an absence of Nitabuch's layer [195]. Abruptio placenta, which leads to high complications in pregnancy, occurs due to the separation of a normally implanted placenta [196]. Placenta bed infarction which is round, mostly anechoic and intraplacental leading to foetal demise is caused by thrombosis in the villous space [35,197]. Different studies have shown that placental thickness is an important parameter in abnormal foetal growth [198]. Different anomalies in placental shape also need to be analysed carefully.

3.3.3. Placental maturity analysis

For identifying the relationship between the appearance of texture and placental maturity, several studies have been conducted [199, 200]. Studies conducted by McKenna et al. [201], analyse the significance of an immature placenta. They suggest that, identification of "at risk" pregnancy, as a result of gestational hypertension and delivery of growth restricted neonate is possible by ultrasound examination of grade 3 placenta at 36 weeks of gestation. Damodaran et al. [36], in 2010 conducted MRI examination of IUGR and established that there exist significant relationship between sternness of foetal growth restriction and appearance of placental pathology.

3.3.4 Classification of placental images

In 2010, Ayache et al. [202] propose the use of DWT to classify placental tissue development. Wavelet coefficients at level 3 decomposition are used for training the neural network. For the classification of 80 images which belong to four grades, an accuracy of 95% has been obtained. Linares et al. [203] use textural features such as GLCM, NGDTM, Laws's operator for the characterization of placenta images. The authors have used 12 ultrasound images. From the manually segmented ROI, features are extracted and classified using decision trees. The accuracy reported is 98 %. Later they have proposed the use of relief-F algorithm for selecting optimal features [30] Liu et al. [204] use multi-classification support vector machines in the B-placenta image classification. They have extracted grey scale statistics from the image and reports 92 % recognition rate. According to Chen et al. [31] quantitative sonography using texture analysis of the placenta is useful in clinical practice to determine gestational age. In this work they have extracted texture features from SGLDM and GLDM matrices after identifying the region of interest. To determine the relationship between gestational age and placental texture they have used multiple regression model. Malathi et al. [205, 206] published papers relating to the classification of placental images into normal and abnormal based on wavelet coefficients, histogram statistics and placental thickness. They have conducted experiments with relatively few numbers of images. K. N. Bhanu Prakash et al. [9] conducted study on foetal lung maturity analysis based on textural features extracted from ultrasound images. The features used are fractal dimension, lacunarity, and features derived from the histogram of the images.

3.4 Content Based Image Retrieval

3.4.1 Introduction

One of the lasting legacies of the twentieth century is the persistent impact of digital techniques in explicit as well as in embedded forms [207]. The power of digital media and the advances in Information Technology offer enormous image archives and repositories for efficient information processing. In early days textual annotation methods were used for image storage and retrieval. Text based retrieval process exhibits number of limitations. In those systems textual annotations are added manually, the process is subjective and incomplete. Text based search gives semantically similar images and content based search gives visually similar images [208]. Non-textual features are suited for efficient query processing. The development of a Content Based Image Retrieval system could meet the storage and retrieval needs of information processing and management by solving the problems in text based search engines [209]. CBIR system retrieves similar images based on low level features such as shape, texture and colour. In the past decades significant progress has been made in the development of CBIR systems. CBIR plays a major role in various fields such as teaching, research, industry and medical diagnosis [210]. Researchers in CBIR have been intensively working to improve the performance of existing techniques using different approaches.

This survey begins with a brief summary of early CBIR developments, and then moves to progress during recent years, which includes a detailed survey of feature extraction techniques, similarity measures and relevance feedback algorithms. In Section 3.4.4 some of the general purpose CBIR systems are discussed. Section 3.4.5 discusses techniques used in Content Based Medical

Image Retrieval such as segmentation, feature extraction and similarity measures. Some of the existing CBMIR systems are listed in the last part of this section. Finally the survey discusses different CBIR methods applied particularly on mammogram images.

3.4.2 The early years of CBIR

The early period of CBIR research is from 1994 to 2000 [209]. In 2000, Smeulders et al. [7] present a review of the progress made in CBIR during this period. The paper discusses the patterns of use, type of images, gaps in image understanding and the different types of features used for describing the image properties. They have classified the image domain into narrow and broad. The variability in narrow domain is limited and predictable while broad domain has unlimited and unpredictable variability in its appearance. According to Smeulders et al. the three categories of image search are: search by association, aimed search and category search. Feature description is divided into two parts, image processing and feature construction. In image processing CBIR is engaged in enhancing the details in images and in feature construction the semantics and understanding of the pictures are important. Major contributions in colour, texture and shape features have been discussed. In 1991 [211], Swain and Ballard uses colour histogram for image indexing. QUBIC [212], VisualSEEK [213], Pitoseek [214] are some of the systems that had excellent choice of colour feature extraction methods. In 1999, Huang et al. [215] introduced colour correlograms, an enhancement to colour histogram. Statistical features characterizing texture are expressed in terms of local statistics such as Tamura texture features [216], and Wold features [217]. Viewpoint features, occlusion invariant local features [218] and local patch based salient features [219], are some of the other works reported in this area. Use of Gabor filters is

explored in Ref. [220]. Daubechies wavelet coefficients for image retrieval were introduced in 1998 [221]. Smeulders et al. [7] grouped similarity measures (used for finding the similarity between query image and database images in a CBIR system) into feature based matching [211], object silhouette based matching [222], structural feature matching [223] , salient feature matching [224], matching at the semantic level [225] and matching based on learning [226]. Later research focused towards methods to improve retrieval accuracy with the help of user interaction like relevance feedback, the process by which user gives judgments on the initial retrieval results in a CBIR system. QUBIC [212], PicHunter [227], VIRAGE [222], VisualSEEK [213], Netra [228] and AMORE [229] were some of the earlier systems that use the concept of relevance feedback.

3.4.3 CBIR at recent years

Most of the CBIR systems use low-level image feature extraction methods which are usually extracted either from the entire image or from regions. Since representation of images at region level is similar to human perception [230], the first step in CBIR is the segmentation of region of interest. Then, low-level features such as colour, texture, shape or spatial location are extracted from the segmented regions. The following section summarizes major feature extraction techniques, similarity measures and relevance feedback mechanisms that are in use.

3.4.3.1 Feature extraction techniques

Colour, texture, shape and their variants are the commonly used feature extraction techniques in CBIR. Table 3.4 lists some of the feature extraction techniques.

Table 3.4 List of major low level features used in CBIR

Feature type	Feature Description	Authors
Colour	Colour-covariance matrix	Jing et al.[2003] [230]
	Colour histogram	Town et al.[2001] [231]Yue et al.[2011] [232] Tong et al.[2001] [233],
	Colour moments	Das et al.[2013] [234]
	Colour coherence vector	Zheng et al.[2004] [235]
	Colour structure descriptor	Park et al.[2007] [236]
	Dominant colour descriptor	Liu et al.[2008] [237]
	Colour co-occurrence matrix	Lin et al.[2009] [238]
	Quantization levels in colour histogram	Rashedi et al.[2013] [239]
	Colour difference histogram	Liu et al.[2013] [240]
Texture	Wavelet features	Wang et al.[2001] [241],
	Edge histogram descriptor	Rashedi et al.[2013] [239]
	Gradient vector	Salembier et al.[2001] [242]
	Difference between pixels of scan pattern	Qi and Y.Han[2003] [243]
	Co occurrence matrix	Lin et al.[2009] [238]
	Local maximum edge binary pattern	Yue et al.[2011] [232], Subrahmanyam et al.[2012] [244]
Shape	Curvature scale space	Salembier et al.[2001] [242]
	Area, Second order moments	Town et al. [2001] [231]
	Eccentricity, Orientation	Mezaris et al.[2003] [245]
	Pseudo-Zernike moments	Wang et al.[2011][246]
	Structural shape features	Lee et al.[2013] [247]

3.4.3.2 Similarity measures

The commonly used distance measures in image retrieval are Minkowski distance, Canberra distance, angular distance, Czekanowski coefficient [248], inner product, dice coefficient, cosine coefficient and Jaccard coefficient [249]. The use of Earth Mover' Distance in CBIR is first reported in Ref. [250]. Earth Mover's Distance measures the minimal cost required to transform one distribution into another based on a traditional transportation problem from linear optimization. Integrated Region Matching (IRM) [251], allows matching a region of one image to several regions of another image and thus decreases the impact of inaccurate segmentation. Dynamic Partial

Distance Function (DPF) [252], which reduces the dimension of feature vectors by dynamically choosing a smaller amount of dimensions is also widely used in CBIR applications. Vasconcelos and Lippman [253] proposed Multi Resolution Manifold Distance (MRMD) for face recognition. In the MRMD, two images to be matched are treated as manifolds, and the distance between the two images is the one which minimizes the error of transforming one manifold into the other. CLUE [254]- Cluster Based Retrieval of Images by Unsupervised Learning is a new technique for improving user interaction with image retrieval systems by fully exploiting the similarity information. Clustering in CLUE is dynamic. Based on a graph-theoretic clustering algorithm CLUE retrieves similar images. A genetic programming framework for content-based image retrieval is proposed by R. da Silva Torres et al. [6]. The problems associated with weighted image similarities and combined feature vector are addressed in this work. The similarity functions are combined through nonlinear combination of image similarities. An extremely fast CBIR system proposed by Yildizer, uses Support Vector Regression (SVR) model to find the class probabilities [255]. Since SVR is mainly defined for binary classification, this study uses multi-class SVR ensemble to handle multi-class image databases. This method reduces dimensions of feature vectors dramatically. A hybrid similarity learning scheme is proposed in Ref. [256]. The proposed method preserves visual and semantic resemblance by integrating short term and long term learning process. Initially the semantic similarity is learned from user's query log and then the visual similarity is learned from a mixture of labelled and unlabelled images. Finally, visual and semantic similarities are fused in a nonlinear way.

3.4.3.3. Relevance feedback

Relevance feedback is a powerful method traditionally used in text-based information retrieval systems [257]. In mid 1990s relevance feedback was introduced to CBIR with the aim to reduce the 'semantic gap' between low level features and high level user understandings. Since then, this topic has got remarkable attention in CBIR research. The use of relevance feedback shows significant improvement in retrieval performance with the help of user interaction [258, 259]. The importance of using relevance feedback is to overcome the ambiguities in interpreting images, easiness of user to give judgments and the continuous representation space of images that describes semantic concepts [260].

A typical scenario for RF in CBIR is as below:

(1) Initial retrieval results are given by the machine through query-by-example, sketch and the like.
(2) User judges the above results as to whether and to what degree, they are relevant or irrelevant to the query.
(3) Machine learns users' feedback. Then go to step (2).

Relevance feedback mechanism can be either treated as density estimation or as a classification process. If image or region is represented as a point in feature space then it is considered as a density estimation problem. Different relevance feedback methods might have adopted different assumptions. Fig.3.1 lists some of the conceptual dimensions, along which some schemes differ greatly from others. These can be separated into two broad classes. Class one includes several aspects of the user behavior model, examples:- what to look for [261], what to feed back [262, 263, 233] greedy vs cooperative [264, 265]. The second class includes algorithmic assumptions

such as feature selection and representation, class distribution [259, 266], objective functions and learning mechanisms [267, 268, 269].

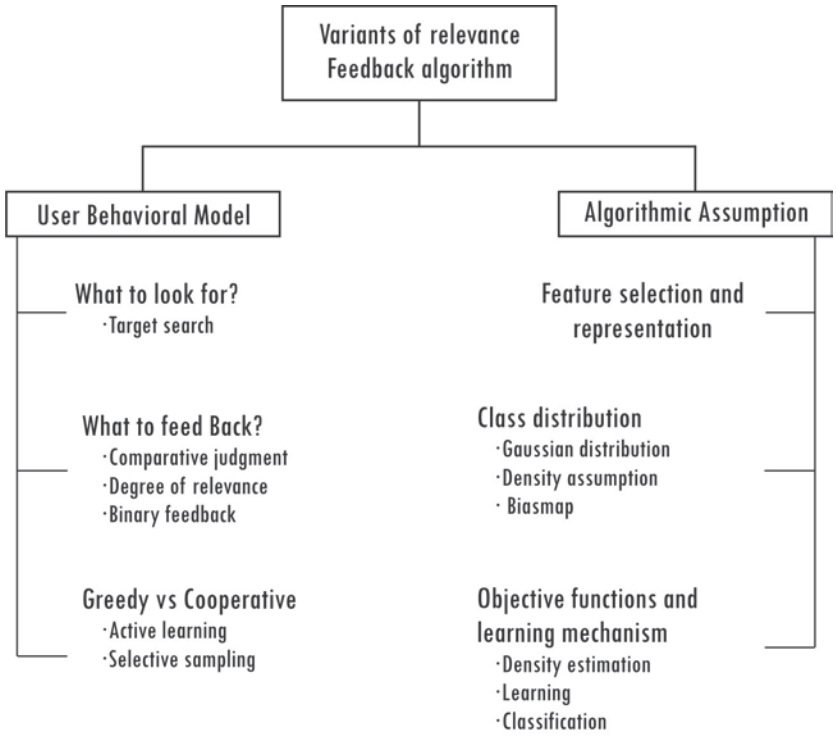

Figure 3.1 Relevance Feedback techniques and their major variants

3.4.4 General purpose CBIR systems

PicSOM [270] is a multi-purpose Content Based Image Retrieval system based on Tree Structured Self-Organizing Maps (TS-SOMs). Given a set of reference images, each TS-SOM is formed with a different image feature representation like colour, texture, or shape. A new approach introduced in PicSOM facilitates automatic grouping of responses from multiple TS-SOMs and their hierarchical levels. In WBIIS, Wang et al. (2001) [271], developed an image retrieval system using Daubechies wavelet transformation. The Red (R),

Green (G) and Blue (B) components, which reflect human perception, are represented in different domains. Low frequency components after 4-level and 5-level Daubechies wavelet transformation and the standard deviation of the matrix calculated after 5-level wavelet transformation are stored. WaveQ [272] which was developed at the University of Calgary is another content based image retrieval system using wavelets. WaveQ uses LUV colour space where L is the luminance of a pixel, U is the red–green colour value of a pixel and V is the blue–yellow colour value of a pixel. First an image is classified as texture or non-texture according to the standard deviation of the U component and different feature vector extraction methods are used for these classes. An Interactive Object-based Image Clustering and Retrieval System (OCRS) have been proposed in Ref. [273]. The system incorporates two major modules: Preprocessing and Object-based Image Retrieval. In preprocessing, an unsupervised segmentation method called WavSeg is used to segment images into meaningful semantic regions (image objects). Techniques based on GA are used to cluster these image objects which reduce the search space for object-based image retrieval. In learning and retrieval module Diverse Density algorithm is used. ImageMiner [274] is a software platform for comparative analysis of expression patterns in imaged microscopy specimens such as tissue microarrays (TMAs). ImageMiner is a federated system of services that offer a reliable set of analytical and data management capabilities for investigative research applications in pathology. It includes a library of image processing methods, like automated registration, segmentation, feature extraction, and classification.

3.4.5 Content Based Medical Image Retrieval

Content Based Medical Image Retrieval is an exciting and active field of research, where disciplines such as Computer Science and Medicine combine forces in order to improve health care [275]. Radiology images are the fundamental part of diagnosis, treatment planning, and treatment. Medical images are equally important for medical education, research and epidemiology. The usage of medical images has been escalating enormously due to production of thousands of digital medical images of different modalities such as Computed Tomography (CT) images, Magnetic Resonance Images (MRI), ultrasound (US) images, X-ray images and so on. Due to the steadily increasing medical image data, the proper management and access of the data is very important [276] Therefore, a lot of CBIR (Content Based Image Retrieval) systems cited medical images as a principal domain for content-based retrieval. CBIR has a potential for building a strong impact in diagnosis, research, and education. CBIR is a promising technology to enhance the core functionality of Picture Archiving and Communication Systems (PACS).

Interpretation of radiology image involves three tasks:- perception of image findings, interpretation of findings to offer proper diagnosis and clinical recommendations [277]. The process is difficult because several hidden problems are associated with the interpretation of medical images. Use of CAD systems, decision support systems and CBIR systems can enhance the perceptual component of image interpretation. Tagare et al. [278] in 1997, published a paper on CBIR using medical images. In 1998 Lowe et al. [279]

published a paper on knowledge-based retrieval of medical images. They have discussed the role of semantic indexing, image content representation and the significance of knowledge-based retrieval. CBIR can be used to distribute the needed information at the right time, in the right place to the right person [280]. Clinical decision support systems such as case based reasoning, evidence based medicine and decision support systems in radiology are also used in CBIR techniques to retrieve images that are valuable for supporting certain diagnoses. In addition to diagnosis, teaching and research widely use visual access methods, since visually interesting images can be chosen easily [280].

The segmentation problem can be seen as the main obstacle towards the use of sophisticated feature extraction methods. Automatic reliable segmentation is a challenge of cases in which objects of interests such as anatomical structures or lesions which are surrounded by complex and arbitrary backgrounds [277]. Segmentation is a major preprocessing step in CBIR systems that describes the image content through regions of interest. Segmentation identifies semantically meaningful regions/objects within an image. Hsu et al. [281] propose the use of two types of hierarchical segmentation algorithms for the segmentation of vertebral bodies from X-ray images. Zamora hierarchical segmentation, which is based on Active Shape Models (ASM) captures the shape of bone spurs by using a combination of hierarchical segmentation and Generalized Hough Transform (GHT), a deformable model (DM).

3.4.5.1 Feature extraction

Comparison of different feature extraction techniques in retrieving medical images is carried out in Ref. [282]. The different techniques are Gabor Transform, Discrete Wavelet Frame, Hu Moment Invariants, Fourier Descriptor, Grey Level Histogram and Grey Level Coherence Vector. Quellec et al. [283] propose a CBIR method for assisting medical diagnosis. In the proposed system, images are indexed in a generic fashion, rather than extracting domain-specific features: a signature is built for each image from its wavelet transform. These image signatures characterize the distribution of wavelet coefficients in each subbands of the decomposition in a database when a query image is submitted by a physician. In medical domain, texture-based descriptors become predominantly vital as they can potentially be a sign of the fine details contained within an image structure [277].

Texture Feature

The common practice to obtain texture-based descriptors is to invoke standard transform domain analysis tools such as Fourier transform, wavelets, Gabor, or Stockwell filters on local image blocks. In addition, one can also derive the so-called Haralick's texture features such as energy, entropy, coarseness, homogeneity and contrast, from a local image neighbourhood or utilize linear system approaches such as simultaneous autoregressive models. Yuan et al. [284] propose the use of non-negative tensor factorization (NTF) for extracting feature of brain CT image. NTF represents local parts of the image set, which is consistent with certain theories in visual recognition, psychological

and physiological evidence that support part-based representations in the brain. NTF treats the whole CT image set as a 3D tensor which keeps each CT image in 2D representation, and therefore preserves the spatial structure information. Subrahmanyam et al. [244] propose the use of Binary wavelet transform (BWT). An 8-bit greyscale image is divided into eight binary bit-planes, and then Binary Wavelet Transform (BWT) which is similar to the lifting scheme in Real Wavelet Transform (RWT) is performed on each bit plane to extract the multi-resolution binary images. The local binary pattern (LBP) features are extracted from the resultant BWT sub-bands. Oberoi et al. [285] propose a framework based on Local Tetra Pattern and Fourier Descriptor for content based image retrieval from medical databases. The proposed approach formulates the relationship between the reference or centre pixel and its neighbours, considering the vertical and horizontal directions calculated using the first-order derivatives. This work also explored the association of Euclidean Distance (ED) with local tetra pattern.

Shape feature

Shape refers to the information that can be inferred directly from images and that cannot be represented by colour or texture [277]. Shape can be represented through perceptually grouped geometric cues such as edges, contours, joints, polylines, and polygonal regions extracted from an image. Shape always provides vital information in detecting a certain disease/lesion or in understanding its characteristics. Thus shape-based descriptors are expected to be useful to accomplish the fine detail constraints of medical image retrieval. Radial distance signature which is expressed by the distance of the boundary

points from the centroid of the shape and Local Area Integral Invariant Signature is explored in Ref. [286].

Table 3.5 List of Image descriptors used in CBMIR

Feature type	Representations	Descriptions
Photometric	Greyscale and colour	Histograms [287, 288, 289] Moments [290, 291] Block-based [292, 293] Intensity features [294]
Geometric	Texture	Tamura features [216] Texture co-occurrence [295] Multiresolution autoregressive model [287] Fourier power spectrum [290] Wavelet-based [288,283] Gabor features [289] Haralick's statistical features [296] Grey level statistical features [297]
	Point sets	Shape spaces [298]
	Contours/curves	Edge histograms[295],[291] Fourier-based [295, 299] Polygon approximation [299] Curvature scale space [300]
	Surfaces	Level sets/distance transforms [301, 302] Gaussian random fields [303]
	Regions and parts	Wavelet-based region descriptors [304] Spatial distributions of ROIs [305] Statistical anatomical parts model [306]
	Other	Global shape :-size, eccentricity, concavity [295, 292, 307] Morphological [302, 308, 307] Location and spatial relationships [307, 302]

3.4.5.2 Feature selection

Feature Selection (FS) algorithms find a reduced number of features that preserves the most significant information of the dataset. FS is usually applied as a preprocessing step in data mining tasks. It reduces the dimensionality of feature set by removing irrelevant or redundant features and thereby leading to more efficient and accurate classification, clustering and similarity searching processes. FS algorithms can be categorized into two groups: filter and wrapper [133]. Filter algorithms evaluate the “properness” of the feature subset by using intrinsic characteristics of the data. Wrapper methods generally select features which are further suited to the mining task than the filter methods, but they normally present a higher computational cost. Correlation based feature selection algorithm and fast correlation based feature selection algorithm employ Pearson's correlation as evaluation criterion of feature subsets. Wrapper FS algorithms are task specific as opposed to filter algorithms. Statistical association rules and genetic algorithms are examples. S. F. da Silva et al. [309], employ a GA using an evaluation function based on the ranking concept to perform FS for CBIR. This study employs a wrapper strategy that searches for the best reduced feature set, while improving the quality of the results of similarity searches. The study by Jiang et al. [310] investigate online feature selection in the relevance feedback learning process to improve the retrieval performance of the region- based image retrieval system.

Other commonly used methods for online feature selection in CBIR are Discriminant Analysis (DA) approach - Multiple Discriminant Analysis (MDA) method, Biased Discriminant Analysis (BDA) method and Symmetric Maximized Minimal Distance in subspace (SMMS) method

[310]. They generalize Linear Discriminant Analysis (LDA) and assume that the "relevant" images group together as one cluster. To meet the asymmetry requirement they do not assume the one-cluster distribution for "irrelevant" images.

3.4.5.3 Similarity measures

Image similarity measures are used for finding the distance between image features. Intuitively, small distances correspond to higher similarity [277]. The choice of metric depends on the type of feature descriptors. The simplest feature representation is a high dimensional vector space. Metrics defined on vector spaces (e.g., the Euclidean distance) are the common similarity measures. Many CBIR systems usually employ such vector distances due to their computational simplicity. These kinds of distance definitions need the features to be continuous within a range for the computed distances to correspond to perceptually coherent similarities. Procrustes methods are used when descriptors consist of landmark points, which usually delineate a shape boundary [298, 299]. In such cases rigid body transformation (translation + rotation) and an isotropic scaling are used for measuring the similarity between two shapes. Using elastic matching methods as in Ref. [311, 312], it is possible to extend this notion of similarity to allow non rigid deformations of the shapes. Approaches based on continuous mappings are also becoming increasingly popular in the medical domain [313, 314].

Sometimes in the diagnosis of disease, fine geometrical differences between imaged structures may be relevant to experts. In such cases, similarity is defined through the notion of elastic deformations required to transform one shape into another [315, 313]. Similarity can also be calculated through the use of statistical classifiers that group new instances using high

level information extracted from a training set of instances with known labels. In such cases retrieval engine can directly optimize the parameters of the similarity model by means of statistical learning as explained in. Ref. [316, 277]. Category-specific statistical similarity matching is proposed on the pre-filtered images by probabilistic multiclass Support Vector Machine (SVM) and Fuzzy C-Means (FCM) clustering for categorization and prefiltering of images to reduce the search space [291]. Iakovidis et al. [317] propose a novel scheme for efficient Content Based Medical Image Retrieval, formalized according to the Patterns for Next generation Database systems (PANDA) framework for pattern representation and management.

3.4.6 Content Based Medical Image Retrieval systems

ASSERT system [295], is designed for High Resolution Computed Tomography (HRCT) images of the lung, where a rich set of textural features is derived from the pathology-bearing regions (PBR). Besides texture, shape, and greyscale properties, attributes that measure the perceptual properties of the anatomy are also used. I-Browse project [318] is aimed at supporting intelligent retrieval and browsing of histological images obtained along the gastrointestinal tract. Using knowledge based systems and reasoning engines, high-level semantic attributes of images are obtained and textual annotation of images are automatically generated in this system. Image Guide [287] is a CBIR system in the domain of cytopathology images. In this system, a classification-based approach is performed to detect different types of blood cells based on the properties of cell nucleus. WebMIRS [319], an ongoing research project, has targeted the retrieval of X-ray images of the human cervical and lumbar spines. The indexing system includes methods for automated image segmentation, image feature extraction, feature vector

computation, feature organization, and text data organization. IRMA [320], a medical image retrieval system is used for the classification of images into anatomical areas, modalities and viewpoints. MIARS (Medical Image Annotation and Retrieval System) [321] provides automatic annotation and supports, text based as well as image based retrieval strategies, which play important roles in medical training, research, and diagnosis. The system utilizes three trained classifiers based on SVM. More medical image retrieval systems are listed in table 3.6.

Table 3.6 List of Content Based Medical Image Retrieval systems

Authors	Description
Liu et al.[1998] [322]	3D X-ray images of Computed Tomography images.
Chbeir et al.[2000] [323]	3D X-ray images of Computed Tomography images of brain.
Antani et al.[2002] [319]	2D-X-ray images of spine.
Petrakis et al.[2002] [308]	MR images.
Mojsilovic et al.[2002] [324]	3D MRI images of brain.
Kuo et al.[2002] [325]	2D ultrasound images of breast.
Kwak et al.[2002] [288]	Abdominal ultrasound images.
Gletsos et al.[2003] [290]	CT liver images.
Glatard et al.[2004] [326]	3D Dynamic Contrast-Enhanced MRI of heart.
Alto et al.[2005] [296]	Mammogram ROIs.
El-Naqa et al.[2004] [327]	Mammogram images.
Aschkenasy et al.[2006] [311]	Cardiac ultrasound images.
Siadat et al.[2005] [328]	Bain MRI images.
Kim et al.[2006] [329]	PET images of brain.
Bai et al.[2007] [330]	3D/4D Functional MRI images of brain.
Hsu et al.[2009] [281]	SPIRS (Spine Pathology & Image Retrieval System).

3.4.7 Content Based Medical Image Retrieval systems for digital mammograms

In spite of the recent advances in medical imaging technologies, mammogram reading is still leftover as a difficult clinical task. Abnormal lesions may produce changes in mammograms that are subtle and difficult to recognize. It is very difficult to discriminate benign lesions from malignant ones in mammograms. Sometimes lesions are misinterpreted during routine screening of mammograms [75]. This increases biopsy rate, causing needless fear and pain to women [331]. This further result in relatively large inter-observer variability that can lead to failure in biopsy. Malignant lesions are difficult to discriminate from benign lesions [332]. Once a suspicious breast mass is either automatically detected by the CAD scheme or visually identified by the observer (radiologist) and manually queried, a CBIR scheme searches the reference database for a group of most 'similar' ROIs. Use of mammogram retrieval system by presenting images with known pathology that are "visually similar" to the image being evaluated, may aid radiologists in their diagnosis, potentially leading to improvement in their diagnostic accuracy [327]. Retrieval system helps to view images of lesions that appear similar.

El-Naqa et al. [327] in 2004 proposed a new approach, in which similarity is learned from training samples given by human observers. They have explored the use of neural networks and support vector machines to predict the user's belief of similarity. They have also incorporated online human interaction by providing relevance feedback. The database consist of 76 mammograms, with clustered microcalcifications (MCs) in it. A new approach to support Computer Aided Diagnosis (CAD) aiming at supporting

the task of classification and similarity retrieval of mammographic mass lesions, based on shape content is proposed in Ref. [333]. Zernike moment features, fractal theory for feature extraction and KNN for retrieval are applied. Kinoshita et al. [334], use breast density as a pattern to retrieve images from a 1080 mammography database. Breast density is characterized using shape descriptors, texture features, moments, Radon transform, granulometry, and histograms. Kohonen self-organizing map (SOM) neural network was used for the retrieval task. Wang et al. [335] conducted studies to assess the performance of three methods, namely mutual information, Pearson's correlation and a multi-feature-based *k*-nearest neighbour (KNN) algorithm, for the search of 15 'the most similar' reference ROIs to each testing ROI from a database of 3000 ROIs. The study demonstrates that due to the diversity and huge collection of medical images, CBIR schemes using multiple image features based on ROIs can accomplish significantly improved performance. J.H. Oh, El-Naqa and Yang [336] propose an online learning mechanism based on relevance feedback for retrieval of 200 mammogram images that contain perceptually similar lesions with clustered microcalcifications. The proposed approach uses support vector machine (SVM) regression for supervised learning and employs the idea of incremental learning to incorporate relevance feedback online. The authors in Ref. [337], propose, implement, and evaluate a CBIR system called MammoSys. They have introduced the two-dimensional Principal Component Analysis (2DPCA) method for the characterization of breast density texture, which allows feature extraction and dimensionality reduction. Retrieval is performed using support vector machine. Wei et al. [338], present a content-based mammogram retrieval system with BIRADS

characteristics. User's perception is modelled using hierarchical similarity measurement scheme based on a distance weighting function. This maximizes the effectiveness of each feature in a mammographic descriptor. A machine learning approach based on support vector machines and relevance feedback is also used. Chandy in 2013 [297], propose a grey level statistical matrix from which four statistical texture features are extracted for the retrieval of mammograms. The data set includes images with architectural distortion, asymmetry and calcifications. It also includes circumscribed, ill-defined, spiculated and normal masses.

3.5 Chapter Summary

This chapter presents a survey on topics relevant to the research work. The key theoretical and empirical contributions in the recent decades related to the classification and retrieval of mammograms and placental sonograms are briefly summarized. The first part includes a comprehensive survey, highlighting current progress, emerging directions in the characterization of digital mammograms and placental sonograms. Progress made in areas such as preprocessing, feature extraction and classification using Machine Learning techniques are discussed. In the second part of the review, techniques used in Content Based Image Retrieval especially in medical image retrieval are discussed. The focus has been put on feature extraction, similarity search and relevance feedback mechanisms.

Chapter 4

PREPROCESSING AND FEATURE EXTRACTION

4.1 Introduction

Preprocessing operations and feature extraction has become a major component of biomedical image analysis and clinical research. Computer Aided Detection and diagnosis is adversely affected by artifacts and unwanted information in the image. For the successful detection and diagnosis, it is vital for clinicians to properly apply the new and innovative techniques in preprocessing and feature extraction. Preprocessing helps to improve the quality of visualization and interpretation of biomedical images. Design of good preprocessing system should consider disease specific features of the medical images and also understand the principles of different imaging modalities. This chapter gives a detailed description of the database, preprocessing steps and feature extraction techniques used in the proposed work.

4.2 Digital Mammograms - Database Description

Mammogram Images are collected from a publically available database – Mammographic Image Analysis Society (MIAS), an organization of UK research groups [339]. The X-ray films in the database have been carefully selected from the United Kingdom National Breast Screening Programme and digitized with a Joyce-Lobel scanning microdensitometer, a device linear in the

optical density range 0-3.2, to a resolution of 50 μm × 50 μm, and each pixel is represented with an 8-bit word. The database contains a total of 322 images of size [1024, 1024] , left and right breast images for 161 patients. Among the 322 images, 210 images are normal, 61 benign and 51 malignant. Information regarding the nature of background tissue (Fatty, Fatty-glandular, and Dense-glandular), class of abnormalities such as calcification, circumscribed masses, speculated masses, ill-defined masses, architectural distortion, asymmetry and normal , and if abnormality is present , its nature, coordinates of centre of abnormality and radius of a circle enclosing the abnormality are given. Fig. 4.1 shows sample images with tissue types. The distribution of data set are given in Fig. 4.2, Fig. 4.3, Fig. 4.4 and Fig.4.5.

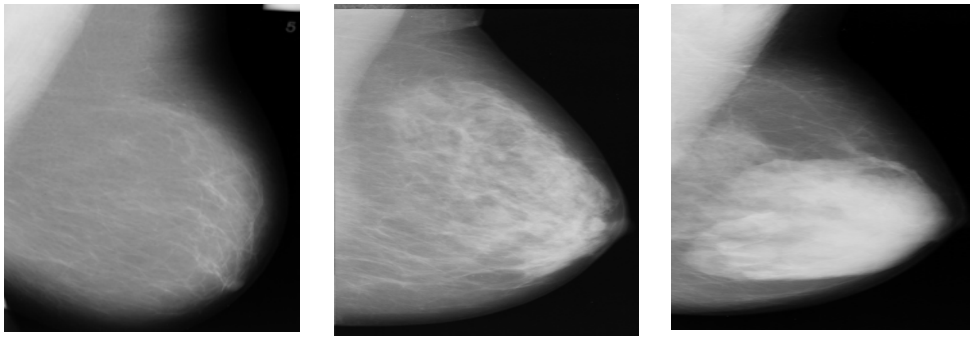

Figure 4.1 Background tissue types. a) Fatty, b) Glandular, c) Dense glandular

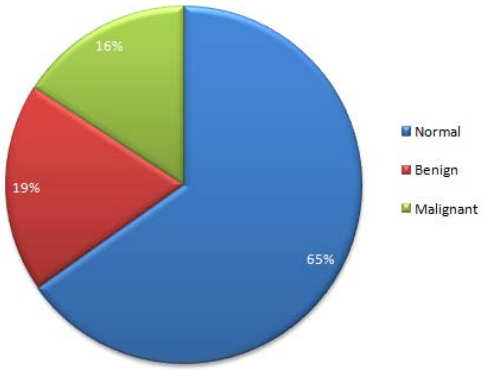

Figure 4.2 Class distribution of MIAS database

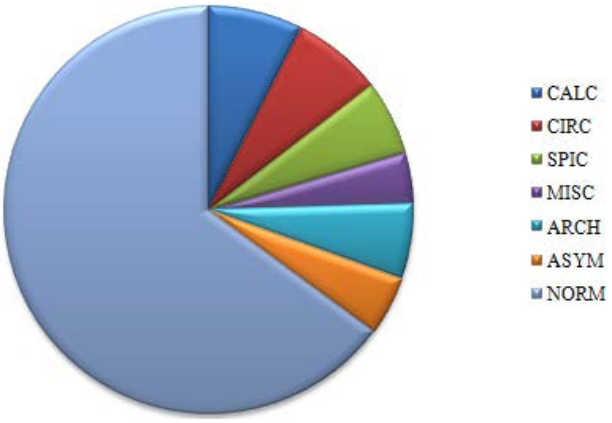

Figure 4.3 Distribution of types of abnormalities in mammogram images

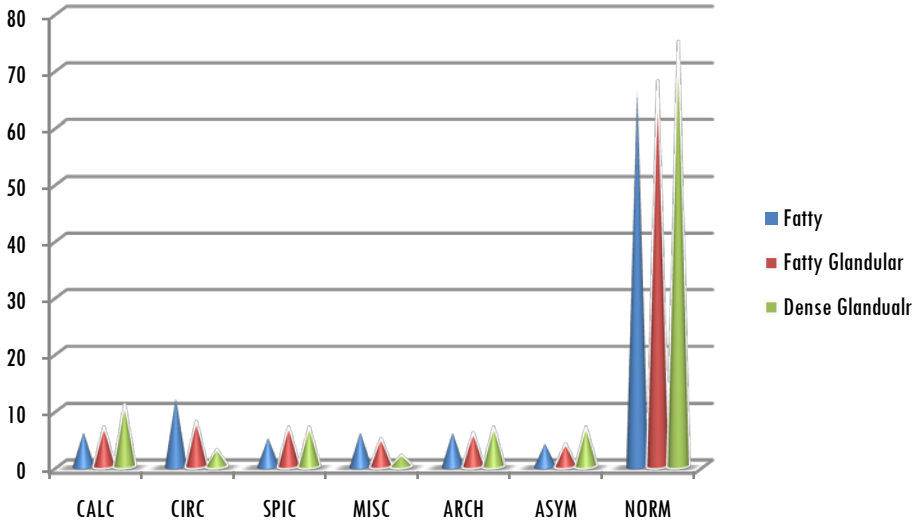

Figure 4.4 Distribution of background tissues in mammogram images

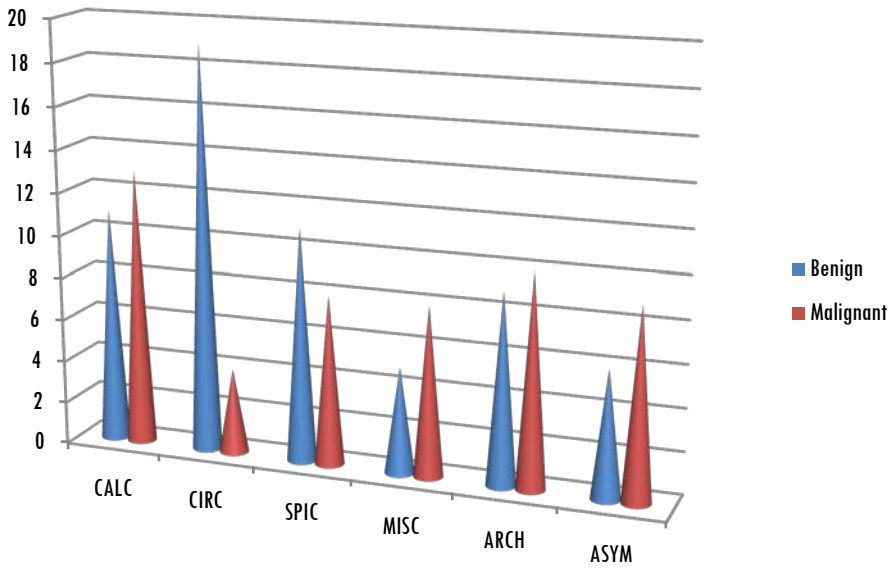

Figure 4.5 Distribution of severity of abnormality in mammogram images

4.3 Preprocessing of Mammogram Images

Images in MIAS database contain breast region, non breast region, background information, pectoral muscle, and several types of noises. This has to be removed for effective analysis and interpretation. Fig. 4.6 shows different types of artifacts such as tape artifact, orientation tag, low intensity label, scanning artifacts and the like, that are usually visible in mammogram images. Removal of these kinds of artifacts is essential for the correct analysis of mammogram images. Different steps involved in preprocessing operation are shown in Fig. 4.7.

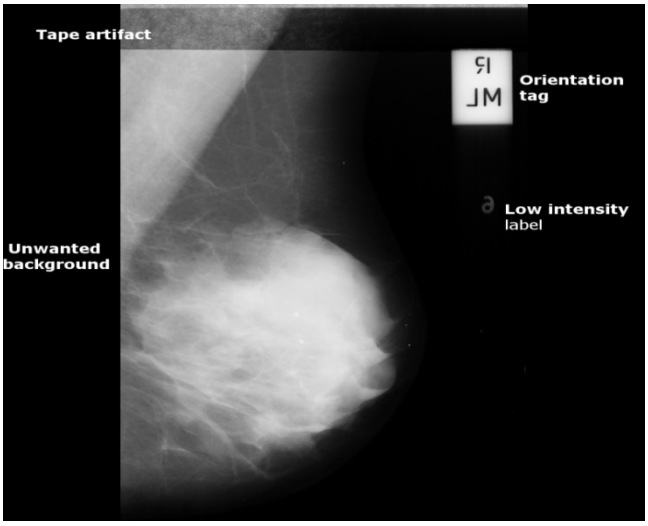

Figure 4.6 Artifacts in mammogram images

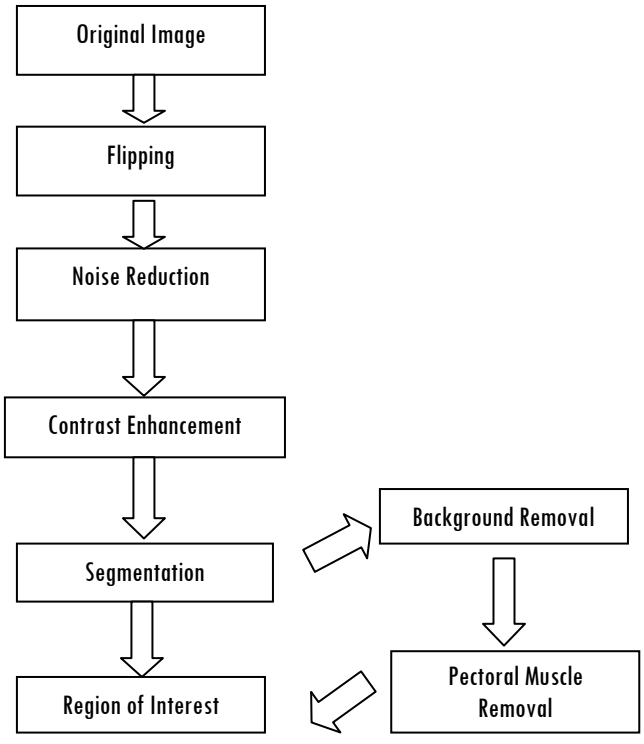

Figure 4.7 Steps in preprocessing - Digital mammogram

4.3.1 Flipping

MIAS database contains image pairs of left and right breasts. Mammogram images of the left breast are processed directly and mammogram images of right breast are flipped horizontally to left.

4.3.2 Contrast enhancement - Adaptive Histogram Equalization

Usually medical images are having poor quality. Contrast enhancement is the process used to alter the appearance of an image. Histogram equalization, computes the greyscale transform of image and ensures that in the resultant image grey values occur at equal frequency. The result is not acceptable always because it does not take into account that the amount of information present in the image depends on the signal level. If we apply histogram equalization to mammogram image, contrast of the background region is expanded at the cost of foreground area. In such cases adaptive histogram equalization in which a different greyscale transform is computed at each location in the image, based on a local neighbourhood will be more appropriated [340]. The size of the neighbourhood is an important parameter. Inorder to reduce the computational complexity involved in finding the transform at every pixel location, the transform is computed at limited locations only. In adaptive histogram equalization the contrast of the noises also increases. To avoid this undesirable result, contrast limited adaptive histogram equalization has been used [341].

The speed and effectiveness of CLAHE in the enhancement of medical images have been proved by scientists over the years and continues to be used in very recent studies [54]. From the literature studies, it is clear that there exists a number of other proven techniques such as fixed neighbourhood method [43], optimal adaptive enhancement [44], adaptive

image enhancement based on first derivative [45], morphological top hat [58], homomorphic filter [52] and LRM [59] for mammogram image enhancement. CLAHE was originally developed for medical images and has proved to be successful for the enhancement of low contrast images. The excellent prevention of noise amplification, ease of implementation and reduced computational complexity [341] led to the use of CLAHE in this study.

4.3.3 Segmentation

Segmentation isolates the object of interest [60]. It is a prerequisite in clinical practice. To separate abnormal lesion from the background parenchyma, the unwanted information has to be removed from the mammogram image. Segmentation is carried out to assist radiologist, so that they can easily locate the suspicious areas that need further analysis. Usually while scanning an image they look for suspicious areas whose characteristics relate to signs of abnormality [37]. Segmentation results in easy discrimination of healthy anatomical structures from the pathological tissue. The segmentation process is based on the fact that, breast contour limits the search for abnormality to the breast region, by removing non-breast region and thereby reduces number of false positives. To define the region of interest, in this study, we propose a three level segmentation. In the first level, background information is removed, in second level pectoral muscle is removed and in final level the breast region is extracted. The procedure is as follows and the algorithm is summarized in Table 4.1.

4.3.3.1 Background removal

Images in the MIAS database contains large portion of unwanted black pixels. The presence of such information will adversely affect further

processing. Therefore it is necessary to remove those pixels. For that we have defined a rectangle over the entire breast region. The procedure is as follows. Scanning from the first position in image, identify the first non zero pixel along the row. By continuing this in each row a straight line that connects the pixels in each row is identified. Move towards right and identify zero pixels along rows. Repeat this process and define a rectangle, covering the entire breast region, thereby removing most of the background information.

4.3.3.2 Pectoral muscle removal

In the Mediolateral Oblique (MLO) view the upper left and right corner on mammogram image shows pectoral muscle as a bright triangular patch. Its intensity is higher than breast tissue and in some cases texture of pectoral muscle shows similar characteristics as that of breast abnormalities. The presence of pectoral muscle causes additional sources of complexity in automated detection of breast cancer. Therefore it has to be removed. Traversing from top to bottom, the width of pectoral muscle decreases. The right side of the shape can be approximated by a straight line. After background subtraction the pectoral muscle starts at the (0,0) position. Scan from this $(0,0)^{th}$ position to find the first black pixel. Draw a straight line from that to the mid point of breast image. Define a rectangle through these points. Apply Canny edge detection algorithm over the rectangular region and plot the principal edge. A clear straight line can be generated, using which a triangular portion that corresponds to pectoral muscle can be identified and removed. The steps involved in Canny edge detection can be summarized as follows [60].

Let $f(x, y)$ denote input image and $G(x, y)$ denote the Gaussian function

$$G(x, y) = e^{-\frac{x^2+y^2}{2\sigma^2}} \tag{4.1}$$

Step 1: Smooth the input image with the Gaussian function

$$f_s(x, y) = G(x, y) * f(x, y) \tag{4.2}$$

Step2: Compute gradient magnitude and direction

$$M(x, y) = \sqrt{g^2 x + g^2 y} \tag{4.3}$$

$$\alpha(x, y) = \tan^{-1}\left[\frac{g_y}{g_x}\right] \tag{4.4}$$

Step 3: Thin the ridges around local maxima using nonmaxima suppression.

Let $g_N(x, y)$ contains the thinned edges

Step 4: Perform double thresholding using a low threshold value and a high threshold value.

Step 5: Use connectivity analysis to identify the principal edges.

4.3.3.3 ROI extraction

The breast boundary is extracted using active contours. An Active contour or snake is a controlled continuity contour which elastically snaps around and encloses a target object by locking onto its edges [27]. Energy function controls this snake. The snake is active because it always tries to reduce the energy. The snake can be imposed to have specific characteristics by specifying appropriate energy function. The energy function constitutes of internal and external energy. Internal energy arises from some fundamental properties of the snake such as length or curvature while external energy depends on image structure and user dependant constraints. Usually to make the

snake to shrink like an elastic band, the internal energy function is defined in such a way that when the length increases, its value also increases. The sum of the squares of the distance between adjacent control points is taken as the internal energy function. The sum is multiplied by an adjustable constant K.

$$E_{\text{internal}} = E_{\text{elastic}} = K\sum_{i=1}^{N}(d_{i,1-1})^{2} \tag{4.5}$$

Where i is the index of the control points with coordinates (x_i, y_i). The force on the i^{th} control point is obtained by differentiating the energy function, as follows.

$$F_i(x) = 2K((x_{i+1} - x_i) - (x_i - x_{i-1})) \tag{4.6}$$

$$F_i(y) = 2K((y_{i+1} - y_i) - (y_i - y_{i-1})) \tag{4.7}$$

These forces pull a control point towards its two nearest neighbours. Forces given on every control point will pull the snake inwards and will pull the control points into line with one another, smoothing the snake.

Each control point is moved by an amount proportional to the force acting on it. That is :-

$$x_i = x_i + CF_i(x) \tag{4.8}$$

$$y_i = y_i + CF_i(y) \tag{4.9}$$

The constant C determines how far the points move for a given force.

The external energy of the snake determines its relationship to the snake. If the snake needs to latch on to bright regions, then negative of the sum of the grey levels of the pixels covered by the snake is the external energy. Reducing this function moves snake towards more brighter areas.

$$E_{\text{external}} = E_{\text{image}} = -K\sum_{i=1}^{N} P_i \tag{4.10}$$

Where P_i is the pixel value of the i^{th} pixel and the constant k is user defined. The forces generated has the form:

$$F_i(x) = \frac{k}{2}(P_{x_{i+1},y_i} + P_{x_{i-1},y_i}) \tag{4.11}$$

$$F_i(y) = \frac{k}{2}(P_{x,y_{i+1}} + P_{x,y_{i-1}}) \tag{4.12}$$

That is, if the pixel in the direction of increasing x is brighter than the pixel in the direction of decreasing x, then the control point is pulled in the positive x direction and likewise for y.

ALGORITHM: MAMMOGRAM ROI SEGMENTATION

Input: *Mammogram Image*

Output: *Segmented Region of Interest*

Method:

Step 1*: Remove black background from mammogram images*

a) *Scan from first position of image and identify the first non zero pixel along row.*
b) *Do the above process until a straight line is identified.*
c) *Move towards right and identify first zero pixel along rows.*
d) *Repeat step c and define a rectangle covering the entire breast region.*

Step2*: Remove pectoral muscle*

a) *Scan from (0,0)th position and find the first black pixel.*
b) *Draw a straight line from the above identified pixel to the centre of breast image. Define a rectangle through these points*
c) *Apply canny edge detection over the rectangle region*
d) *Using the above formed straight line, identify a triangular portion corresponding to pectoral muscle*

Step3*: Use active contours to extract the breast region*

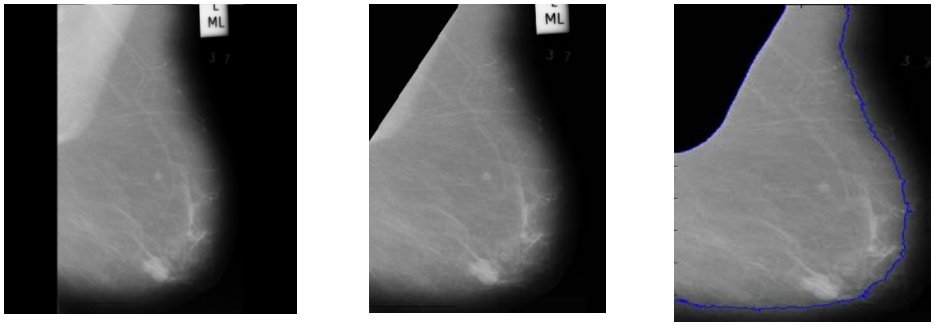

Original image | Pectoral muscle removed | Breast boundary

Figure 4.8 Result of preprocessing - Digital mammogram

So far we have seen the database description and preprocessing of digital mammogram. In the next section description of placental images and its preprocessing techniques are given.

4.4 Placental Sonograms - Database Description

The ultrasound examination was carried out using Sonoline G50 ultrasound system with frequency ranging from 3.5 to 5 MHz. Machine settings were optimized to ensure that images with uniform visibility and uniform echo texture are obtained. The assessment of placenta and grading were done transabdominally by an experienced radiologist. The gestational age of subject under examination varies from 6 to 40 weeks. A total of 530 images are used in this study. Out of this 530 images, 150 images fall into grade 0, 190 into grade 1, 130 into grade2 and 60 into grade3. Fig. 4.9 shows the distribution of different classes in placental images. Fig. 4.10 shows sample sonogram images of placenta. The main challenges in data collection are difficulty in segmentation due to the similarity of placental tissue with its surroundings, biovariability and similarity of subject's texture, variability in ultrasound examination with probe and tissue parenchyma.

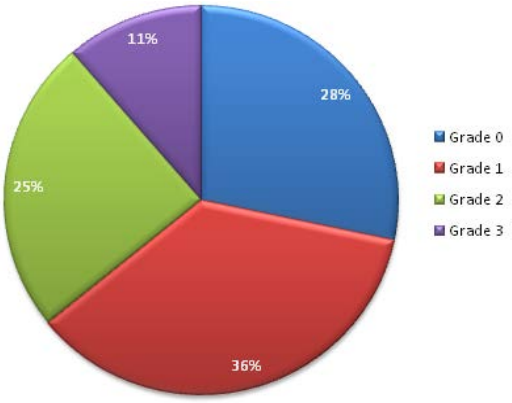

Figure 4.9 Distribution of different classes in placental sonograms

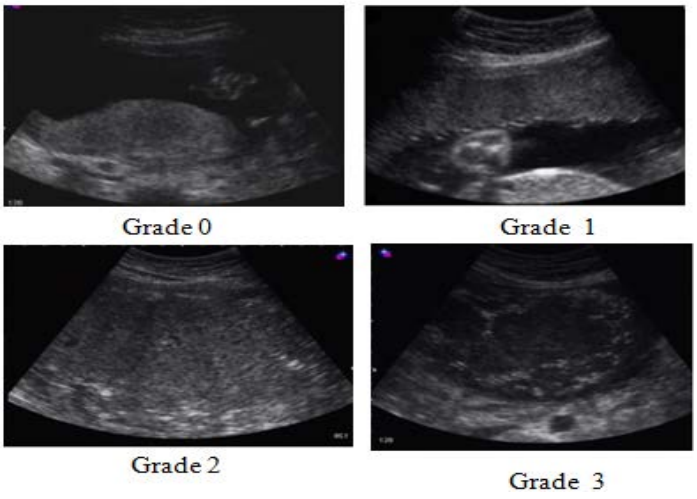

Figure 4.10 Sample images of placental sonograms

4.5 Preprocessing of Placental Sonogram

Ultrasound imaging is an important tool in many clinical diagnoses. The quality of ultrasound images is often degraded with speckle noise. Preprocessing is carried out to improve the quality of images by altering the raw image. It can increase the contrast between background and foreground region along with removing insignificant regions thereby emphasizing the desired part. Fig.4.11 shows the different steps in preprocessing of placental images.

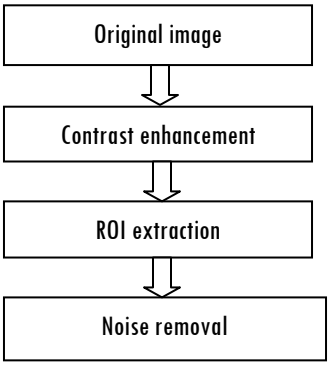

Figure 4.11 Steps in Preprocessing - Placental sonograms

4.5.1 Contrast enhancement

Contrast Limited Adaptive Histogram Equalization is applied to improve the contrast of the placenta images. Theoretical background is given in section 4.3.2.

4.5.2 ROI extraction

Automated extraction of region of interest is difficult because in some cases the regions are not uniform and homogeneous with respect to texture characteristics. The similarity between adjacent regions also causes difficulty in segmentation. The boundaries are not simple or accurate. Ultrasound images are having echo structures, which are formed as a result of different transmission speed of sound waves. In order to extract the object of interest, seed points are selected manually. Then using interpolation, region of interest is extracted. Fig 4.12 shows result of ROI extraction in placental sonograms.

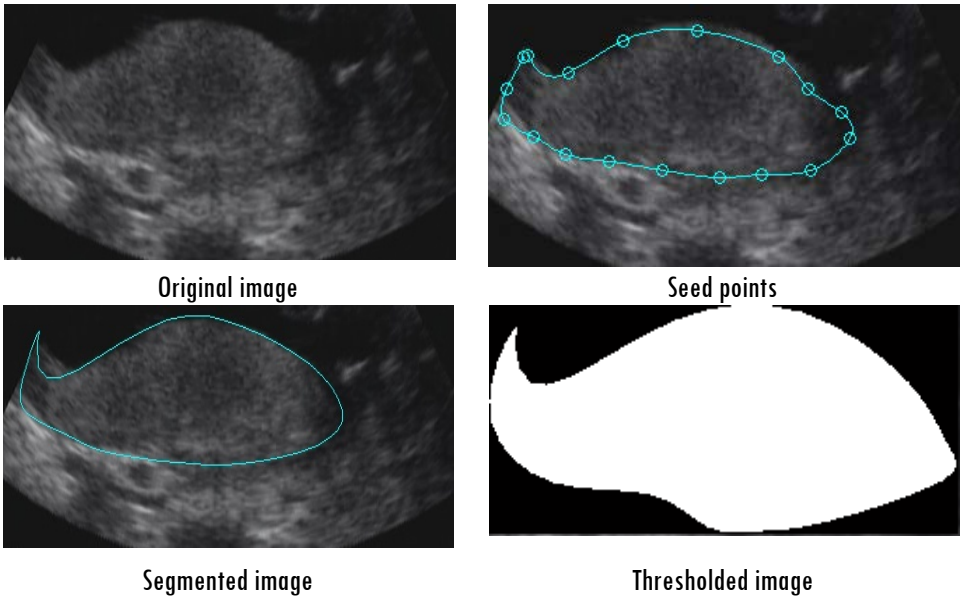

Figure 4.12 ROI extraction - Placental sonograms

4.5.3 Proposed despeckling algorithm

Speckle noise formed as a result of the coherent nature of ultrasound imaging, affects the lesion detectability. Here we are proposing a new weighted linear filtering approach using Local Binary Patterns (LBP) for reducing the speckle noise in ultrasound images. The new filter achieves good results in reducing the noise without affecting the image content.

Ultrasound machine uses high frequency sound waves to capture pictures. Speckle noises are multiplicative in nature that appear as a granular pattern which varies depending upon the type of biological tissue. The interference of backscattered signals results in speckle noise and its apparent resolution is beyond the functionalities of the imaging system. Noise content is usually stronger than the microstructure of tissue parenchyma and reduces the visibility and masks the tissue under investigation. Therefore the main challenge in despeckling is to filter the noise content without affecting the microstructures and edges.

Despeckling can be done in two ways. It can be applied directly on phase of RF signal [342] and it can also be used as post processing techniques applied on images. Different methods like linear and non linear filtering, wavelet based despeckling and the like have been proposed to reduce the noise. Chinrungrueng and Suvichakorn et al. [343, 344] propose edge preserving noise reduction method using two dimensional Savitsky Golay filters which is based on the least square fitting of a polynomial function to image intensities. Though it takes less computation time than median filter, the effect of noise reduction is the same as that of median filter. A modified hybrid median filter and adaptive weighted median filter have been reported in the literature [345, 346]. Sivakumar et al. propose an improved mean filter using fuzzy similarity [347]. A cumulative speckle reduction algorithm for spatial and diffusion filter and the modified anisotropic diffusion filter based on partial differential equation has been developed [348, 349]. Filtering using wavelet transformation, multi scale wavelet domain transformation, wavelet shrinkage, wavelet thresholding and anisotropic diffusion can be found in various studies [350-354]. Another method based on Ricardo reduces the split spectrum processing that occurs as a result of one dimensional narrow band filters [348]. Yang et al. [355] propose an edge preserving denoising method based on bilateral filter and Gaussian scale mixtures in shiftable complex directional pyramid domain. Bhadauria et.al propose an adaptive fusion of curvelet transform and total variation for denoising medical images [356].

Characteristics of speckle noise

Speckle is a form of multiplicative noise that affects the quality of ultrasound images. In ultrasound imaging the tissue under examination is a

sound absorbing medium containing scatters. The inhomogenity of the tissue and the small size of image detail than the wavelength of the ultrasound results in the scattering of signals and lead to the formation of a granular pattern called speckle noise [357]. Multiple examination of the same object under different machine conditions forms identical speckle patterns. Speckle patterns generally change with the change in machine condition. There exists no relation between the speckle and texture pattern which depicts the actual histological structure of object. The output of ultrasound signal can be modelled as,

$$g(x,y) = f(x,y)n(x,y) + \eta(x,y) \tag{4.13}$$

Where $g(x,y)$ is the noisy pixel, $f(x,y)$ is the noise free pixel, $n(x,y)$ and $\eta(x,y)$ represents the multiplicative and additive noise respectively, x and y are the indices of the spatial locations which belong to the 2D space of real numbers. The effect of additive noise is less than that of multiplicative noise, therefore the above equation after logarithmic compression we can write as the sum of noise free pixel and noise component.

$$g(x,y) = f(x,y) + n(x,y) \tag{4.14}$$

Better image quality helps in easy and accurate diagnostic decision making. The widespread use of ultrasound imaging necessitates the need for developing despeckling filters for reducing noise. The performance of the proposed filter is compared with some of the existing filters such as mean filter, median filter, diffusion filter and wiener filter.

Mean Filter

Conventional mean filter replaces the value of every pixel in the image by the mean of the intensity level defined over a neighbourhood [60].

As a result sharp transitions in intensity get reduced. Mean filters fail to preserve edges and small details in an image. The basic linear filtering operation can be represented as,

$$f(x,y) = \bar{g} + w(x,y)(g(x,y) - \bar{g}) \quad (4.15)$$

Where $\bar{g}$ is the local mean value of a region surrounding and including the pixel $g(x,y)$, $w(x,y)$ is the weight with values in the range [0, 1]. The image obtained will be blurred.

Median Filter

Median filter is a non linear order static filter that replaces the middle pixel in the neighbourhood window with the median value [346]. Generally an odd number is chosen as the size of the neighbourhood so that a well defined centre value exists. If the neighbourhood region of a median filter contains an edge, it preserves the edge under the following conditions:- 1: The edge is straight within the neighbourhood region, 2: The signal difference of the two regions on either side of the edge exceeds the noise amplitude, 3: The signal is locally constant within each of the two regions [358]. Its performance is poor when the number of noise pixels is greater than or equal to half the number of pixels in the neighbourhood.

Wiener Filter

Wiener filter is more data driven and relies on the homogeneous appearance of the image. It is developed, based on the assumption that the image properties and the characteristics of noise are same over different regions [359]. This is not true in practical situation. Therefore adaptive wiener filtering has been developed. Wiener filter also uses local statistics in

a moving window. The term $w(x, y)$ in equation 4.15 becomes

$$w(x, y) = (\sigma^2 - \sigma_n^2) / \sigma^2 \qquad (4.16)$$

Where σ^2 and σ_n^2 represent the variance in the moving window and the variance of noise in the image. In frequency domain, wiener filter tends to weaken low energy components which give more information regarding image detail. In the power spectrum, the noise and image content show similar properties [360].

Diffusion Filter

Perona and Malik [361] proposed a PDE (Partial Differential Equation) based speckle noise reduction method using the concept of scale space. In scale space representation the original image is embedded into a family of more simpler and global representation where semantic information can be extracted easily. They tried to reduce the diffusivity of edge like locations in which a transition in intensity level occurs. The diffusion coefficient is adjusted to give more priority to intra-regional smoothing than inter-regional smoothing. Perona Malik diffusion is based on the flowing equation.

$$\partial_t u = div(g(|\nabla_u|^2)\nabla_u \qquad (4.17)$$

The diffusivity $g(s^2) = \dfrac{1}{1 + s^2 / \lambda^2}$ $(\lambda \succ 0)$

The disadvantage of diffusion filtering is the correspondence problem which occurs mainly due to the dislocation of edge from finer to coarser region. Also there exists the chance of losing some relevant information while smoothing.

Proposed Linear Filter Based on Local Binary Pattern

LBP is a grey scale invariant that describes local primitives such as curved edges, points, spot, flat areas and the like [362]. LBP methodology has contributed a vital role in texture analysis. It is extensively used in different computer vision problems such as face recognition, motion analysis, medical image analysis, finger print recognition, palm print recognition, vessel extraction of conjunctiva images and level identification of brain MRI images [363-369]. Over the past ten years different variant to LBP such as uniform patterns, dominant local binary pattern, combination of Gabor and LBP, centre symmetric local binary pattern and the like has been reported in the literature [370-373]. To generate LBP code for a neighbourhood, the weight assigned to each pixel is multiplied with a numerical threshold. The process is repeated for a set of circular samples. Fig. 4.13 shows the process of LBP code generation for a circular neighbourhood.

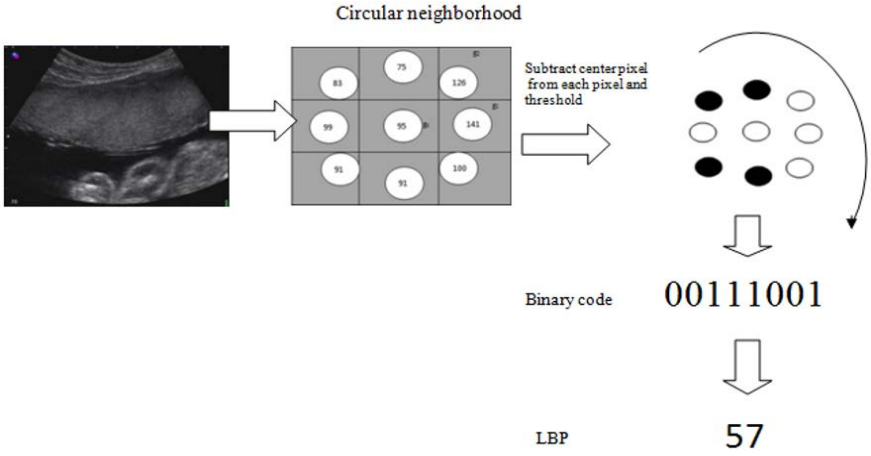

Figure 4.13 LBP calculation

According to Ref. [362], texture T, over a neighbourhood of pixels can be defined as the joint distribution of the grey value of a central pixel of the

neighbourhood, say g_c and grey value of circular pixels of radius R located at distance P.

$$T = t(g_c, g_0, g_{1,}....g_{p-1}) \tag{4.18}$$

The local texture pattern of a neighbourhood can be obtained from the difference of central pixels and each pixel in the neighbourhood. As the differences are independent this joint distribution can be factorized:

$$T \approx t\left(g_c\right)t(g_0 - g_c, ..., g_{p-1} - g_c) \tag{4.19}$$

To make this invariant against all transformations the signs of the difference are also considered and the overall luminance $t(g_c)$ is ignored as it does not contribute anything to texture analysis.

$$T \approx t(s(g_0 - g_c), ...s(g_{p-1} - g_c)) \tag{4.20}$$

$$s\left(x\right) = \begin{cases} 1x \geq 0 \\ 0x < 0 \end{cases}$$

By assigning weight, this difference is converted to a Local Binary Pattern Code which is equivalent to the local texture. The following expression will generate 2^p LBP values for a neighbourhood of pixels located at distance P .

$$LBP_{P,R}(x_c, y_c) = \sum_{p=0}^{P-1} s(g_p - g_c)2^p \tag{4.21}$$

Where g_c is the grey value of a central pixel of the neighbourhood. The process is repeated for a set of circular samples. The histogram of the LBP codes is widely used as texture descriptor. To reduce the size of the descriptors only uniform patterns- binary patterns that occurs more frequently than others are considered. These values are normalized and used for the filtering operation. The proposed approach uses the local binary patterns as the coefficient of

filtering. The proposed method follows a weighted linear filtering approach. It replaces the conventional local statistics in weighted linear filtering by local binary pattern approach. This method uses LBP to calculate the weight in the linear filter of the form $f(x,y) = \overline{g} + w(x,y)(g(x,y) - \overline{g})$.

The despeckling algorithm is implemented using Matlab 7 with Windows 7 as operating system. Initially, the well known median filtering has been applied to make the ultrasound image noise free. To the noise free image, speckle noise of zero mean and variance 0.2 are added. Then the original image is reconstructed using despeckling filters. Fig. 4.14 shows the example of a noisy image.

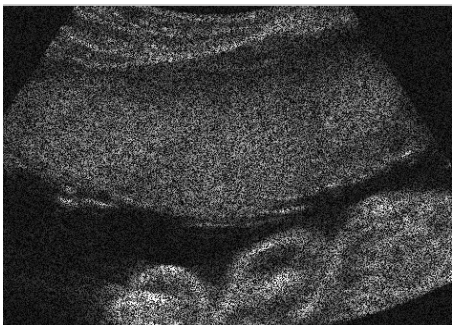

Figure 4.14 Sample noisy ultrasound image

We compare the performance of the proposed method with some of the conventional approaches in speckle reduction: diffusion filtering, mean filtering and wiener filtering. The quantitative measurements used for performance evaluation are Mean Squared Error (MSE), Root Mean Squared Error (RMSE), Signal to Noise Ratio (SNR), Peak Signal to Noise Ratio (PSNR) and Structural Similarity Index (SSIN). The performance of the system is also evaluated using one of the best quantitative measurements - Universal Quality Index (UQI). It models any distortions in image as a combination of loss of correlation, luminance distortion and contrast distortion. The following equations are used for computing these measures [357].

$$MSE = \frac{1}{MN}\sum_{i=1}^{M}\sum_{j=1}^{N}(g(x,y) - f(x,y))^2 \tag{4.22}$$

$$RMSE = \sqrt{\frac{1}{MN}\sum_{i=1}^{M}\sum_{j=1}^{N}(g(x,y) - f(x,y))^2} \tag{4.23}$$

$$SNR = 10\log_{10}\frac{\sum_{i=1}^{M}\sum_{j=1}^{N}(g(x,y)^2 - f(x,y)^2)}{\sum_{i=1}^{M}\sum_{j=1}^{N}(g(x,y) - f(x,y))^2} \tag{4.24}$$

$$PSNR = 10\log_{10}(\frac{g^2_{\max}}{MSE}) \tag{4.25}$$

$$SSIN = \frac{(2\overline{g}\overline{f} + c_1)(2\sigma_{gf} + c_2)}{(\overline{g}^2 + \overline{f}^2 + c_1)(\sigma^2{}_g + \sigma^2{}_f + c_2)}, -1 < SSIN < 1 \tag{4.26}$$

$$UQI = \frac{\sigma_{gf}}{\sigma_f \sigma_g}\frac{2\overline{f}\overline{g}}{(\overline{f})^2 + (\overline{g})^2}\frac{2\sigma_f \sigma_g}{\sigma^2{}_f + \sigma^2{}_g}, -1 < UQI < 1 \tag{4.27}$$

Where $g(x,y)$ is the noisy pixel, $f(x,y)$ is the noise free pixel, $\overline{g}$ and $\overline{f}$ are the local mean value of a region in the noise free and noisy image, c_1 and c_2 represents the dynamic range of ultrasound images ; $\sigma_g \sigma_f$ represents the standard deviations of original and despeckled values of the analysis window and σ_{gf} represents the covariance between original and despeckled windows.

The results in Table 4.1 clearly demonstrate that, the proposed method outperforms the other filters. The edge map of the proposed filter in Fig. 4.15 shows high similarity to edge map of original image than the other filters which indicate the superior performance of the proposed method in edge preservation. Fig. 4.16 shows the horizontal intensity profile of a scan line passing through the centre of the original image and despeckled image using different filters such as diffusion, mean, wiener and proposed LBP filter. We

can observe a close similarity between the intensity profile of the proposed LBP method and that of original image. The proposed method is also tested with ultrasound kidney images collected from ultrasound-images.com. The quantitative results are shown in Table 4.2.

Table 4.1 MSE, RMSE, SNR, PSNR, SSIN, UQI values obtained for various filters on sonogram images

Grade 0 Placenta						
	MSE	**RMSE**	**SNR**	**PSNR**	**SSIN**	**UQI**
diffusion filter	30.0673	5.4834	24.4235	35.1172	0.8126	0.4227
mean filter	30.2667	5.5015	24.3765	35.0885	0.8291	0.5468
wiener filter	19.7550	4.4447	26.2505	36.9414	0.8677	0.6335
proposed filter	11.1425	3.3380	28.7395	39.4283	0.9329	0.7991
Grade 1 Placenta						
	MSE	**RMSE**	**SNR**	**PSNR**	**SSIN**	**UQI**
diffusion filter	23.4549	4.8430	4.8430	35.7524	0.8602	0.4019
mean filter	25.9858	5.0976	25.4537	35.3073	0.8736	0.5741
wiener filter	13.0994	3.6193	28.4503	38.2822	0.9167	0.6502
proposed filter	7.8416	2.8003	30.6802	40.5106	0.9561	0.7668
Grade 2 Placenta						
	MSE	**RMSE**	**SNR**	**PSNR**	**SSIN**	**UQI**
diffusion filter	42.6805	6.5330	22.1915	32.5531	0.7860	0.4586
mean filter	63.3604	7.9599	20.4313	30.8372	0.7494	0.4717
wiener filter	36.9114	6.0755	22.8177	33.1838	0.8152	0.5792
proposed filter	19.1188	4.3725	25.6826	36.0408	0.9195	0.8236
Grade 3 Placenta						
	MSE	**RMSE**	**SNR**	**PSNR**	**SSIN**	**UQI**
diffusion filter	20.3646	4.5127	22.8805	35.4047	0.8757	0.4078
mean filter	20.9073	4.5724	22.7414	35.2905	0.8895	0.5346
wiener filter	10.8094	3.2878	25.6424	38.1555	0.9266	0.6403
proposed filter	5.5919	2.3647	28.5127	41.0179	0.9671	0.8464

Table 4.2 MSE, RMSE, SNR, PSNR, SSIN, UQI values obtained for various filters on ultrasound kidney images

	MSE	**RMSE**	**SNR**	**PSNR**	**SSIN**	**UQI**
diffusion filter	42.2944	6.5034	21.553	34.8783	0.8106	0.5223
mean filter	72.9593	8.5416	19.1161	32.5103	0.7715	0.6543
wiener filter	41.8041	6.4656	21.5932	34.9289	0.8283	0.7313
proposed filter	21.2596	4.6108	24.5443	37.8655	0.9351	0.8975

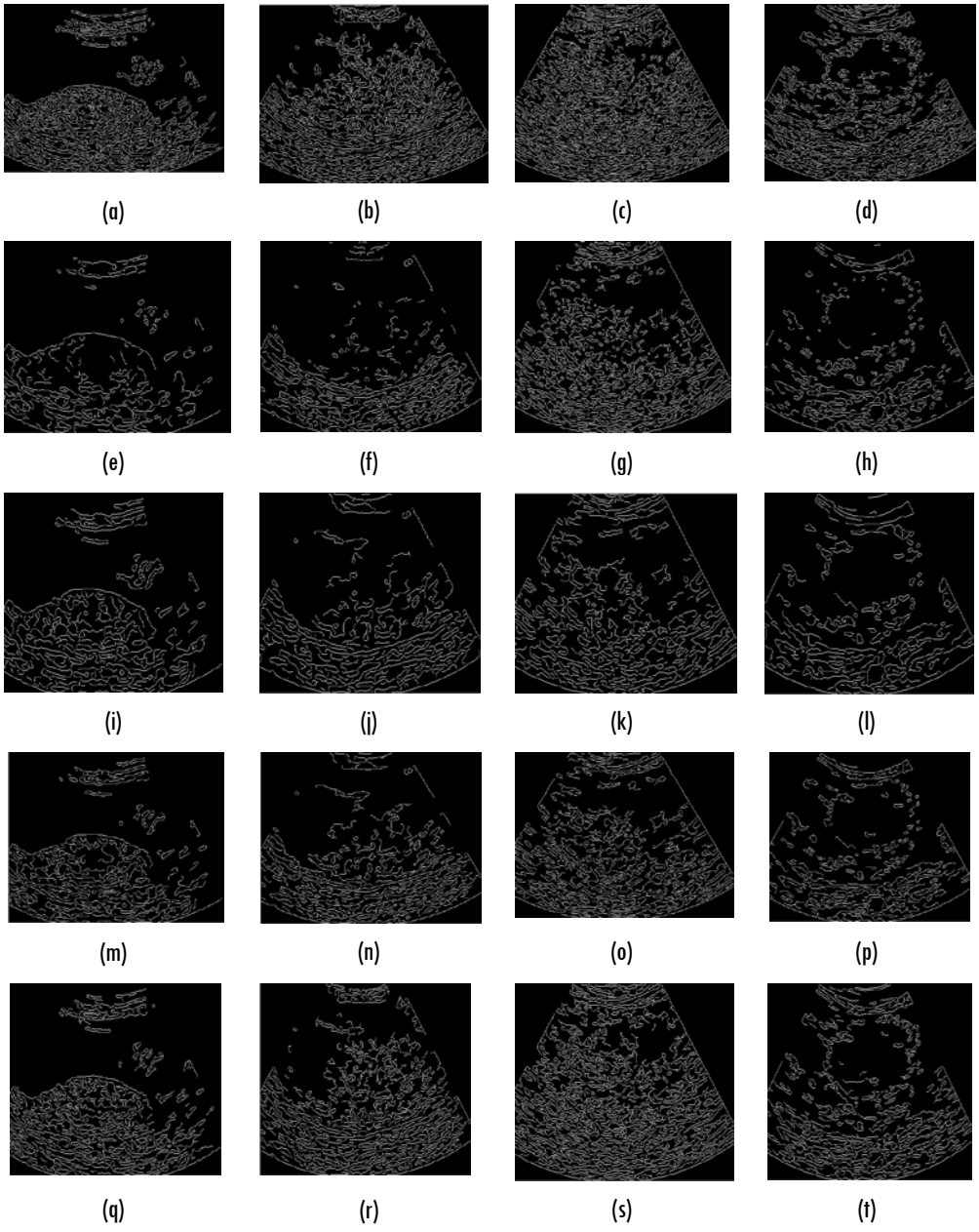

Figure 4.15 (a-d) Edge maps of noise free placental images - grade 0 to grade 3, (e-h) edge maps of despeckled placenta images using diffusion filter , (i-l)) edge maps of despeckled placenta images using mean filter, m-p)) edge maps of despeckled placenta images using wiener filter, (q-t)) edge maps of despeckled placenta images using proposed LBP filter

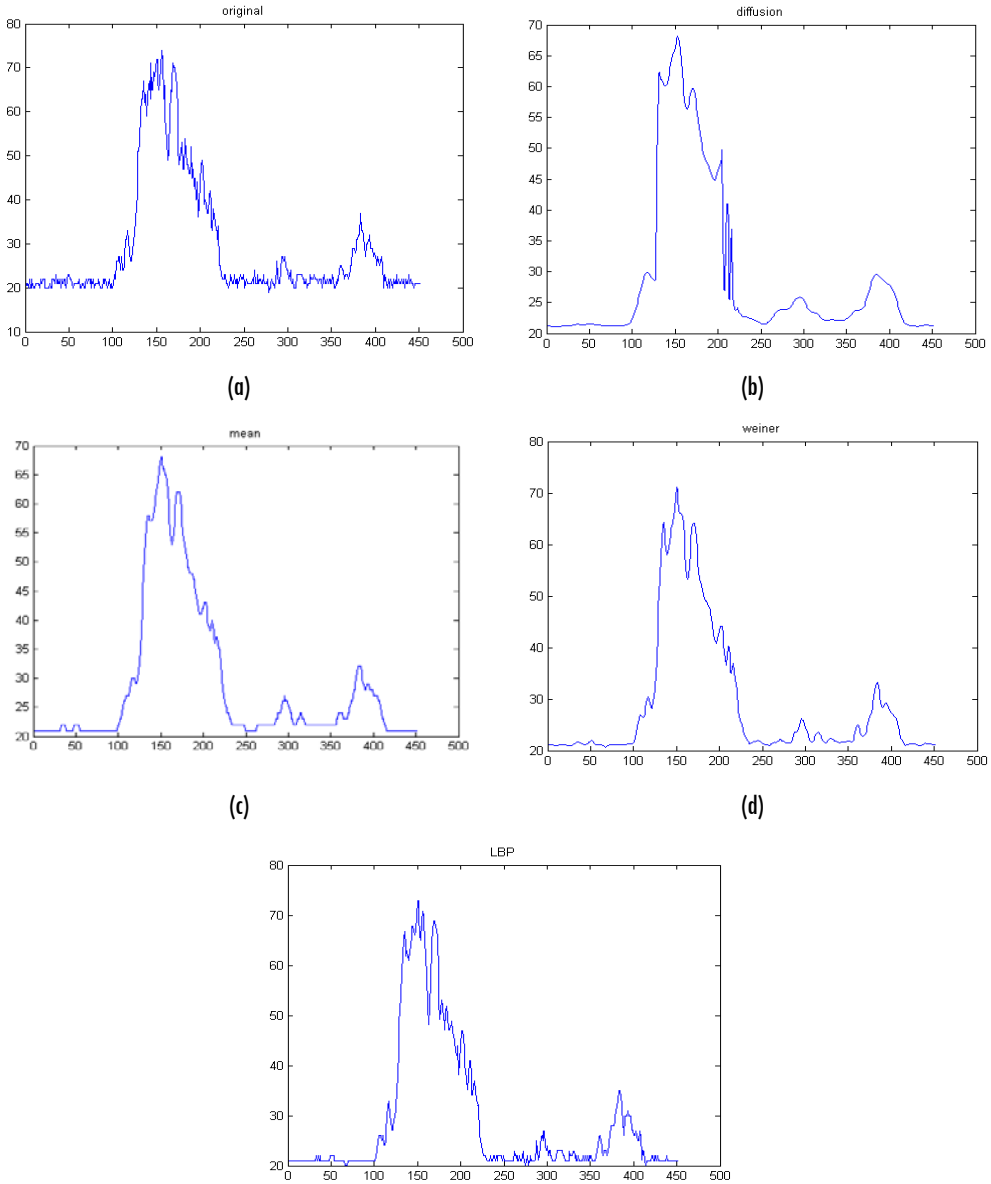

Figure 4.16 Intensity profile of a scan line through the centre of the image- grade 1.(a) original image, (b-e) despeckled image using diffusion filter, mean filter, wiener filter and proposed LBP filter.

ALGORITHM: PREPROCESSING OF PLACENTAL SONOGRAM

Input: *Original Placenta image*

Output: *Preprocessed image*

Method:

Step 1*: Apply Contrast Limited Adaptive Histogram Equalization to improve the contrast of the placental images.*

Step 2*: Extract the region of interest by manually selecting the seed points and interpolating them.*

Step 3*: Remove noises using linear filter based on Local Binary Patterns.*

The first part of this chapter describes databases used in this work and their preprocessing. In the next section the mathematical background of different feature extraction techniques used are given.

4.6 Feature Extraction Techniques

A feature of a given parameter set refers to an attribute described by one or more elements of the original pattern vector. The features of digital images can be extracted either from the spatial domain or from the frequency domain. In spatial domain, features are extracted directly from the pixels whereas in frequency domain, image is transformed into its frequency representation. Feature extraction is an important step in CAD. This step helps to improve the performance of the CAD scheme, because the extracted features in effect describes the specific properties or characteristics of object of interests [26]. The choice of appropriate features depends on the particular image and the application at hand. However they should be [27]

- Robust :- Features should be invariant to translation, orientation, scale and illumination and partially invariant to noises and artifacts.

- ❖ Discriminating :- the range of values for objects in different classes should be dissimilar and if possible, be well separated and non overlapping.
- ❖ Reliable :- All objects of the same class must have similar values.
- ❖ Independent :- Features should be uncorrelated.

Texture Analysis

Textures are repetitive patterns with varying intensity [17]. It defines the basic units of image. The qualitative descriptions that are used for representing textures are: coarseness, homogeneity, orientation, spatial relationship between pixel values and the like. According to Amadasun, texture can be defined as the spatial interrelationships and arrangements of the fundamental elements of an image [374]. Visually these spatial relationship and arrangements of the image pixels appear as variations in the intensity patterns or grey tones. Therefore texture features have to be derived from the grey tones of the image. Thus, texture cannot be defined for a point. The resolution at which an image is captured determines the scale at which the texture is perceived. Human beings can easily recognize texture patterns, but for digital computers it is difficult to interpret [26]. The three different approaches in texture analysis are statistical, structural and spectral [60]. In statistical approach texture is characterized as smooth, coarse, grainy patterns, while in structural approach image primitives are used. Spectral techniques are based on Fourier spectrum. Sample texture images are given in Fig.4.17. This study concentrates on the statistical approach of texture analysis.

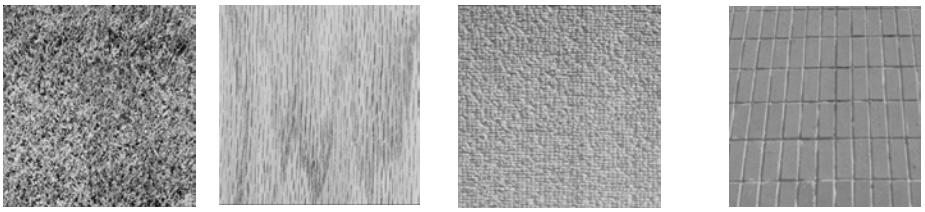

Figure 4.17 Sample texture images

4.6.1 Histogram Statistics

Histogram based approach to texture analysis is based on the intensity value concentrations on all or part of an image represented as a histogram [375]. Let $P(v)$ is the first order histogram estimate of an image; $P(v) = \frac{N(v)}{S}$, Where S is the size of the image and $N(v)$ is the number of pixels of intensity value v in the image [376]. The histogram of intensity levels is thus a concise and simple summary of the statistical information contained in the image. Calculation of the grey-level histogram involves single pixels. The following first order histogram statistics are used in this work.

Histogram Statistics

Mean	$\sum_v vP(v)$	(4.28)
Variance	$\sum_v (v-\bar{v})^2 P(v)$	(4.29)
Skewness	$\frac{1}{\sigma_v^3}\sum_v (v-\bar{v})^3 P(v)$	(4.30)
Kurtosis	$\frac{1}{\sigma_v^4}\sum_v (v-\bar{v})^4 P(v) - 3$	(4.31)
Energy	$\sum_v [P(v)]^2$	(4.32)
Entropy	$-\sum_v P(v)\log_2[P(v)]$	(4.33)

Texture analysis depending on the grey level histogram suffers from the limitation that it provides no information about the relative pixel pairs in the image.

4.6.2 Autocorrelation

In autocorrelation model, a single pixel and its grey level is considered which access the amount of regularity, coarseness of the image texture [377]. Correlation coefficient is used to describe the texture and to evaluate the linear spatial relationship between pixels. Autocorrelation function can be defined as follows:

$$C_{ff}(p,q) = \frac{MN}{(M-p)(N-q)} \frac{\sum_{i=1}^{M-p}\sum_{j=1}^{N-q} f(i,j) f(i+p, j+q)}{\sum_{i=1}^{M}\sum_{j=1}^{N} f^2(i,j)} \tag{4.34}$$

Where p,q are the pixel positions in the i,j direction and M,N are the image dimensions. If the texture primitives are comparatively large, the autocorrelation function value diminishes slowly with increasing distance, while it decreases quickly if texture consists of small primitives. If primitives are placed periodically in a texture, the autocorrelation increases and decreases periodically with distance.

4.6.3 Spatial Grey-Level-Dependence Matrix (SGLDM)

Haralick [378] proposes Grey Level Dependence Matrix (GLDM), which is one of the widely accepted texture feature extraction methods based on second order statistics. Suppose the function, $f(i,j,d,\theta)$ is the probability that two pixels (k,l) and (m,n), with distance d in the direction specified by the angle θ, have intensities of grey level i and grey level j. The

estimated values for this probability density functions will be denoted by $P(i, j, d, \theta)$. GLDM characterizes how often pairs of pixels with specific values and in a specified spatial relationship occur in an image. The following Haralick features which are having high discriminating powers, are extracted from the GLDM.

Notations:

$p(i, j)$ is the $(i, j)^{th}$ entry in the normalized spatial grey level dependence matrix.

$P(i, j) = P(i, j)\big|R$ Where R is a normalizing constant.

$p_x(i)$ is the i^{th} entry in the marginal probability matrix obtained by summing the rows of $p(i, j) = \sum_{j=1}^{N_g} p(i, j)$

N_g - Number of distinct grey levels in the quantized image

$\sum_i$ means $\sum_{i=1}^{N_g}$ and $\sum_j$ means $\sum_{j=1}^{Ng}$

SGLDM Features

Angular Second Moment $$\sum_i \sum_j \{p(i, j)\}^2 \quad (4.35)$$

Contrast $$\sum_{i=1}^{N_g - 1} n^2 \left\{ \sum_{\substack{i=1 \\ |i-j|=n}}^{N_g} \sum_{j=1}^{N_g} p(i, j) \right\} \quad (4.36)$$

Correlation $$\frac{\sum_i \sum_j (i, j)\, p(i, j) - \mu_x \mu_y}{\sigma_x \sigma_y} \quad (4.37)$$

Variance $$\sum_i \sum_j (i - \mu)^2 p(i, j) \quad (4.38)$$

Inverse difference Moment	$\sum_i \sum_j \frac{1}{1+(i-j)^2} p(i,j)$	(4.39)
Entropy	$-\sum_i \sum_j p(i,j) \log(p(i,j))$	(4.40)

4.6.4 Grey Level Difference Statistics (GLDS)

The **Grey Level Difference Statistics (GLDS)-** [117] uses absolute differences between pairs of grey level or average grey level to extract local statistics. Let $I(x,y)$ be the image intensity function, and for any given displacement $\delta \equiv (\Delta_x, \Delta_y)$, let $I_\delta(x,y) = \left| I(x,y) - I(x+\Delta x, y+\Delta y) \right|$. Let p_δ be the probability density of $I_\delta(x,y)$. For m grey levels, this has the form of an m-dimensional vector whose i^{th} component is the probability that $I_\delta(x,y)$ will have the value i. The probability density p_δ can be easily computed by counting the number of times each value of $I_\delta(x,y)$ occurs, where Δ_x and Δ_y are integers.

The following measures of the spread of values in p_δ away from the origin with different magnitude of δ are calculated to analyse texture coarseness. Features were calculated for $\delta = (0,1),(1,1),(1,0),(1,-1)$, and their mean values are taken.

GLDS Features

Contrast	$CON = \sum_i i^2 p_\delta(i)$	(4.41)
Angular Second Moment	$ASM = \sum_i p_\delta(i)^2$	(4.42)
Entropy	$ENT = -\sum_i p_\delta(i) \log(p_\delta(i))$	(4.43)
Mean	$MEAN = (1/m) \sum_i i p_\delta(i)$	(4.44)

4.6.5 Neighbourhood Grey-Tone-Difference Matrix (NGTDM)

NGTDM is proposed by Amadasun and King [374]. Let $f(k,l)$ be the grey tone of a pixel at (k,l) having grey tone value i. The average grey tone over a neighbourhood centred at, but excluding , (k,l) is

$$\bar{A}_i = \bar{A}(k,l) = \frac{1}{W-1}\left[\sum_{m=-d}^{d}\sum_{n=-d}^{d} f(k+m,l+n)\right] \tag{4.45}$$

Where $(m,n) \neq (0,0), d$ specifies the neighbourhood size, and $W = (2d+1)^2$. Then the i^{th} entry in the NGTDM is

$$s(i) = \sum \left| i - \bar{A}_i \right| \text{ for } i \in N_i \text{ if } N_i \neq 0 = 0 \text{ if } N_{i=0} \tag{4.46}$$

Where $\{N_i\}$ is the set of all pixels having grey tone i.

NGTDM Features

Coarseness
$$f_{\cos} = \left[\varepsilon + \sum_{i=0}^{G_h} p_i s(i)\right]^{-1} \tag{4.47}$$

Contrast
$$f_{con} = \left[\frac{1}{N_g(N_g-1)}\sum_{i=0}^{G_h}\sum_{j=0}^{G_h} p_i p_j (i-j)^2\right]\left[\frac{1}{n^2}\sum_{i=0}^{G_h} s(i)\right] \tag{4.48}$$

Busyness
$$f_{bus} = \sum_{i=0}^{G_h} p_i s(i) \Big/ \sum_{i=0}^{G_h}\sum_{j=0}^{G_h} i p_i - j p_j,\ p_i \neq 0,\ p_j \neq 0 \tag{4.49}$$

Complexity
$$f_{com} = \sum_{i=0}^{G_h}\sum_{j=0}^{G_h} \left\{ \left(|i-j|\right) / \left(n^2 (p_i + p_j)\right)\right\}\left\{ p_i s(i) + p_j s(j)\right\},\ p_i \neq 0,\ p_j \neq 0 \tag{4.50}$$

Strength
$$f_{str} = \left[\sum_{i=0}^{G_h}\sum_{j=0}^{G_h} (p_i + p_j)(i-j)^2\right]\left[\varepsilon + \sum_{i=0}^{G_h} s(i)\right],\ p_i \neq 0,\ p_j \neq 0 \tag{4.51}$$

Where G_h is the highest grey tone value present in the image, ε is a small number to prevent $f_{\cos}$ from becoming infinite. For an $N \times N$ image, p_i is the

probability of occurrence of grey-tone value i and is given by $p_i = N_i / n^2$, $n = N - 2d$, N_g is the total number different grey levels present in the image.

4.6.6 Statistical Feature Matrix (SFM)

The **statistical feature matrix** [379] measures the statistical properties of pixel pairs at several distance within an image. Let $I(x, y)$ be the intensity at point (x, y) and let $\delta = (\Delta x, \Delta y)$ represent the inter-sample spacing distance vector, where Δx and Δy are integers. The δ contrast, δ covariance, and δ dissimilarity are defined as

$$CON(\delta) = E\left\{\left[I(x, y) - I(x + \Delta x, y + \Delta y)\right]^2\right\} \quad (4.52)$$

$$COV(\delta) = E\left\{\left[I(x, y) - \eta\right]\left[I(x + \Delta x, y + \Delta y) - \eta\right]\right\} \quad (4.53)$$

$$DSS(\delta) = E\left\{\left[I(x, y) - I(x + \Delta x, y + \Delta y)\right]\right\} \quad (4.54)$$

Where $E\{\ \}$ denotes the expectation operation, and η is the average grey level of the image.

A statistical-feature matrix (SFM), M_{sf}, is an $(L_r + 1) \times (2L_c + 1)$ matrix whose (i, j) element is the d statistical feature of the image, where $d = (j - L_c, i)$ is an inter sample spacing distance vector for $i = 0,1,..., L_r$, $j = 0,1,..., L_c$ and where L_r, L_c are the constants that determine the maximum inter sampling spacing distance. In a similar way, the contrast matrix (M_{con}), covariance matrix (M_{cov}) and dissimilarity matrix (M_{dss}) can be defined as the matrices whose (i, j) elements are the d contrast, d covariance and d dissimilarity, respectively. Based on the SFM, the following texture features can be computed:

SFM Features		**SFM**
Coarseness	$F_{CRC} = c / \sum_{(i,j)\in N_r} DSS(i,j) / n$	(4.55)
Contrast	$F_{CON} = \left[\sum_{(i,j)\in N_r} CON(i,j) / 4 \right]^{\frac{1}{2}}$	(4.56)
Periodicity	$F_{PER} = \frac{\bar{M}_{dss} - M_{dss}(valley)}{\bar{M}_{dss}}$	(4.57)
Roughness	$F_{RGH} = (D_f^{(h)} + D_f^{(v)}) / 2$	(4.58)

Where c is a normalizing factor, N_r is the set of displacement vectors defined as $N_r = \{(i,j) : |i|, |j| \le r\}$, n is the number of elements in the set, $\bar{M}_{dss}$ is the mean of all elements in M_{dss}, $M_{dss}(valley)$ is the deepest valley in the matrix, D_f is the fractal dimension in horizontal and vertical directions.

4.6.7 Local Binary Patterns

The method of calculation of LBP for a circular neighbourhood of pixels is explained in 4.5.3. After calculating the LBP codes for the entire image its histogram is used as the texture descriptor.

4.6.8 Wavelet energy descriptors

Two dimensional wavelet transform requires a two dimensional scaling function, $\varphi(x,y)$, and three two dimensional wavelets ; $\psi^H(x,y)$, $\psi^V(x,y)$ and $\psi^D(x,y)$, the products of two one dimensional functions [60]. The scaling function is separable whereas the wavelets are separable and directionally sensitive. It can be represented as follows

$$\varphi(x,y) = \varphi(x)\varphi(y)$$
$$\psi^H(x,y) = \psi(x)\varphi(y)$$
$$\psi^V(x,y) = \varphi(x)\psi(y)$$
$$\psi^D(x,y) = \psi(x)\psi(y)$$

These wavelets measure functional variations-intensity variations for images-along different directions: ψ^H measures variations along columns like horizontal edges, ψ^V response to variations along rows like vertical edges, and ψ^D corresponds to variations along diagonals.

The scaled and translated basis functions can be defined as:

$$\varphi_{j,m,n}(x,y) = 2^{j/2}\varphi(2^j x - m, 2^j y - n) \tag{4.59}$$

$$\psi^i{}_{j,m,n}(x,y) = 2^{j/2}\psi^i(2^j x - m, 2^j y - n), i = \{H,V,D\} \tag{4.60}$$

Where the index i identifies the directional wavelets that assumes the values H,V and D. The discrete wavelet transform of image $f(x,y)$ of size $M \times N$ is

$$W_\varphi(j_0,m,n) = \frac{1}{\sqrt{MN}}\sum_{x=0}^{M-1}\sum_{y=0}^{N-1} f(x,y)\varphi_{j_0,m,n}(x,y) \tag{4.61}$$

$$W_\psi{}^i(j,m,n) = \frac{1}{\sqrt{MN}}\sum_{x=0}^{M-1}\sum_{y=0}^{N-1} f(x,y)\psi^i{}_{j,m,n}(x,y), i = \{H,V,D\} \tag{4.62}$$

Where j_0 is an arbitrary starting scale and the $W_\varphi(j_0,m,n)$ coefficients define an approximation of $f(x,y)$ at scale j_0. The $W_\psi{}^i(j,m,n)$ coefficients add horizontal , vertical and diagonal details of scales $j \geq j_0$. We normally let $j_0 = 0$ and select $N = M = 2^J$ so that $j = 0,1,...,J-1$ and $m = n = 0,1,...,2^j - 1$. Using $W\varphi$ and $W_\psi{}^i$ and $f(x,y)$ can be obtained via the inverse discrete wavelet transform.

For implementing 2D - Discrete Wavelet Transform (DWT) digital filters and down samplers are used. With separable two dimensional scaling and wavelet functions, we take the 1D Fast Wavelet Transform (FWT) of the

rows of $f(x, y)$, followed by the 1D FWT of the resulting columns. Fig. 4.18 shows the process in block diagram form. The 2D FWT "filters" the scale $j+1$ approximation coefficients to construct the scale j approximation and detail coefficients. In the two dimensional case, however, we get three sets of detail coefficients- the horizontal, vertical and diagonal details.

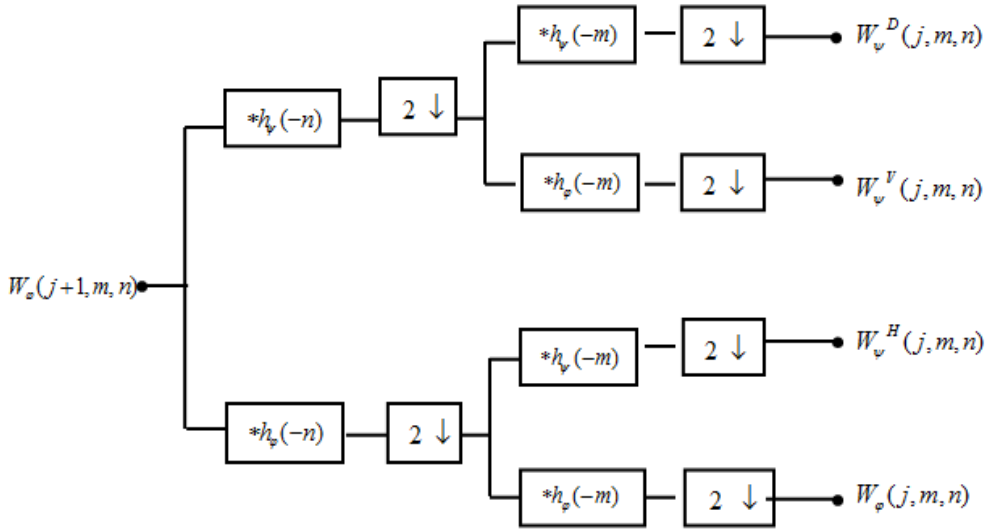

Figure 4.18 Analysis of filter bank in wavelet decomposition

The single scale filter bank of Fig. 4.18 can be "iterated" to produce a P scale transform in which scale $j = J-1, J-2, ..., J-P$. Here, image $f(x, y)$ is used as the $W_\varphi(J, m, n)$ input. Convolving its rows with $h_\varphi(-n)$ and $h_\psi(-n)$ and down sampling its columns we get two subimages whose horizontal resolutions are reduced by a factor of 2. The high pass or detail component characterizes the image's high frequency information with vertical orientation. The low pass, approximation component contains its low frequency, vertical information. Both subimages are then filtered column

wise and downsampled to yield four quarter size output subimages $W_{\varphi}, W_{\psi}^{H}, W_{\psi}^{V}$ and W_{ψ}^{D}. These subimages are the inner products of $f(x,y)$ and the two dimensional scaling and wavelet functions in equation, followed by downsampling by 2 in each dimension. Two iterations of the filtering process produce the two scale decomposition.

An image is decomposed into orthogonal sub-bands with low–low (LL), low–high (LH), high–low (HL), and high–high (HH) components which correspond to approximation, horizontal, vertical and diagonal coefficients respectively. The second level decomposition is performed at the LL band. This study follows a 2 level decomposition in which the image is divided into 7 sub bands as shown in Fig. 4. 19.

Features:

- Percentage of Energy corresponding to level 2 approximation coefficient.
- Percentage of Energy corresponding to sum of detail coefficient of level 1 & 2.

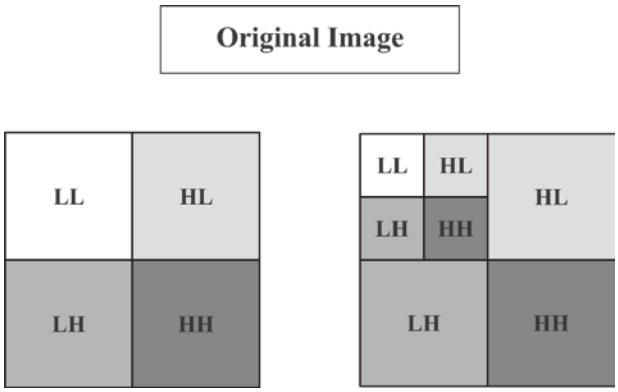

Figure 4.19 Wavelet decomposition

4.6.9 Shape Features

4.6.9.1 Invariant moments

The two dimensional moments of order $(p+q)$ of an image $f(x,y)$ are defined as [380]

$$\mu_{pq}=\int\int x^p y^q f(x,y)d_x d_y \tag{4.64}$$

$p,q=0,1,2,...,$ .These are not invariant to any distortion, therefore the central moments are defined as

$$\mu_{pq}=\int\int (x-x')^p (y-y')^q f(x,y)d(x-x')d(y-y') \tag{4.65}$$

$$x'=\frac{m_{10}}{m_{00}} \text{ and } y'=\frac{m_{01}}{m_{00}}$$

The normalized central moments are

$$\eta_{pq}=\frac{\mu_{pq}}{\mu_{00}^{\ r}}$$

Where $r=1+\frac{p+q}{2}$ for $(p+q)=2,3,...$

The following are the Hu [380] invariant moments

$$\varphi_1=\eta_{20}+\eta_{02} \tag{4.66}$$

$$\varphi_2=(\eta_{20}-\eta_{02})^2+4\eta_{11}^2 \tag{4.67}$$

$$\varphi_3=(\eta_{30}-3\eta_{12})^2+(3\eta_{21}-\eta_{03})^2 \tag{4.68}$$

$$\varphi_4=(\eta_{30}-\eta_{12})^2+(\eta_{21}-\eta_{03})^2 \tag{4.69}$$

$$\varphi_5=(\eta_{30}-3\eta_{12})(\eta_{30}+\eta_{12})^2\left[(\eta_{30}-\eta_{12})^2-3(\eta_{21}+\eta_{03})^2\right]+(3\eta_{21}-\eta_{03})(\eta_{21}+\eta_{03})\left[3(\eta_{30}+\eta_{12})^2-(\eta_{21}+\eta_{03})^2\right] \tag{4.70}$$

$$\varphi_6 = (\eta_{20} - \eta_{02})(\eta_{30} + \eta_{12})^2 - (\eta_{21} - \eta_{03})^2 + 4\eta_{11}(\eta_{30} + \eta_{12})(\eta_{21} + \eta_{03}) \quad (4.71)$$

$$\varphi_7 = (3\eta_{21} - \eta_{03})(\eta_{30} + \eta_{12})\left[(\eta_{30} - \eta_{12})^2 - 3(\eta_{21} + \eta_{03})^2\right] - 3\eta_{12})(\eta_{21} + \eta_{03})\left[3(\eta_{30} + \eta_{12})^2 - (\eta_{21} + \eta_{03})^2\right] \quad (4.72)$$

4.6.9.2 Regional descriptors

Various features are used for describing image regions. The *Area* of a region is the number of pixels in the region, P*erimeter* is the number of pixels in the boundary of the object, *Compactness* express the extent to which a shape can be considered as a circle. *Circularity* gives the area to perimeter ratio, it is a measure of roundness. The lengthiness of ROI is named as *Eccentricity* [381].

4.7 Chapter Summary

The use of appropriate preprocessing operations helps to remove the unwanted information from the images, enhances the contrast of the images and extracts the region of interest. A major contribution in this direction is the development of a new filter for removing the speckle noise in ultrasound images. The proposed linear filter is based on Local Binary Patterns (LBP), which follows a weighted linear filtering approach. The statistical features extracted are capable of capturing the essential differences between objects or classes of objects. The conceptual boundary between feature extraction and classification is somewhat arbitrary. A perfect feature extractor would yield a representation that makes the job of the classifier trivial.

Chapter 5

CLASSIFICATION USING SUPERVISED LEARNING ALGORITHMS

5.1. Introduction

Last several years witnessed immense growth in Machine Learning techniques that are capable to stir up knowledge from raw data by design, development and implementation of various learning algorithms [382]. Machine learning has a wide spectrum of applications including natural language processing, medical diagnosis, bio-informatics, speech recognition, character recognition, object recognition and the like. Machine learning framework consists of a learning system, concept examples and background knowledge. The learning system learns description of a given concept from examples and background knowledge, the process is explained in Fig.5.1. Major types of learning systems are supervised learning, unsupervised learning and reinforcement learning [383]. In supervised learning, a set of objects and their class labels are given, by which the learning system builds a mapping between objects and classes which can be used for classifying new objects. In this case, labelling or categorization of the initial set of objects is done by an agent external to the system. Unsupervised learning automatically discovers hidden patterns in data where labelled objects are not used. Reinforcement learning can be placed in between supervised and unsupervised learning schemes, in which information in the form of reinforcement signals are provided.

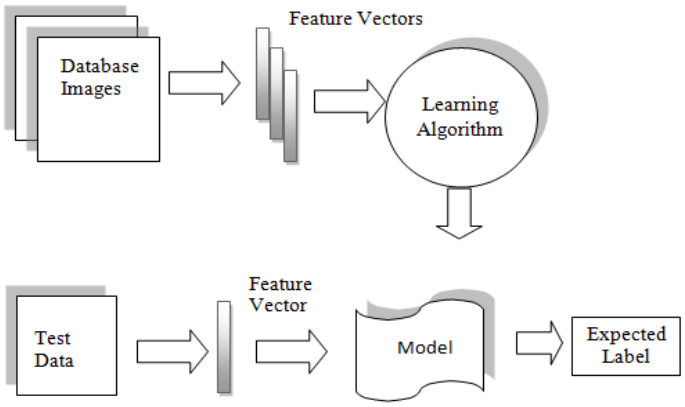

Figure 5.1 Learning system model

Classification is a kind of supervised learning, which assigns data items to target classes [384]. The design of a classifier depends on the nature of data, its distribution, number of classes, learning algorithms and validation procedures. In learning process the entire data set is grouped into training set and test set. Using the training data set, the classifier builds a model capable of generalizing new test cases.

In this study we have used different classifiers such as Multilayer Perceptrons (MLP), decision trees, Support Vector Machines (SVM), Extreme Learning Machines (ELM) and ensembles of classifiers as shown in Fig.5.2 for the classification of digital mammograms and placental sonograms. We propose a novel approach by using a combination of different statistical texture features for the classification of mammogram images. A new approach based on Extreme Learning Machines and ensemble classifiers for the classification of placental sonograms is also proposed. The proposed approach to use a combination of shape and hybrid texture features is a novelty. Performance is evaluated using different statistical measures.

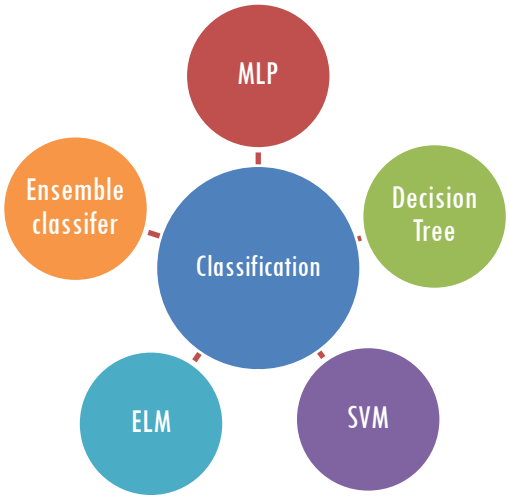

Figure 5.2 List of classifiers used in the proposed work

5.2 Neural Network Classification

The pioneers in neural network research are Warren McCulloch, a neuro-physiologist, and the Mathematical prodigy Walter Pitts [385]. They have developed the theory of formal neural networks in 1943, which is still, used in modern artificial neural network concepts. Using electrical circuits they have modelled the neurons in brain. The first artificial neural network was the perceptron, developed in 1958 [386]. The concept of learning using weight adjustment was introduced in 1962 by Widrow and Hoff [387]. In 1986 Widrow-Hoff rule was extended to networks with multi layer. Neural network has been widely used in many classification problems in recent years [388]. They are best suited and applied in variety of fields such as medical imaging, character recognition, stock market prediction, image compression, process control, quality control and so on .

The simplest architecture of a neural network is given in Fig.5.3. The architecture or topological structure of an ANN is characterized by the

arrangement of different layers, neurons, nodal connectivity and nodal transfer functions. Inputs are fed to the input nodes [384]. The number of input nodes and output nodes depends on the size of feature set. Similar to biological neurons, the weights in artificial neurons are adjusted during training phase. From an optimization point of view, learning in a neural network, is similar to minimizing a global error function, which is a multivariate function [389]. The learning process depends on the weights in the network, which are adjusted to minimize the error function. One of the most popular architectures is multilayer feedforward network with backpropagation learning algorithm [384]. In backpropagation algorithm the weights are adjusted in the steepest descent direction, the direction in which the performance function is decreasing most rapidly. Although the function decreases most rapidly along the negative of the gradient, it does not necessarily produce the fastest convergence. In conjugate gradient algorithms a search is performed along conjugate directions, which produces generally faster convergence than steepest descent directions. Most of the gradient algorithms require line search at each iteration. This line search is computationally expensive, because it requires the network response to all training inputs to be computed several times for each search. The Scaled Conjugate Gradient algorithm (SCG), developed by Moller [389], was designed to avoid the time-consuming line search. Scaled Conjugate Gradient algorithms are all-purpose second order techniques that help to minimize goal functions of several variables. By using a step size scaling mechanism, SCG avoids the time consuming line-search per learning iteration, which makes the algorithm faster than other second order algorithms recently proposed.

Gradient based learning and stochastic learning are the two basic ways to train feed forward networks.

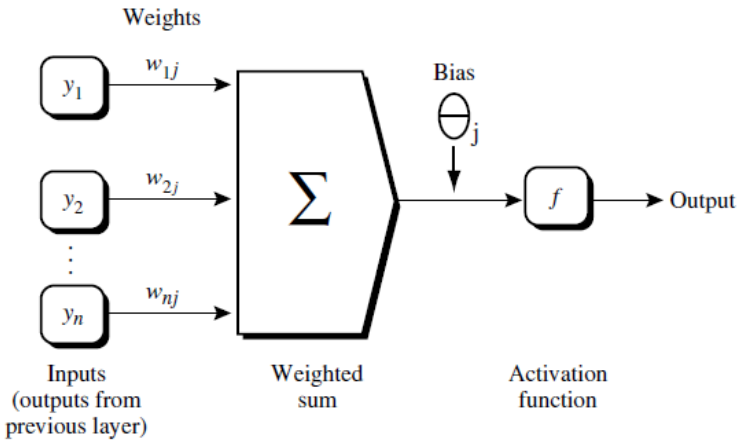

(Source: Data mining: concepts and techniques, Han and Kamber)

Figure 5.3 Architecture of feed forward neural network

ALGORITHM: SCALED CONJUGATE GRADIENT

Input: *Let* w_1 *be the weight vector,* $E(w)$ be the error function

Output: *Trained network*

Method:

Step1: Choose weight vector w1 and scalars $\sigma > 0, \lambda_1 > 0$ *and* $\bar{\lambda}_1 = 0$.

Set $p_1 = r_1 = -E'(w_1), k = 1$ *and success=true.*

Step 2: If success=true then calculate second order information :

$$\sigma_k = \frac{\sigma}{|p_k|},$$

$$s_k = \frac{E'(w_k + \sigma_k p_k) - E'(w_k)}{\sigma_k},$$

$$\delta_k = p_k^T s_k.$$

Step 3: Scale s_k :

$$s_k = s_k + (\lambda_k - \bar{\lambda}_k) p_k$$

$$\delta_k = \delta_k + (\lambda_k - \bar{\lambda}_k) |p_k|^2 .$$

Step 4: If $\delta_k \le 0$ *then make the Hessian matrix positive definite.*

$$s_k = s_k + (\lambda_k - 2\frac{\delta_k}{|p_k|^2}) p_k$$

$$\bar{\lambda}_k = 2(\lambda_k - \frac{\delta_k}{|p_k|^2}),$$

$$\delta_k = -\delta_k + \lambda_k |p_k|^2 , \lambda_k = \bar{\lambda}_k .$$

Step 5: Calculate the step size :

$$\mu_k = p_k^T r_k , \alpha_k = \frac{\mu_k}{\delta_k}$$

Step 6: Calculate the comparison parameter

$$\Delta_k = \frac{2\delta_k \left[E(w_k) - E(w_k + \alpha_k p_k) \right]}{\mu_k^2}$$

Step 7: If $\Delta_k \ge 0$ *then a successful reduction in error can be made:*

$$w_{k+1} = w_k + \alpha_k p_k ,$$

$$r_{k+1} = -E'(w_{k+1}),$$

$$\bar{\lambda}_k = 0, success = true$$

a) If $K \bmod N = 0$ *then restart algorithm:* $p_{k+1} = r_{k+1}$

else create new conjugate direction.

$$\beta_k = \frac{|r_{k+1}|^2 - r_{k+1} r_k}{\mu_k},$$

$$p_{k+1} = r_{k+1} + \beta_k p_k.$$

b) If $\Delta_k > 0.75$ *then reduce the scale parameter:* $\lambda_k = \frac{1}{2}\lambda_k$

else a reduction in error is not possible: $\bar{\lambda}_k = \lambda_k$, *success=false.*

Step 8: If $\Delta_k < 0.25$ *then increase the scale parameter:* $\lambda_k = 4\lambda_k$

Step 9: If the steepest descent direction $r_k \neq 0$ *then set* $k = k+1$ *and go to step2.*

Else terminate and return w_{k+1} *as the desired minimum.*

5.3 Decision Trees

In early 1980s Quinlan developed the first decision tree algorithm known as ID3 [390]. Later he proposed C4.5, a benchmark to which other learning algorithms are judged. Decision tree, an inductive learning task, uses specific facts to make general conclusions. Decision tree algorithms have been very successful to solve large number of real world problems in data mining and machine learning [391]. Decision tree represents a sequence of decisions that are to be followed and their resulting recommendations. Decision trees are having flow chart like tree structure, with root node, leaf node, internal nodes and branches [384]. If a tuple with unknown class label is given, the attribute values of the tuple are tested against the decision tree. A path is traced from the root node to the leaf node that holds the class prediction for that tuple. Each non-leaf node of the tree contains a split point where it checks the condition based on attribute values.

Decision tree induction algorithm consists of three parameters, *the data partition,* which is a set of training tuples and their associated class

labels, *the attribute list,* set of candidate attributes and *the attribute selection method* [384]. *Attribute selection method* specifies a heuristic procedure for selecting the attribute that "best" discriminates the given tuples. The best attribute that classifies all the training instances at each node is identified using *information gain* [392]. Information gain for an attribute is defined as the reduction in *entropy* obtained by splitting the instances based on values taken by the attribute. The information gain for an attribute *A* at a node is calculated using

$$InformationGain(S, A) = Entropy(S) - \sum_{v \in Values(A)} \left(\frac{|S_v|}{|S|} Entropy(S) \right) \quad (5.1)$$

where *S* is the set of instances at that node and $|S|$ is its cardinality, S_v is the subset of *S* for which attribute *A* has value *v*, and entropy of the set *S* is calculated as

$$Entropy(S) = \sum_{i=1}^{numclasses} -p_i \log_2 p_i \quad (5.2)$$

where p_i is the proportion of instances in S that have the i^{th} class value as output attribute.

The algorithm works as follows. It starts with a single node representing the training tuples in dataset. If all the tuples in the root node are having same class label, the root node can be labelled using that class label. If the tuples in root node are different, then using attribute selection method, it finds the best attribute to partition the data. The process repeats with each partition until each leaf contains similar class label. Simple decision trees often perform much better than complex decision trees [392]. The noise and

outliers in the data will result in different kinds of anomalies in the generated decision tree. Use of tree pruning solves this problem by eliminating the least reliable branch. Two commonly used approaches in pruning are, prepruning and postpruning. In prepruning, the decision to stop developing subtrees is taken, during the tree building process while in post pruning, the complete tree is derived first then starts pruning.

5.4 Support Vector Machines

Support Vector Machines (SVM) are supervised learning algorithm derived from statistical learning theory and developed by Vapnik and Lerner in 1963 [393]. They have introduced the Generalized Portrait algorithm. Later many researchers have worked to improve the theory and concept so that it could solve many complex real world problems in classification and prediction. The history and development of support vector machines can be found in [394]. SVMs have attracted attention from the medical imaging community due to a number of theoretical and computational merits derived from the statistical learning theory. The mathematical background of SVM is as follows [395], Consider a linearly separable binary classification problem (as shown in Fig. 5.4)

$$\{(x_i, y_i)\}_{i=1}^{N} \text{ and } y_i = \{+1, -1\} \tag{5.3}$$

where x_i is an n-dimension vector and y_i is the label of the class that the vector belongs to. SVM separates the two classes of points by a hyperplane

$$w^T x + b = 0 \tag{5.4}$$

where w is an input vector, x is an adaptive weight vector, and b is a bias. SVM finds the parameters w and b for the optimal hyperplane to maximize the geometric margin $\frac{2}{\|w\|}$, subject to

$$y_i(w^T x_i + b) \geq +1. \tag{5.5}$$

The solution can be found through a Wolfe dual problem with the Lagrangian multiplied by α_i:

$$Q(\alpha) = \sum_{i=1}^{m} \alpha_i - \sum_{i,j=1}^{m} \alpha_i \alpha_j y_i y_j (x_i . x_j) / 2 \tag{5.6}$$

Subject to $\alpha_i \geq 0$ and $\sum_{i=1}^{m} \alpha_i y_i$.

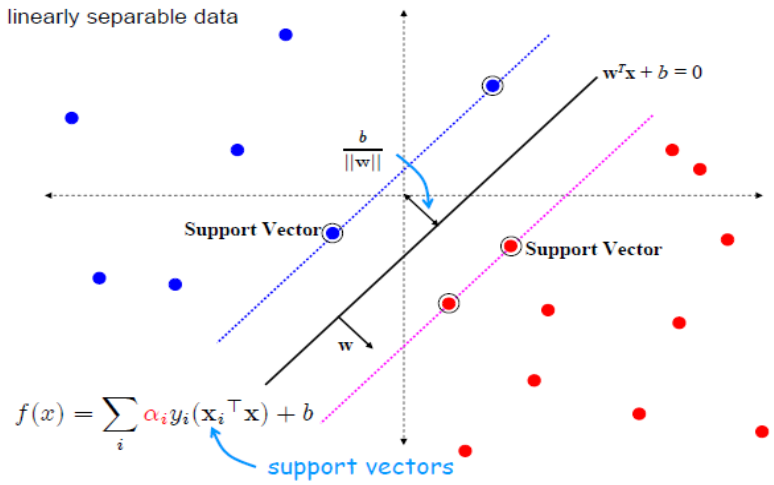

Figure 5.4 SVM for a linearly separable binary classification problem

The original optimal hyperplane algorithm proposed by Vladimir Vapnik in 1963 was a linear classifier. However, in 1992, Boser et al. [396] proposed a method to create non-linear classifiers by applying the kernel trick to maximum-margin hyperplanes. The resulting algorithm is formally similar,

except that every dot product is replaced by a non-linear kernel function. For linearly inseparable data, SVM uses a nonlinear mapping to transform the original training data into a higher dimension. Within this new dimension, it searches for the linear optimal separating hyperplane. Using an appropriate nonlinear mapping to a sufficiently high dimension, data from two classes can always be separated by a hyperplane, Fig.5.5 explains the same.

$$x_i.x_j \rightarrow \phi(x_i).\phi(x_j) = K(x_i, x_j), \tag{5.7}$$

where $K(.)$ is a kernel function. Thus, for a given kernel function, the SVM classifier is given by

$$F(x) = \text{sgn}(f(x)), \tag{5.8}$$

Where $f(x) = \sum_{i=1}^{l} \alpha_i y_i K(x_i, x) + b$ is the output hyperplane decision function of the SVM.

The common choices for kernel functions are:

Polynomial kernel of degree d $\quad k(x, y) = (\langle x, y \rangle + 1)^d \quad (5.9)$

Gaussian Radial Basis kernel $\quad k(x, y) = \exp(-\frac{\|x - y\|^2}{2\sigma^2}) \quad (5.10)$

Sigmoid Kernel $\quad k(x, y) = \tanh(\langle x, y \rangle - \sigma) \quad (5.11)$

SVM is based on the principle of structural risk minimization which leads to good generalization capability. The use of kernel function to map the data into a higher dimension is an over fitting task. SVMs tend to limit this effect by controlling the capacities of the machine by maximizing the margin of the hyperplane. During the learning process SVM tends to find a global solution because the model complexity is treated as a structural risk

minimization. Support vectors with non zero slack variable, and those that do not appear in the margin do not have any role in the classification task.

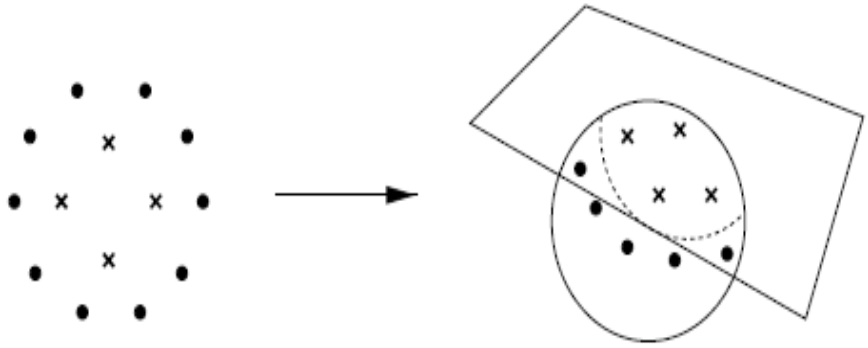

Figure 5.5 Nonlinear transformation of input data to higher dimension

5.5 Extreme Learning Machines

Extreme Learning Machine (ELM) is originally developed by Huang et al. [397] in 2004. Recently extreme learning machine has attracted many researches as a learning technique to solve classification and regression problems. Over the past decade, remarkable contributions have been made both in theoretical study and in the development of applications [398]. ELM and its enhancements such as C-ELM [399], I-ELM [400], OS-ELM [401] are widely used in various classification problems in medical diagnosis [402] and pattern recognition [403]. These classifiers were originally developed for Single Layer Feedforward Networks (SLFNs).

For function approximation in a finite training set, Huang et al. [404], showed that a single hidden layer feedforward neural network (SLFN) with at most N hidden nodes with almost any non linear activation function can exactly learn N distinct observation.

Approximation in SLFNs

For N samples $\{(\mathrm{x}_k, \mathrm{t}_k)\}_{k=1}^{N}$, where $\mathrm{x}_k = [x_{k1}, x_{k2}, ..., x_{kn}]^T$ and $\mathrm{t}_k = [t_{k1}, t_{k2}, ..., t_{km}]^{T\,N}_{k=1},$, a standard SLFN with $\tilde{N}$ hidden neurons and activation function $g(x)$ can be mathematically modelled as follows [405]

$$\sum_{i=1}^{\tilde{N}} \beta_i g(\mathrm{w}_i.\mathrm{x}_k + b_i) = \mathrm{o}_k, k = 1, ..., N \tag{5.12}$$

Where $\mathrm{w}_i = [w_{i1}, w_{i2}, ..., w_{in}]^T$ is the weight vector connecting the i^{th} hidden neuron and the input neurons, $\beta_i = [\beta_{i1}, \beta_{i2}, ..., \beta_m]^T$ is the weight vector connecting the i^{th} hidden neuron and the output neurons, $\mathrm{o}_k = [o_{k1}, o_{k2}, ..., o_{km}]^T$ is the output vector of the SLFN, and b_i is the threshold of the i^{th} hidden neuron. $\mathrm{w}_i.\mathrm{x}_k$ denote the inner product of w_i and x_k, these N equations can be written as,

$$\mathrm{H}\beta = \mathrm{O} \tag{5.13}$$

Where

$$\mathrm{H} = \begin{bmatrix} g(\mathrm{w}_1.\mathrm{x}_1 + b_1)...g(\mathrm{w}_{\tilde{N}}.\mathrm{x}_1 + b_{\tilde{N}}) \\ \vdots \quad ... \quad \vdots \\ g(\mathrm{w}_1.\mathrm{x}_N + b_1)...g(\mathrm{w}_{\tilde{N}}.\mathrm{x}_N + b_{\tilde{N}}) \end{bmatrix}_{NX\,N} \tag{5.14}$$

$$\beta = \begin{bmatrix} \beta_1^T \\ \vdots \\ \beta_{\tilde{N}}^T \end{bmatrix}_{\tilde{N}Xm} \tag{5.15}$$

$$O = \begin{bmatrix} o_1^T \\ \vdots \\ o_N^T \end{bmatrix}_{\tilde{N}Xm} \tag{5.16}$$

Here H is the hidden layer output matrix.

ELM learning

In conventional gradient based algorithms, to minimize the error function, input weights and hidden layer parameters are to be adjusted which makes the process very slow. According to ELM theories, the hidden layer SLFNs need not be tuned. The input weights and hidden layer biases can be randomly assigned if the activation functions in the hidden layer are infinitely differentiable. The input weight w_i and the hidden layer bias b_i need not be tuned and the hidden layer output matrix H can actually remain unchanged once these parameters are initialized randomly. For fixed input and hidden layer bias, to train SLFNs is simply equivalent to finding a least square solution. The number of hidden neurons required to achieve a proper generalization performance on novel pattern can be minimized by solving the following problem.

$$\min_{w_i, b_i, \beta} \left\| H(w_1, ..., w_{\tilde{N}}, b_1, ...b_{\tilde{N}})\beta - T \right\|^2, \tag{5.17}$$

$$\text{Where } T = \begin{bmatrix} t_1^T \\ \vdots \\ t_N^T \end{bmatrix}_{\tilde{N}Xm} \tag{5.18}$$

The above problem is a linear system optimization problem. Its unique least-square solution with minimum norm is given by

$$\hat{\beta} = H^{\dagger}T \tag{5.19}$$

Where H^{+} is the Moore-Penrose generalized inverse of the matrix H [406]

ALGORITHM : ELM

Input: Let *training set* $\aleph = \{(x_k, t_k) / x_k \in R^n, t_k \in R^m, k = 1,..., N\}$, *activation function* $g(x)$ *and hidden node number* $\tilde{N}$,

Output: *Trained network*

Method:

Step 1*: Randomly assign input weight* w_i *and bias* $b_i, i = 1,..., \tilde{N}$

Step 2*: Calculate the hidden layer output matrix H*

Step 3: *Calculate the output weight* $\hat{\beta} = H^{+}T$

5.6 Ensemble Classification for Performance Improvement

An ensemble of two regression models has been developed in early 1977 [407]. At the end of 1980s Hansen and Salamon [408] proved that prediction made by a combination of more than one classifier is accurate than using a single classifier. In 1989 Schapire, [409] proved that boosting of a weak learner to a strong learner can improve the classification accuracy. Ensemble methods are widely used in fields such as finance, bioinformatics, healthcare, manufacturing and geography [383]. In ensemble based classification method, an ensemble of potentially weak classifier is built to solve complex real world problems. The total expected error of a classifier arises from both bias and variance. Bias measures how well the learning model matches the problem. The expected error of a learned model over all possible training set of the given size and all possible test set, is called variance of the learning model for that problem. Use of combined classifiers

reduces the expected error by reducing the variance component [392]. The more classifier models are build and included, the greater is the reduction in variance. The classifier model is shown in Fig. 5.6.

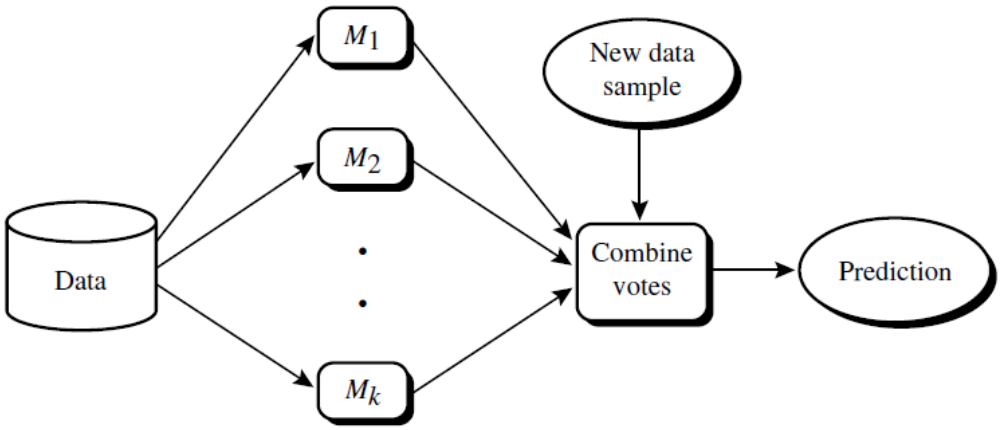

(Source: Data mining: concepts and techniques, Han and Kamber)

Figure 5.6: Ensemble classification

Two prominent ensemble classifiers are bagging and boosting [384]. In this study we have used bagging approach of combining different classifier models to classify data items. Bagging stands for Bootstrap aggregation. Each training set is a bootstrap sample. It creates an ensemble of models for a learning scheme where each model gives an equally weighted prediction. Use of bagging can reduce the instability of learned model. Sampling with replacement is used to create the data set. This causes some instances to replicate and some gets deleted. The algorithm for bagging is given below [410].

ALGORITHM: BAGGING

Input : *Data set* $D = \{(x_1, y_1), (x_2, y_2), ..., (x_m, y_m)\}$;

Base learning algorithm L

Number of learning rounds T.

Process :

for $i = 1, ...T$:

$D_t = Bootstrap(D)$

$h_t = L(D_t)$

End

Output : $H(x) = \arg\max_{y \in Y} \sum_{t=1}^{T} 1(y = h_t(x))$

$$1(a) = \begin{cases} 1 & if\ a\ is\ true \\ 0 & otherwise \end{cases}$$

5.7 Principal Component Analysis for Dimensionality Reduction

The use of large number of features does not improve the classification performance and the use of features, without any discriminative power, increases the complexity of the characterization process. The variability involved in prediction will be large and the classifier is sensitive to outliers. Therefore selection of optimal feature subset is an important problem [26]. In feature selection we compute a smaller set of new features which are more informative. In this work we have used the well known dimensionality reduction techniques, PCA (Principal Component Analysis). Earlier descriptions of Principal Component Analysis as 'lines and planes of

closest fit to systems of points in space', is given by Pearson in 1901 [411]. Later Hotelling in 1933, [412] developed PCA to its present stage and since then PCA has been used in diverse areas. Major applications of PCA are dimensionality reduction, lossy compression, feature extraction and visualization [413]. PCA generates a new set of variables called *principal components*, a linear combination of the original variables. Principal components are orthogonal to each other and therefore there is no redundant information. The first principal component is a single axis in space. When each observation is projected on to that axis, the resulting values form a new variable. And the variance of this variable is the maximum among all possible choices of the first axis. The second principal component is another axis in space, perpendicular to the first. Projecting the observations on this axis generates another new variable. The variance of this variable is the maximum among all possible choices of this second axis.

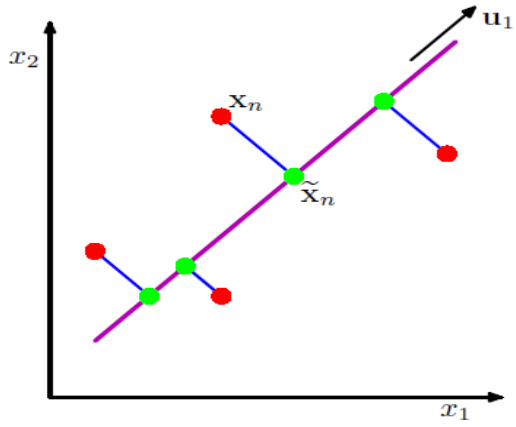

Principal Component Analysis seeks a space of lower dimension which is called as principal subspace, so that orthogonal projection of data points onto this subspace maximizes the variance of the projected points.

(Source: C. M. Bishop, and N. M. Nasrabadi, *Pattern recognition and machine learning*)

Figure 5.7 Principal subspace and orthogonal projection of principal components

Steps: PCA :- Transform an $N \times d$ matrix X into an $N \times m$ matrix Y

Step 1: Centralize the data by subtracting mean.

Step 2: Calculate the $d \times d$ covariance matrix: $C = \frac{1}{N-1} X^T X$

$C_{i,i}$ is the variance of variable.

$C_{i,j}$ is the covariance between variables i and j.

Step 3: Calculate the eigenvectors of the covariance matrix.

Step 4: Select *m* eigenvectors that correspond to the largest *m* eigenvalues to be the new basis.

5.8 Performance Measures

Kappa Statistics

Kappa statistics introduced by Fleiss et al. [414] is a measure of inter observer agreement. Kappa is calculated as a measure of agreement between the classifications and the true classes. It is defined as the proportion of agreement after chance agreement is removed from consideration.

$$K = \frac{P(A) - P(E)}{1 - P(E)} \tag{5.20}$$

Where $P(A)$ is the percentage agreement between the classifier and the ground truth, and $P(E)$ is the chance agreement. K=1 indicates perfect agreement, K=0 indicates chance agreement.

Confusion Matrix

The *confusion matrix* is a useful tool for analysing how well the classifier can recognize tuples of different classes [384]. Given m classes, a confusion matrix is a table of at least size m by m. An entry, $CM_{i,j}$ in the first m rows and m columns indicates the number of tuples of class i that were labelled by the classifier as class j.

Predicted Class			
		Yes	No
Actual Class	yes	True Positive	False Negative
	no	False Positive	True Negative

True positive rate (Recall) is the proportion of positive samples that are correctly classified. The false positive rate (FP) is the proportion of negative cases that were incorrectly classified as positive. Precision (P) is the proportion of the predicted positive cases that were correct. F-measure is a combined measure for precision and recall.

Measure	Formula
True positive rate	TP / (TP + FN)
False positive rate	FP / (FP + TN)
Precision	TP / (TP + FP)
Recall	TP / (TP + FN)
F-measure	2*Precision*Recall/(Precision+Recall)

ROC Curves

ROC stands for Receiver Operating Characteristic. It depicts the performance of a classifier without regard to class distribution or error cost. It shows the trade-off between true positive rate and false positive rate for a given model. The vertical axis represents true positive rate and horizontal axis represents false positive rate. The accuracy of a classification model is determined by calculating the area under ROC. The measure of area under ROC = 1, represents a model with perfect accuracy.

Error Measures

Following are the error measures used in this study, y_i is the actual value , y' is the predicted value and $\overline{y}$ is the mean values of y_i's.

$$\text{Mean Absolute Error} = \frac{\sum_{i=1}^{d} |y_i - y_i'|}{d} \quad (5.21)$$

$$\text{Root Mean Squared Error} = \sqrt{\frac{\sum_{i=1}^{d} (y_i - y')^2}{d}} \quad (5.22)$$

$$\text{Relative Absolute Error} = \frac{\sum_{i=1}^{d} |y_i - y_i'|}{\sum_{i=1}^{d} |y_i - \bar{y}|} \quad (5.23)$$

$$\text{Root Relative Squared Error} = \sqrt{\frac{\sum_{i=1}^{d} (y_i - y')^2}{\sum_{i=1}^{d} (y_i - \bar{y})^2}} \quad (5.24)$$

5.9 Experimental Set up and Result Analysis

The work is implemented using Matlab 7, a numerical computing environment and fourth generation programming language. Matlab is a high performance language for technical computing, visualization, and programming. The problems and solutions are expressed in familiar mathematical notation. Matlab provides a high level scientific and engineering programming environment with capabilities for plotting and visualizing data. It has an extensive library of built-in functions for data manipulations. In this study we have mainly used Image Processing, Neural Network and Wavelet toolboxes.

5.9.1 Result analysis of digital mammograms

The proposed method is experimented on mammogram images described in section 4.2. Different preprocessing techniques are applied to improve the quality of mammogram images. Contrast Limited Adaptive

Histogram Equalization enhances the contrast of mammogram images. After removing the background information and pectoral muscle, active contours are applied to segment the region of interest. Features extracted from 322 mammogram images are used for classification. The performances of different classifiers are evaluated based on the number of correct classification of images- normal, benign and malignant. The distribution of features: - types and numbers, are given in Table 5.1. The proposed approach combines 285 different statistical texture features for the classification of mammogram images. Performance is evaluated using different classifiers with entire feature set and reduced feature set. After principal component analysis the size of feature set is reduced to 5. Fig.5.8 shows scatter plot of first two principal components. Fig.5.9 shows the two dimensional scatter plot of principal components and the percent variability of each principal component. It is clear that the first principal component accounts for a majority of the variance in the model. First component by itself explains more than 40 % of the total variance. By considering first five components maximum variability is achieved and there by the dimension of the feature set get reduced.

Table 5.1 Number of features in each group-Mammogram images

Type of Feature	Number of Features
Histogram Statistics	6
Autocorrelation	1
Spatial Grey-Level-Dependence Matrix Features	6
Grey Level Difference Statistics	4
Neighbourhood Grey-Tone-Difference Matrix Features	5
SFM features	4
Local Binary Patterns	256
Wavelet Energy Descriptors	3
Total	**285**

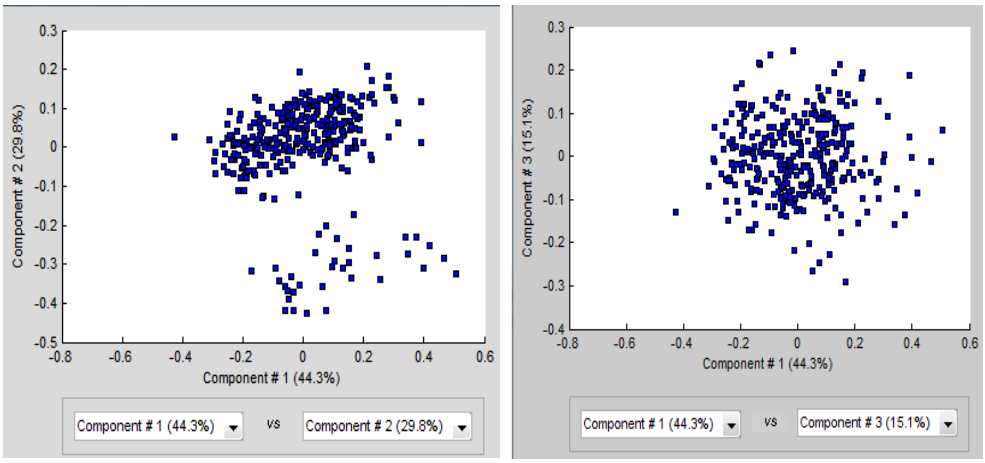

Figure 5.8 Scatter plot of first two principal components - Mammogram images.

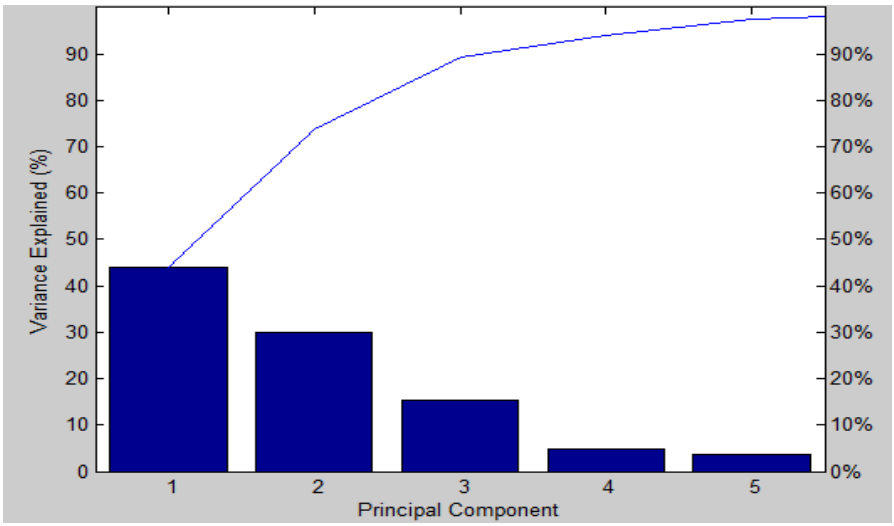

Figure 5.9: Variance explained by principal components - Mammogram images

MLP for Mammogram Image Classification

Multilayer perceptrons with Scaled Conjugate Gradient algorithm is used in this study. The complexity of the decision boundary and the power of neural network are determined by the number of hidden neurons. Half of the

total number of features, plus number of classes is taken as the number of hidden neurons. The activation function used is sigmoid. Weights are initialized to ensure fast and uniform learning. It is observed that a learning rate of 0.3 guarantees minimum error and helps to avoid getting stuck at local minima. Incorporation of momentum to stochastic gradient descent, reduces variation in overall gradient direction and increases speed of learning. To satisfy this, we have chosen the value 0.2 as momentum. Weight decay can cause the learning rate to decrease. Therefore the process divides the starting learning rate by the epoch number, to determine the current learning rate. This helps to stop the network, diverging from the target output as well as to improve the overall performance. Table 5.2, Table 5.3 and Table 5.4 shows the classification results of mammogram images using multilayer perceptrons. Fig.5.10 shows the change in performance of MLP classifier with varying number of hidden neurons. The experimental analysis shows that a maximum value is obtained when number of hidden neurons is 100. When the number of hidden neurons is increased to 120, the accuracy remains unchanged. Beyond the value 120, the accuracy decreases.

Table 5.2 Classification results using MLP-Mammogram images

Particulars	Full feature set	After PCA
Correctly Classified Instances	312	310
Incorrectly Classified Instances	10	12
Kappa statistic	0.9395	0.9249
Mean absolute error	0.211	0.2326
Root mean squared error	0.1438	0.2906
Relative absolute error	6.1542 %	67.7035 %
Root relative squared error	34.754 %	70.2134 %

Table 5.3 Detailed classification accuracy using MLP-Mammogram images

	Class	TP Rate	FP Rate	Precision	Recall	F-Measure	ROC Area
Full Feature Set	Benign	0.934	0.023	0.905	0.934	0.919	0.958
	Normal	0.986	0.027	0.986	0.986	0.986	0.981
	Malignant	0.941	0.004	0.98	0.941	0.96	0.969
	Weighted Average	**0.969**	**0.022**	**0.969**	**0.969**	**0.969**	**0.975**
Reduced Feature Set	Benign	0.852	0	1	0.852	0.92	0.94
	Normal	1	0.107	0.946	1	0.972	0.946
	Malignant	0.941	0	1	0.941	0.97	0.971
	Weighted Average	**0.963**	**0.07**	**0.965**	**0.963**	**0.962**	**0.949**

Table 5.4 Confusion matrix of classification using MLP - Full feature set & reduced feature set-Mammogram images

A	B	C	< --- Classified as
57	3	1	A=Benign
3	207	0	B=Normal
3	0	48	C=Malignant

A	B	C	< --- Classified as
52	9	0	A=Benign
0	210	0	B=Normal
0	3	48	C=Malignant

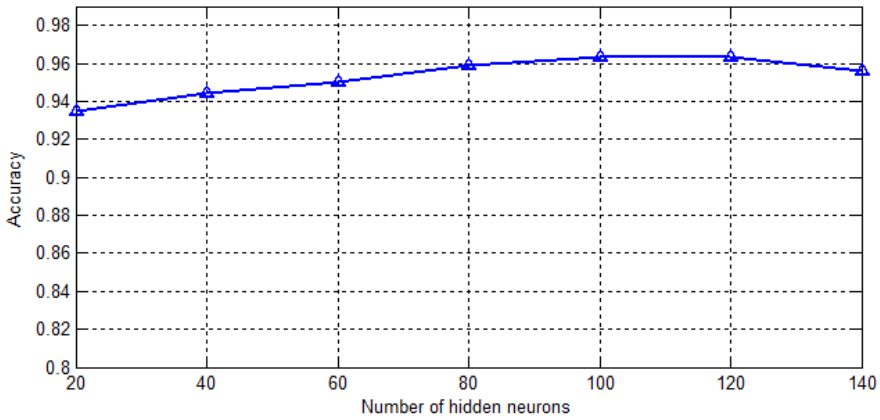

Figure 5.10 MLP classifier accuracy variation with respect to hidden neurons - Mammogram images

Decision Tree for Mammogram Image Classification

The Decision tree algorithm used in this study is J48. At each node of the tree, the algorithm chooses one attribute of the data to split the samples into subsets. Information gain is used to split the attribute. In this study we have used post pruning strategies to identify features that perform, weak individually but excellent when combined together. To remove the least reliable branches, which reflect anomalies in training data, postpruning is applied. Subtree raising and subtree replacement are the two ways to do post pruning. The selection is decided based on the error rate that would be expected at a particular node when an independent test set is given. By comparing the estimated error of the subtree with that of the raised tree, the decision to replace or raise the subtree is made. We have implemented reduced error pruning which is simply the verification with independent test set. The disadvantage is that the actual tree is based on less data. Table 5.5, Table 5.6 and Table 5.7 shows the classification results of mammogram images using Decision trees.

Table 5.5 Classification results using Decision tree- Mammogram images

Particulars	Full feature set	After PCA
Correctly Classified Instances	308	307
Incorrectly Classified Instances	14	15
Kappa statistic	0.9119	0.9055
Mean absolute error	0.234	0.2346
Root mean squared error	0.2929	0.2941
Relative absolute error	68.1053 %	68.3062 %
Root relative squared error	70.785 %	71.0691 %

Table 5.6 Detailed classification accuracy using Decision tree - Mammogram images

	Class	TP Rate	FP Rate	Precision	Recall	F-Measure	ROC Area
Full Feature Set	Benign	0.82	0	1	0.82	0.901	0.926
	Normal	1	0.125	0.938	1	0.968	0.938
	Malignant	0.941	0	1	0.941	0.97	0.97
	Weighted Average	**0.957**	**0.082**	**0.959**	**0.957**	**0.955**	**0.941**
Reduced Feature Set	Benign	0.82	0.004	0.98	0.82	0.893	0.908
	Normal	1	0.125	0.938	1	0.968	0.938
	Malignant	0.922	0	1	0.922	0.959	0.97
	Weighted Average	**0.953**	**0.082**	**0.956**	**0.953**	**0.952**	**0.937**

Table 5.7 Confusion matrix of classification using Decision tree - Full feature set & reduced feature set- Mammogram images

A	B	C	< --- Classified as
50	11	0	A=Benign
0	210	0	B=Normal
0	3	48	C=Malignant

A	B	C	< --- Classified as
50	11	0	A=Benign
0	210	0	B=Normal
1	3	47	C=Malignant

SVM for Mammogram Image Classification

The proposed work using SVM is experimented with polynomial kernel and RBF kernel. These kernel functions, project the data into a high dimensional space. The overfitting is controlled by maximizing the margin of the hyperplane. The parameter C-regularization constant, is used to control the tradeoff between the complexity of SVM and the number of non-separable points. The classifier is trained using two thirds of the data which are randomly selected. The remaining one third is used for testing by which the performance of the classifiers is

evaluated. The results obtained with RBF kernels are better when compared with that of polynomial kernels. Best results after doing a fivefold cross validation are recorded in Table 5.8, Table 5.9 and Table 5.10. To evaluate the robustness of SVM classifier, performance evaluation by varying the regularization parameter C and kernel parameters are done. Repeated trials are done for both polynomial kernels of degree upto 3 and RBF kernels. Results are shown in Fig.5.11 and Fig.5.12 respectively. Best value is obtained for RBF kernel with regularization value 1000 and gamma 0.1. Beyond that accuracy decreases. For polynomial kernel of degree 2 with regularization parameter value 100, maximum accuracy is observed. Further increase in regularization parameter degrades the performance of the classifier.

Table 5.8 Classification results using SVM- Mammogram images

Particulars	Full feature set	After PCA
Correctly Classified Instances	309	308
Incorrectly Classified Instances	13	14
Kappa statistic	0.9207	0.9148
Mean absolute error	0.0403	0.0433
Root mean squared error	0.1551	0.1546
Relative absolute error	12.623 %	12.6135 %
Root relative squared error	37.4769 %	37.3686 %

Table 5.9 Detailed classification accuracy using SVM- Mammogram images

	Class	TP Rate	FP Rate	Precision	Recall	F-Measure	ROC Area
Full Feature Set	Benign	0.918	0.023	0.903	0.918	0.911	0.982
	Normal	0.981	0.063	0.967	0.981	0.974	0.979
	Malignant	0.922	0	1	0.922	0.959	0.963
	Weighted Average	**0.96**	**0.045**	**0.96**	**0.96**	**0.96**	**0.977**
Reduced Feature Set	Benign	0.918	0.27	0.889	0.918	0.903	0.981
	Normal	0.976	0.063	0.967	0.976	0.972	0.983
	Malignant	0.922	0	1	0.922	0.959	0.979
	Weighted Average	**0.957**	**0.046**	**0.957**	**0.957**	**0.957**	**0.982**

Table 5.10 Confusion matrix of classification using SVM - Full feature set & reduced feature set-Mammogram images

A	B	C	< --- Classified as
56	5	0	A=Benign
4	206	0	B=Normal
2	2	47	C=Malignant

A	B	C	< --- Classified as
56	5	0	A=Benign
5	205	0	B=Normal
2	2	47	C=Malignant

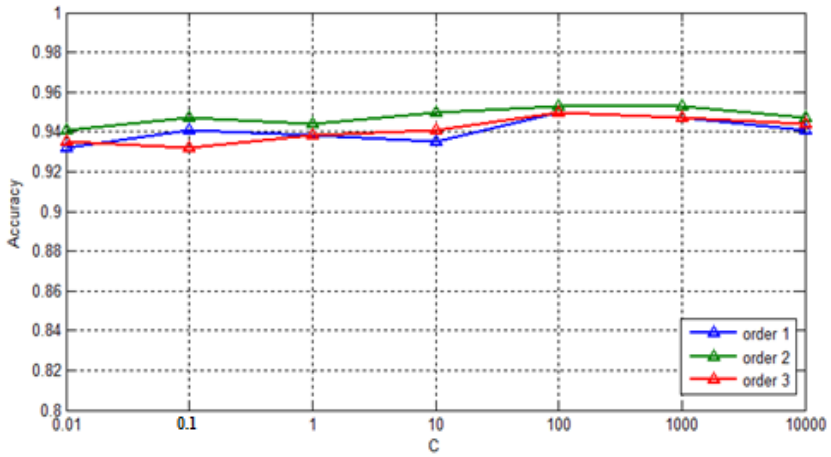

Figure 5.11 SVM with polynomial kernel - classifier accuracy variation with regularization parameter - Mammogram images

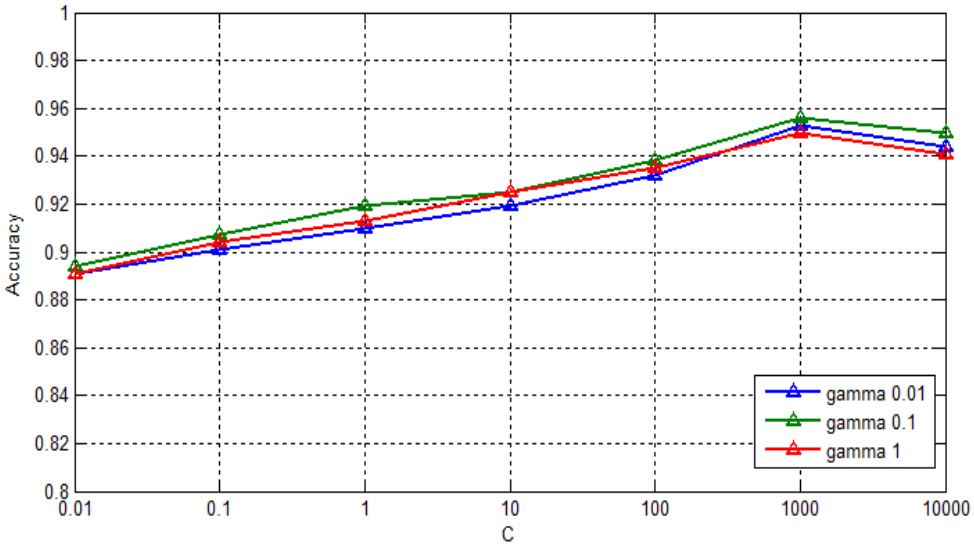

Figure 5.12 SVM with RBF kernel - classifier accuracy variation with regularization parameter- Mammogram images

ELM for Mammogram Image Classification

Classification using ELM, proposed herewith, uses unipolar sigmoid activation function. For each iteration of the algorithm, parameters are initialized randomly. The result of ELM varies with the number of hidden neurons. For each hidden neuron, fivefold cross validation is performed to find the best parameters of W and B. Experiments are conducted with different number of neurons in steps of 20, starting from 20 upto 140. Change in accuracy with respect to the number of hidden neurons is plotted in Fig.5.13 under the assumption that, for each neuron, the best B and W are selected by conducting different runs. An apparent increase in accuracy can be noted with the increase in number of hidden neurons upto 120. Beyond the value 120, accuracy remains unchanged. Table 5.11, Table 5.12 and Table 5.13 shows the classification results of mammogram images using ELM.

Table 5.11 Classification results using ELM-Mammogram images

Particulars	Full feature set	After PCA
Correctly Classified Instances	306	304
Incorrectly Classified Instances	16	18
Kappa statistic	0.8993	0.8899
Mean absolute error	0.2367	0.05
Root mean squared error	0.2976	0.1694
Relative absolute error	68.8663 %	14.533 %
Root relative squared error	71.8912 %	40.9099 %

Table 5.12 Detailed classification accuracy using ELM-Mammogram images

	Class	TP Rate	FP Rate	Precision	Recall	F-Measure	ROC Area
Full Feature Set	Benign	0.814	0.008	0.96	0.814	0.881	0.92
	Normal	1	0.125	0.938	1	0.968	0.938
	Malignant	0.906	0	1	0.906	0.95	0.945
	Weighted Average	**0.95**	**0.083**	**0.952**	**0.95**	**0.949**	**0.936**
Reduced Feature Set	Benign	0.864	0.03	0.864	0.864	0.864	0.979
	Normal	0.981	0.071	0.963	0.981	0.972	0.983
	Malignant	0.887	0.007	0.959	0.887	0.922	0.962
	Weighted Average	**0.944**	**0.053**	**0.944**	**0.944**	**0.944**	**0.979**

Table 5.13 Confusion matrix of classification using ELM - Full feature set & reduced feature set- Mammogram images

A	B	C	< --- Classified as
209	1	0	A=Benign
12	49	0	B=Normal
0	3	48	C=Malignant

A	B	C	< --- Classified as
207	3	0	A=Benign
12	49	0	B=Normal
0	3	48	C=Malignant

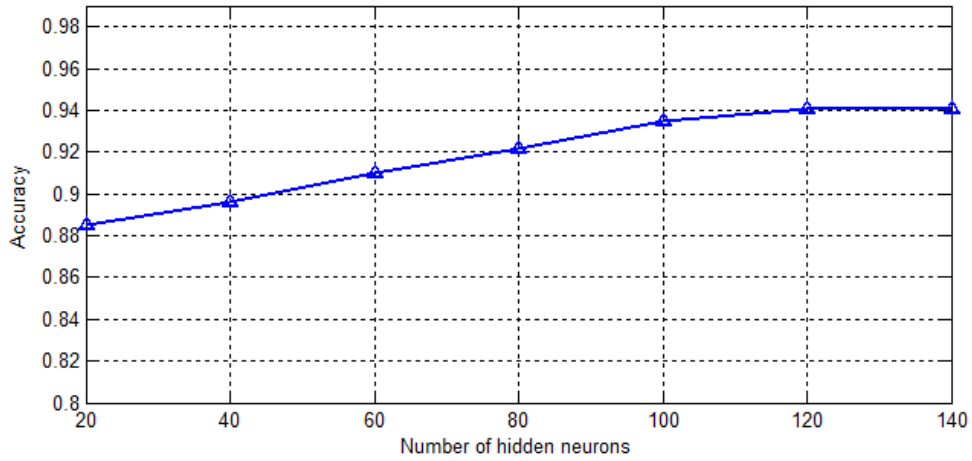

Figure 5.13 ELM classifier accuracy variation with hidden neurons - Mammogram images

Ensemble Classifiers for Mammogram Image Classification

Among the different classifiers, viz: decision tree, SVM , MLP and ELM, MLP with scaled conjugate gradient algorithm gives highest accuracy of 96.27 with reduced feature set for the classification of mammogram images. Therefore experiments are also conducted with bagging using MLP as the base classifier. The accuracy obtained is 97.20. Table 5.14, Table 5.15 and Table 5.16 shows marked increase in classification accuracy using bagging.

Table 5.14 Classification results using Bagging- Mammogram images

Particulars	Full feature set	After PCA
Correctly Classified Instances	315	313
Incorrectly Classified Instances	7	9
Kappa statistic	0.9572	0.9454
Mean absolute error	0.0693	0.225
Root mean squared error	0.1229	0.133
Relative absolute error	20.1705 %	6.5511 %
Root relative squared error	29.69 %	32.1439 %

Table 5.15 Detailed classification accuracy using Bagging-Mammogram images

	Class	TP Rate	FP Rate	Precision	Recall	F-Measure	ROC Area
Full Feature Set	Benign	0.934	0.11	0.95	0.934	0.942	0.998
	Normal	1	0.036	0.981	1	0.991	0.999
	Malignant	0.941	0	1	0.941	0.97	0.999
	Weighted Average	**0.978**	**0.025**	**0.978**	**0.978**	**0.978**	**0.999**
Reduced Feature Set	Benign	0.951	0.019	0.921	0.951	0.935	0.965
	Normal	0.986	0.036	0.981	0.986	0.983	0.977
	Malignant	0.941	0	1	0.941	0.97	0.98
	Weighted Average	**0.972**	**0.027**	**0.973**	**0.972**	**0.972**	**0.975**

Table 5.16 Confusion matrix of classification using Bagging - Full feature set & reduced feature set-Mammogram images

A	B	C	< --- Classified as
57	4	0	A=Benign
0	210	0	B=Normal
3	0	48	C=Malignant

A	B	C	< --- Classified as
58	3	0	A=Benign
3	207	0	B=Normal
2	1	48	C=Malignant

5.9.1.1 Comparative analysis and discussion

Proposed work has been compared with some of the recently published papers which use MIAS and DDSM as databases. The works used here for comparison mainly depend on intensity, texture, shape, density features and wavelet, curvelet coefficients. Table 5.17 shows their relevant details and results. Results include accuracy, area under ROC and true positive rate. The distinguishing features of the proposed method are:-

- Use of better preprocessing techniques.
- Design of a novel feature set :- Histogram statistics, Autocorrelation, SGLDM features, GLDS features, NGTDM features, SFM features, Local Binary Patterns and Wavelet Energy Descriptors.
- Dimensionality reduction using Principal Component Analysis.
- Experimental analysis with different powerful classifiers: - ANN, Decision Tree, Support Vector Machine and Extreme Learning Machines.
- Classification of all the kinds of abnormality: - Images in MIAS database are classified into normal, benign and malignant.
- Performance improvement by Ensemble classification using Bagging.

Table 5.17 Comparative analysis of mammogram image classification

Authors	Features	Classifier	Results (%)
Ren J. et al.[2011] [103]	Intensity statistics, shape features, linear structure features	ANN	80
J. Dheeba et al.[2011] [105]	Laws texture features	Swarm optimized ANN	91
Subashini et al.[2010] [116]	Statistical features	SVM	95
Sampaio et al.[2011] [117]	Shape, texture using geostatic function	SVM	80
Zhang et al.[2012] [118]	Shape, margin of masses	Ensemble	72
Verma et al.[2009] [127]	Density features, Mass shape, mass margin features	ANN	94
Verma et al.[2010] [128]	Density features, Mass shape, mass margin features, Patient age	SCBDL	97
Wang et al.[2009] [130]	Curvilinear, GLCM, Gabor, Multi-resolution statistical features	sSVM	91.4
Meselhy et al.[2010][133]	Wavelet, curvelet coefficients	KNN	94.2
Arikidis et al.[2008] [35]	Wavelet coefficients	Genetic Programming	98
Nanni et al.[1971] [86]	LTP, LPQ	SVM	97
Proposed work	**Intensity features, Texture features, Wavelet Energy**	**Ensemble**	**97.20**

5.9.2. Result analysis of placental sonograms

A total of 530 images, in which 150 images are of grade 0, 190 of grade 1, 130 of grade2 and 60 of grade3 are used. Preprocessing operations such as contrast enhancement, noise reduction using proposed linear filter based on local binary pattern and ROI extraction are applied to improve the quality of ultrasound image. In the proposed work for classifying placenta images of different grade, a total of 297 different features are extracted. The type of features and the number of features in each class is given in Table 5.18. Performance is evaluated with different classifiers using full feature set and reduced feature set. The size of feature set is reduced to 5 after principal component analysis. Fig.5.14 shows the percent variability of each principal

component. First component by itself explains more than 50 % of the total variance. The result of experimental analysis using the first 5 principal components shows near values as that of the result of entire data set. Table 5.19, Table 5.20 and Table 5.21 shows the classification accuracy of placental images using MLP whereas Fig. 5.15 shows the variation in classification accuracy with hidden neurons using MLP. Table 5.22, Table 5.23 and Table 5.24 shows the classification accuracy of placental images using Decision trees. Table 5.25, Table 5.26 and Table 5.27 shows the classification accuracy of placental images using SVM. Fig.5.16 and Fig.5.17 shows classification accuracy variation using SVM with Polynomial kernel and RBF kernel respectively. Table 5.28, Table 5.29 and Table 5.30 shows the classification accuracy of placental images using ELM and Fig.5.18 shows the variation in classification accuracy with hidden neurons.

Table 5.18 Number of features in each group- Sonogram images

Type of Feature	Number of Features
Histogram Statistics	6
Autocorrelation	1
Spatial Grey-Level-Dependence Matrix Features	6
Grey Level Difference Statistics	4
Neighbourhood Grey-Tone-Difference Matrix Features	5
SFM Features	4
Local Binary Patterns	256
Wavelet Energy Descriptors	3
Moment Invariants	7
Regional Descriptors	5
Total	**297**

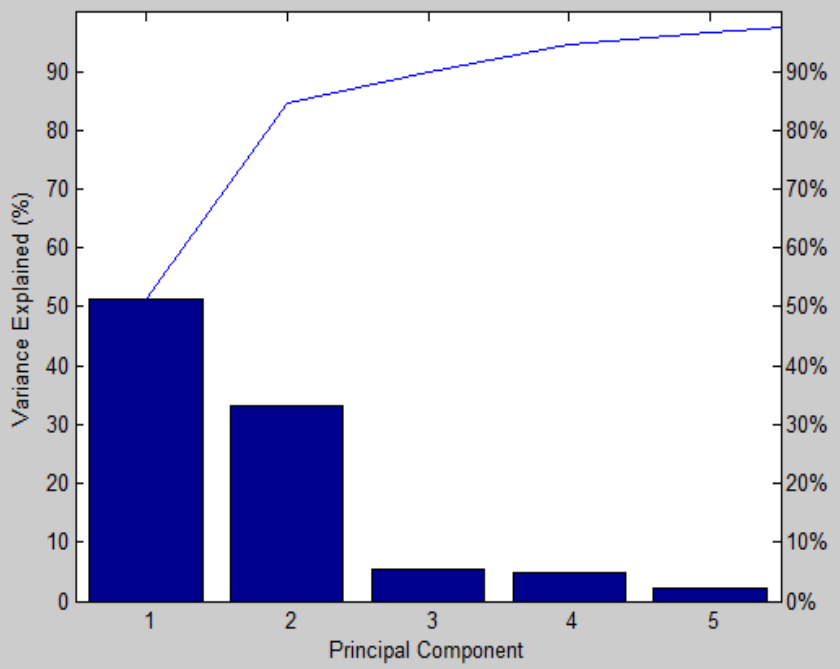

Figure 5.14 Variance explained by principal components - Sonogram images

MLP for Sonogram Image Classification

Table 5.19 Classification results using MLP- Sonogram images

Particulars	Full feature set	After PCA
Correctly Classified Instances	408	406
Incorrectly Classified Instances	122	124
Kappa statistic	0.6789	0.6744
Mean absolute error	0.146	0.1464
Root mean squared error	0.3199	0.3066
Relative absolute error	40.6008 %	40.7284 %
Root relative squared error	75.4689 %	72.3274 %

Table 5.20 Detailed classification accuracy using MLP-Sonogram images

	Class	TP Rate	FP Rate	Precision	Recall	F-Measure	ROC Area
Full Feature Set	Grade 0	0.92	0.026	0.932	0.92	0.926	0.965
	Grade 1	0.677	0.145	0.603	0.677	0.638	0.782
	Grade 2	0.833	0	1	0.833	0.909	0.984
	Grade 3	0.695	0.159	0.71	0.695	0.702	0.758
	Weighted Average	**0.77**	**0.1**	**0.779**	**0.77**	**0.773**	**0.848**
Reduced Feature Set	Grade 0	0.92	0.016	0.958	0.92	0.939	0.962
	Grade 1	0.692	0.165	0.577	0.692	0.692	0.801
	Grade 2	0.833	0	1	0.833	0.909	0.984
	Grade 3	0.674	0.153	0.711	0.674	0.692	0.825
	Weighted Average	**0.766**	**0.1**	**0.781**	**0.766**	**0.771**	**0.876**

Table 5.21 Confusion matrix of classification using MLP - Full feature set & reduced feature set- Sonogram images

A	B	C	D	< --- Classified as
138	0	0	12	A = Grade 0
0	88	0	42	B = Grade 2
0	10	50	0	C = Grade 3
10	48	0	132	D = Grade 1

A	B	C	D	< --- Classified as
138	0	0	12	A = Grade 0
0	90	0	40	B = Grade 2
0	10	50	0	C = Grade 3
6	56	0	128	D = Grade 1

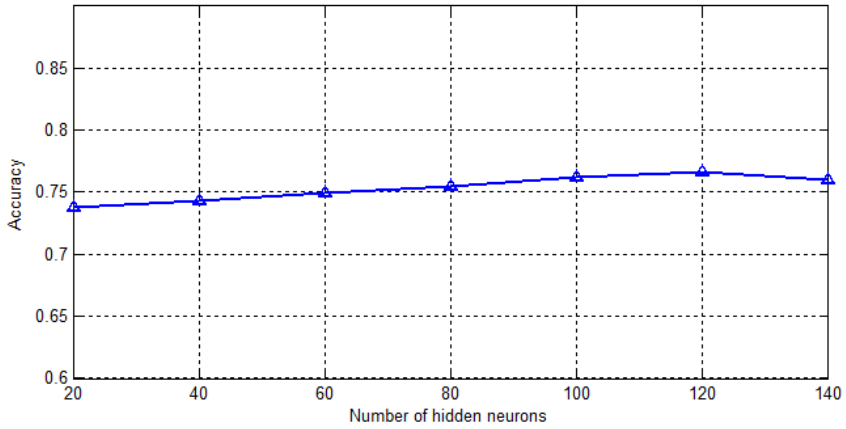

Figure 5.15 MLP classifier accuracy variation with hidden neurons - Sonogram images

Decision Tree for Sonogram Image Classification

Table 5.22 Classification results using Decision tree- Sonogram images

Particulars	Full feature set	After PCA
Correctly Classified Instances	400	396
Incorrectly Classified Instances	130	134
Kappa statistic	0.6555	0.6453
Mean absolute error	0.1472	0.1419
Root mean squared error	0.2982	0.3046
Relative absolute error	40.9419 %	41.5158 %
Root relative squared error	70.3443 %	71.8618 %

Table 5.23 Detailed classification accuracy using Decision tree - Sonogram images

	Class	TP Rate	FP Rate	Precision	Recall	F-Measure	ROC Area
Full Feature Set	Grade 0	0.92	0.021	0.945	0.92	0.932	0.969
	Grade 1	0.554	0.13	0.581	0.554	0.567	0.838
	Grade 2	0.833	0	1	0.833	0.909	0.987
	Grade 3	0.737	0.206	0.667	0.737	0.7	0.85
	Weighted Average	**0.755**	**0.112**	**0.762**	**0.755**	**0.757**	**0.896**
Reduced Feature Set	Grade 0	0.92	0.021	0.945	0.92	0.932	0.966
	Grade 1	0.554	0.14	0.563	0.554	0.558	0.83
	Grade 2	0.833	0	1	0.833	0.909	0.988
	Grade 3	0.716	0.206	0.66	0.716	0.687	0.846
	Weighted Average	**0.747**	**0.114**	**0.755**	**0.747**	**0.75**	**0.892**

Table 5.24 Confusion matrix of classification using Decision tree - Full feature set & reduced feature set- Sonogram images

A	B	C	D	< --- Classified as
138	0	0	12	A = Grade 0
0	72	0	58	B = Grade 2
0	10	50	0	C = Grade 3
8	42	0	140	D = Grade 1

A	B	C	D	< --- Classified as
138	0	0	12	A = Grade 0
0	72	0	58	B = Grade 2
0	10	50	0	C = Grade 3
8	46	0	136	D = Grade 1

SVM for Sonogram Image Classification

Table 5.25 Classification results using SVM- Sonogram images

Particulars	Full feature set	After PCA
Correctly Classified Instances	438	422
Incorrectly Classified Instances	92	108
Kappa statistic	0.7486	0.7113
Mean absolute error	0.2651	0.2695
Root mean squared error	0.3351	0.3416
Relative absolute error	75.3906 %	74.9614 %
Root relative squared error	79.9628 %	80.6031 %

Table 5.26 Detailed classification accuracy using SVM- Sonogram images

	Class	TP Rate	FP Rate	Precision	Recall	F-Measure	ROC Area
Full Feature Set	Grade 0	0.973	0	1	0.973	0.986	0.987
	Grade 1	0.429	0	1	0.429	0.6	0.714
	Grade 2	1	0	1	1	1	1
	Grade 3	1	0.271	0.674	1	0.805	0.865
	Weighted Average	**0.826**	**0.097**	**0.883**	**0.826**	**0.81**	**0.865**
Reduced Feature Set	Grade 0	0.92	0.016	0.958	0.92	0.939	0.966
	Grade 1	0.492	0.06	0.727	0.492	0.587	0.804
	Grade 2	0.867	0.004	0.963	0.867	0.912	0.991
	Grade 3	0.884	0.224	0.689	0.884	0.774	0.844
	Weighted Average	**0.796**	**0.1**	**0.805**	**0.796**	**0.791**	**0.885**

Table 5.27 Confusion matrix of classification using SVM - Full feature set & reduced feature set- Sonogram images

A	B	C	D	< --- Classified as
146	0	0	4	A = Grade 0
0	66	0	88	B = Grade 2
0	0	36	0	C = Grade 3
0	0	0	190	D = Grade 1

A	B	C	D	< --- Classified as
138	0	0	12	A = Grade 0
0	64	2	64	B = Grade 2
0	8	52	0	C = Grade 3
6	16	0168		D = Grade 1

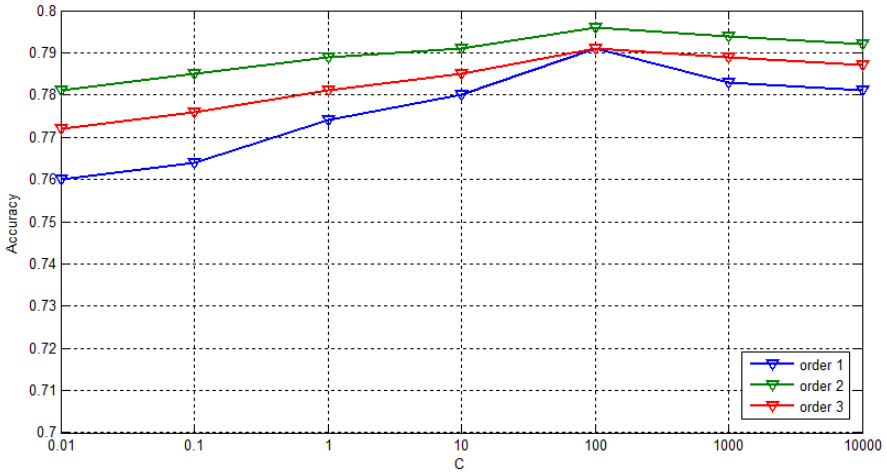

Figure 5.16 SVM with polynomial kernel - classifier accuracy variation with regularization parameter -Sonogram images

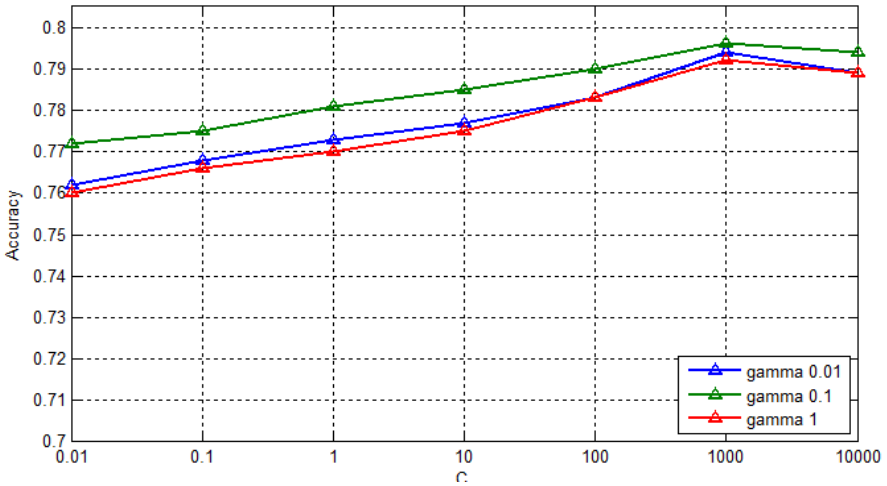

Figure 5.17 SVM with RBF kernel - classifier accuracy variation with regularization parameter - Sonogram images

ELM for Sonogram Image Classification

Table 5.28 Classification results using ELM-Sonogram images

Particulars	Full feature set	After PCA
Correctly Classified Instances	410	404
Incorrectly Classified Instances	120	126
Kappa statistic	0.6816	0.674
Mean absolute error	0.1549	0.1511
Root mean squared error	0.2951	0.3003
Relative absolute error	43.0863 %	42.0369 %
Root relative squared error	69.6134 %	70.8521 %

Table 5.29 Detailed classification accuracy using ELM-Sonogram images

	Class	TP Rate	FP Rate	Precision	Recall	F-Measure	ROC Area
Full Feature Set	Grade 0	0.92	0.026	0.932	0.92	0.926	0.946
	Grade 1	0.779	0.2	0.685	0.779	0.729	0.826
	Grade 2	0.569	0.1	0.649	0.569	0.607	0.843
	Grade 3	0.833	0.004	0.962	0.833	0.893	0.987
	Weighted Average	**0.774**	**0.104**	**0.778**	**0.774**	**0.773**	**0.882**
Reduced Feature Set	Grade 0	0.92	0.021	0.945	0.92	0.932	0.956
	Grade 1	0.705	0.159	0.713	0.705	0.709	0.844
	Grade 2	0.646	0.145	0.592	0.646	0.618	0.835
	Grade 3	0.833	0.009	0.926	0.833	0.877	0.984
	Weighted Average	**0.766**	**0.099**	**0.773**	**0.766**	**0.769**	**0.889**

Table 5.30 Confusion matrix of classification using ELM - Full feature set & reduced feature set- Sonogram images

A	B	C	D	< --- Classified as
118	10	6	16	A = Grade 0
6	168	6	10	B = Grade 2
22	6	84	18	C = Grade 3
8	12	0	40	D = Grade 1

A	B	C	D	< --- Classified as
114	12	8	16	A = Grade 0
6	168	6	10	B = Grade 2
22	8	82	18	C = Grade 3
8	12	0	40	D = Grade 1

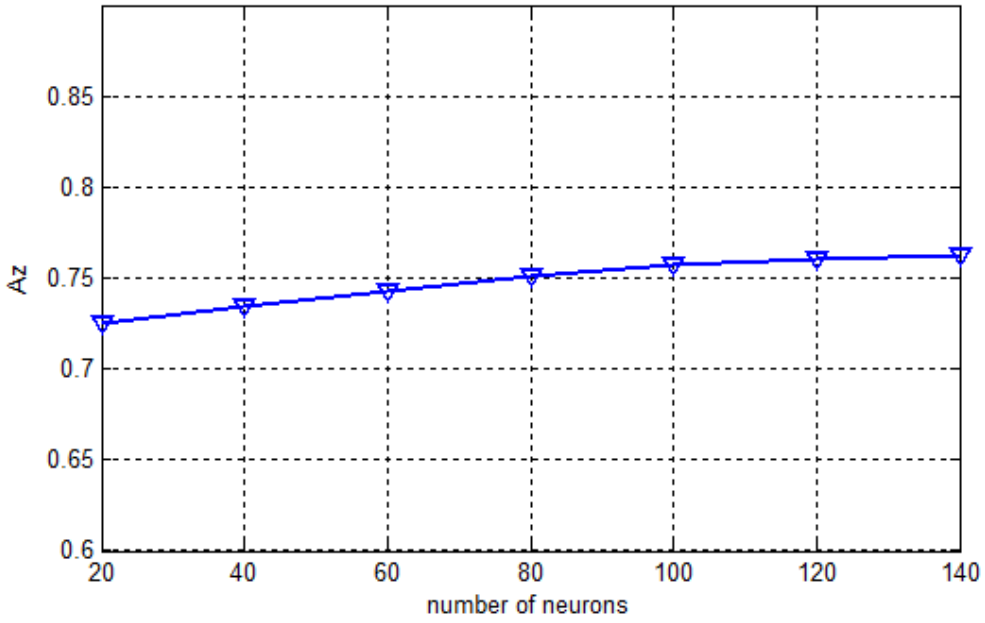

Figure 5.18 ELM classifier accuracy variation with hidden neurons-Sonogram images

Ensemble Classifiers for Sonogram Image Classification

Among the classifiers, MLP, decision tree, SVM and ELM, for the classification of placental images, maximum accuracy of 79.62 is obtained for SVM using the features mentioned in Table 5.18. Therefore for bagging, SVM has been used as the base classifier. The accuracy obtained is 83.77 for

reduced feature set. Table 5.31, Table 5.32 and Table 5.33 shows the classification accuracy of ensemble classification.

Table 5.31 Classification results using Bagging - Sonogram images

Particulars	Full feature set	After PCA
Correctly Classified Instances	446	444
Incorrectly Classified Instances	84	86
Kappa statistic	0.7765	0.7715
Mean absolute error	0.0792	0.0811
Root mean squared error	0.2815	0.2848
Relative absolute error	22.0423 %	22.5671 %
Root relative squared error	66.4152 %	67.2012 %

Table 5.32 Detailed classification accuracy using Bagging-Sonogram images

	Class	TP Rate	FP Rate	Precision	Recall	F-Measure	ROC Area
Full Feature Set	Grade 0	0.92	0.016	0.958	0.92	0.939	0.952
	Grade 1	0.677	0.06	0.786	0.677	0.727	0.808
	Grade 2	0.8330	0	1	0.833	0.909	0.917
	Grade 3	0.895	0.159	0.759	0.895	0.821	0.868
	Weighted Average	**0.842**	**0.076**	**0.849**	**0.842**	**0.841**	**0.883**
Reduced Feature Set	Grade 0	0.92	0.021	0.945	0.92	0.932	0.949
	Grade 1	0.692	0.065	0.776	0.692	0.732	0.814
	Grade 2	0.833	0	1	0.833	0.909	0.917
	Grade 3	0.874	0.153	0.761	0.874	0.814	0.86
	Weighted Average	**0.838**	**0.077**	**0.844**	**0.838**	**0.838**	**0.881**

Table 5.33 Confusion matrix of classification using Bagging - Full feature set & reduced feature set-Sonogram images

A	B	C	D	< --- Classified as
138	0	0	12	A = Grade 0
0	88	0	42	B = Grade 2
0	10	50	0	C = Grade 3
6	14	0	170	D = Grade 1

A	B	C	D	< --- Classified as
138	0	0	12	A = Grade 0
0	90	0	40	B = Grade 2
0	10	50	0	C = Grade 3
8	16	0	166	D = Grade 1

5.9.2.1 Comparative analysis and discussion

In literature, a few works are reported regarding the classification of placental images. The works used for comparison are mainly depended on intensity, texture, wavelet coefficients and the like. In most of the works, the number of images used is very less compared to the proposed work. There is no clarity in the preprocessing procedures and in the use of classification algorithms. Technical details of the existing works are given in section 3.3. Table 5.34 shows the comparative analysis of sonogram image classification in the proposed work with existing works. The distinguishing features of the proposed method are.

- Design and use of efficient noise removing filter.
- Design of a novel feature set which includes Histogram statistics, Autocorrelation, SGLDM features, GLDS features, NGTDM features, SFM features, Local Binary Patterns, Wavelet Energy Descriptors, moment invariants and regional descriptors.
- Identification and use of 297 different features.
- Dimensionality reduction using Principal Component Analysis.
- Experimental analysis with different powerful classifiers: - ANN, Decision Tree and Support Vector Machines.

- Design of a novel approach using Extreme Learning Machines.
- Performance improvement with the help of Ensemble classification by bagging with SVM as base classifier.
- Promising results are obtained for the automated classification of placenta into different grades.

Table 5.34 Comparative analysis of sonogram image classification

Authors	Features	Classifier	Accuracy (%)
Mohammag Ayache et al.[19]	Wavelet coefficients	ANN	95
Linares at al. [20]	GLCM, NGDTM, Laws's operator features	Decision tree	92
Zhi Liu et al. [22]	Grey scale statistics	SVM	92
Proposed work	**Intensity features, Texture features, Wavelet Energy, Shape features**	**Ensemble**	**83.77**

5.10 Chapter Summary

This chapter has described the classification of both digital mammograms and placental sonograms using supervised classification algorithms such as ANN, Decision Trees, SVM and ELM. Different types of features that are discussed in the previous chapter are used for the classification purpose. For both digital mammograms and placental sonograms, the best classifier is identified, with which ensemble classification is done to improve the accuracy. To reduce the dimensionality of feature vector, principal component analysis is applied. The results obtained after PCA show its ability to identify most discriminating features. The proposed work identifies the best suited statistical texture features for mammogram image classification. The novelty of the work in placental classification is the use of ELM and ensemble classifiers. Comparison of the proposed work with some of the existing works shows the distinguishing features of the proposed work.

Chapter 6

MULTIPLE IMAGE QUERY SYSTEM FOR MEDICAL IMAGE RETRIEVAL

6.1 Introduction

Developments in image acquisition and data storage have facilitated the creation of large image datasets. To manage these large collections of images, it becomes necessary to develop appropriate information systems. With the popularization of digital information in the present era, the demand for effective storage and retrieval mechanism has reached an all time high level [277]. The most needed approach is the so-called Content-Based Image Retrieval (CBIR) systems. Basically, these systems try to retrieve images similar to a user-defined specification or pattern (e.g., shape sketch, image example). Their goal is to support image retrieval based on content properties (e.g., shape, colour, texture), usually encoded into feature vectors. The function of CBIR in medical domain is potentially very dominant:- CBIR could provide Computer Aided Diagnostic assistance based on image content or properties as well as on other metadata linked with medical images [280]. The integration of Content Based Image Retrieval approaches to daily clinical practice is helpful in clinical decision making. In medical field CBIR system allows the doctors to compare their diagnosis with the earlier findings in the respective domain in case of any doubt regarding the diagnosis. Thus

by the use of human perception together with machine intelligence, best results can be arrived at, which is of great help for the physician. Modern works in image processing, medical informatics, and information retrieval areas provide building blocks that can noticeably increase the significance of CBIR to radiology practice in the future.

This chapter presents the basic concepts of CBIR. Description of a general CBIR framework with its applications and the components like feature extraction and similarity computation are given. Then we move to CBMIR systems. Finally a new method for improving the retrieval accuracy has been proposed. The proposed method uses multiple images to retrieve desired images from database. The multiple images in the query are combined using logical AND, OR and NOT.

6.2 System Architecture

Fig.6.1 shows the architecture of a general purpose CBIR system which consists of two major process - offline process and online process. The offline process is called data insertion stage by which images are added to the database. The process involves preprocessing steps to improve the quality of images, segmentation for extracting region of interest, feature extraction and formation of feature vector. The online processing is called query processing stage. The user uses image queries from which the system extracts features and evaluates the similarity between query image and database images. The images are sorted according to the distance and the interface displays most similar images that are retrieved.

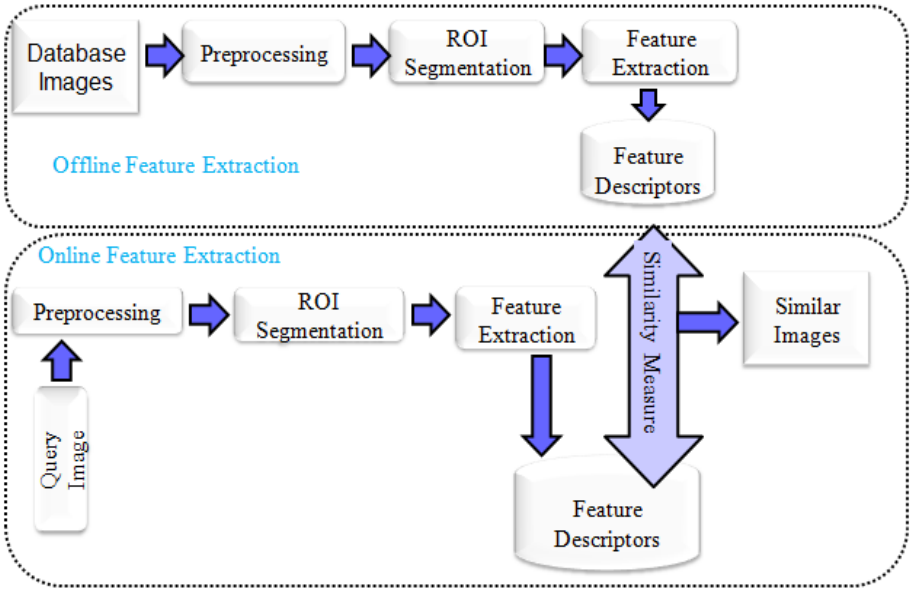

Figure 6.1 CBIR system architecture

6.3 Basic Concepts in CBIR

Image, Feature vectors, and Image descriptors

Solution to CBIR problems requires construction of an **image descriptor**, which is characterized by: (i) an extraction algorithm to encode image features into feature vectors; and (ii) a similarity measure to compare two images [6]. The similarity measure is a matching function, which gives the degree of similarity for a given pair of images as represented by their feature vectors, often defined as an inverse function of the distance , that is, the larger the distance value, the less similar the images are.

An **image** $\hat{I}$ is a pair $(D_I, \vec{I})$, where

D_I : is a finite set of pixels and

$\vec{I} : D_I \to R^n$ is a function that assigns to each pixel p in D_I a vector $\vec{I}(p) \in R^n$

A **feature vector** $\vec{v}_{\hat{I}}$ of an image $\hat{I}$ can be thought of as a point in R^n space: $\vec{v}_{\hat{I}} = (v_1, v_2, ..., v_n)$, where n is the dimension of the vector.

A **simple image descriptor** is defined as a tuple $(\in_D, \delta_D)$: where

$\in_D : \{\hat{I}\} \to R^n$ is a function, which extracts a *feature vector* $\vec{v}_{\hat{I}}$ from an *image* $\hat{I}$.

$\delta_D : R^n \times R^n \to R$ is a *similarity function* that computes the similarity between two mages as the inverse of the distance between their corresponding *feature vectors.*

Query

Usually, two kinds of queries are supported by CBIR systems [11]. In a *K-nearest neighbour query (KNNQ),* the user specifies the number k of images to be retrieved that are closest to the query pattern. In a *range query (RQ),* the user defines a search radius r, and wants to retrieve all database images whose distances to the query pattern are less than r. In this case, both the specification of k in the KNNQ and the specification of r in *RQ* needs to be incorporated into Q.

Two intrinsic problems in CBIR

1. How to mathematically describe an image - Features.
2. How to access similarity between images - Similarity Measures.

Features

Quantitative features calculated automatically are employed for characterizing image content [207]. General visual features and domain specific semantic features are the two broad groups of image features. General visual features typically comprise primitive image information that refers to the constituents and composition of images, such as colour, shape, texture and spatial relationships. While domain specific semantic features are application dependent and consist principally of abstract information that refers to the meaning of an image, describing high level semantic content in focused domains. Often medical images contain varied, rich, and often subtle features that are important clinically and that take apart this domain from other multimedia applications. Therefore appropriate selection of clinically relevant features is an important task in CBIR.

Similarity Measure

The second intrinsic problem is the assessment of similarities between image features based on mathematical analysis, which evaluate descriptors across different images. Preferably, the computed similarity should be partly similar to the similarity between images when analyzed by the human visual system alone. In a typical CBIR system, database images are retrieved and displayed in the decreasing order of their computed similarity to a query image provided by the user. The proposed work uses the following distance measure to assess the similarity between query image and database images.

Eucledian Distance - $\sqrt{\sum_{i=1}^{n}((f_i(Q) - f_i(P_j))^2)}$

Where $f_i(Q)$ is the ith feature of query image, $f_i(P_j)$ is the corr-esponding feature of the image P_j in the data base.

6.4 General Purpose CBIR System

The generic CBIR system has two main components. The first component stands for representing the visual information contained in image pixels in the form of quantitative features/descriptors and intend to reduce the gap between the visual content and its numerical representation. The features mainly arise from colour, texture properties of the image, the spatial layout of objects, and geometric shape characteristics of structures within the image.

The second component is used for assessing the similarities between features of query image and database images. The database images are returned and displayed in the decreasing order of their computed similarity to the query image presented by the user. This is the basic requirement for any CBIR application. The developed CBIR system can be used for any particular application. According to the requirement we can add additional functionalities like new preprocessing, feature extraction and similarity measures to this system. This system has been tested with applications such as face recognition [415], character recognition [416] and mammogram image classification and placental image classification.

6.5 Content Based Medical Image Retrieval System

Content Based Medical Image Retrieval is an exciting and active field of research [275]. Most frequently, radiology images are the fundamental part of diagnostics, treatment planning, and treatment, but medical images are equally important for medical education, research and epidemiology. The

usage of medical images in medical institutions has been escalating enormously day by day due to production of thousands of medical digital images of different modalities such as Computed Tomography (CT) images, Magnetic Resonance Images (MRI), ultrasound (US) images, X-ray images and so on. Due to the steadily increasing medical image data, it is very important to manage and access the data properly [417]. Therefore, a lot of CBIR (Content Based Image Retrieval) systems cited medical images as a principal domain for content-based retrieval. CBIR has a potential for building a strong impact in diagnostics, research, and education. CBIR is a promising technology to enhance the core functionality of picture archiving and communication systems (PACS).

In this work mammogram images and sonogram images are used. In digital mammogram the CBMIR system is used for retrieving images with similar abnormality while in sonogram images the system retrieves similar grade images.

Problems with Existing Systems

From the literature survey conducted in section 3.4, certain challenges and problems that exist in the current content based medical image retrieval systems are observed.

1. Lack of intelligible features to express the visual content in images.
2. Usually in a general purpose CBIR system the subtle difference between images are ignored for matching. But in medical image retrieval systems subtle differences are highly relevant. Therefore the identification of small and fine details is a challenging problem in medical image retrieval.

3. Dimensionality of features highly affects the quality and retrieval efficiency.
4. Difficulty in representing the user's requirement.

To overcome the above mentioned problems we have designed excellent methods for noise reduction, contrast enhancement and for the extraction of most relevant features. Principal component analysis is used to reduce feature dimension. Finally a multiple image query system is proposed using logical operations.

6.6 Proposed Multiple Image Query System

Most of the existing systems support single image queries or image queries with single ROI. Tang et al. propose a method that uses multiple images for querying [418]. This method extracts one type of feature from one image and another type of feature from the other. The extracted features are combined and used for further similarity comparison. In Ref. [419], multiple image examples are preprocessed and combined to form a single query. Each query image is evaluated independently and the results are combined. In Ref. [420] a linear combination of the distances of a test image to all images in the query image set was used for distance calculation. Multitiered CBIR system for microscopic images is proposed in [421]. To protect the semantic consistency among the retrieved images, this system enables both multi-image query and slide level image retrieval. None of the existing systems use the concept of relational logical operators to combine different images in query.

We are proposing a multiple image query system in which images are combined using relational logical operators. The use of distance function is

characterized by the logical operation in the given query. To express the information need, single image or single region is not sufficient. The distinguishing feature of the proposed system is the use of complex queries with AND, OR and NOT logical operations. The query builder can build complex queries. According to the logical connective used, the system retrieves desired images. The similarity between the query image and the images in the database is obtained by calculating the distance of each feature of the query image and that of database image. In general, the distance function of query image and database image can be written as, $D(P_i, Q)$, where P_i is an image in the database and Q is the query image. Q can be single image or multiple images. The distance will be minimum for highly similar images and will be maximum for highly dissimilar images. The distance measure used in this study is Euclidean distance. Application of logical operations simplifies the retrieval process. For AND operation, the resultant image should be similar to both query images. It implies that the distance of each query image to the database images should be minimum. The distance function in this case is, $D(P_i,Q) = Max(d(P_i, Q_i))$, where (P_i, Q_i) is the distance between images P_i and Q_i in the feature space. For an OR operation the retrieved images should be highly similar to one of the query images. Images that are closest to either query image 1 or query image 2 are retrieved and the distance function is $D(P_i,Q) = Min(d(P_i, Q_i))$. If the user selects a 'NOT' operation the distance should be maximum. The algorithm is given below. Fig.6.2 shows the possible feature space for logical AND, OR and NOT operations.

ALGORITHM : MULTIPLE IMAGE QUERY CONTENT BASED IMAGE RETRIEVAL

Input **:** *Given the Compound Query Q*

Output **:** *Set of k similar images satisfying the condition given in the query*

Method:

Let $P_1, P_2, ..., P_m$ *be the database of images, Q be the given compound query.*

Step 1 **:** *Calculate feature vector of query images.*

Step 2 **:** *Compute the distance between query images and database images,* $D(P_i, Q)$ *as*

a) If AND then

$D(P_i,Q) = Max\ (d(P_i, Q_i))$

b) If OR then

$D(P_i,Q) = Min\ (d(P_i, Q_i))$

c) If NOT then

$D(P_i,Q) = -\ (d(P_i,Q))$

Where $d(P_i, Q_i)$ *is the distance between images* P_i *and* Q_i *in the feature space.*

Sort images according to $D(P_i, Q)$ *in ascending order and retrieve set of k similar images.*

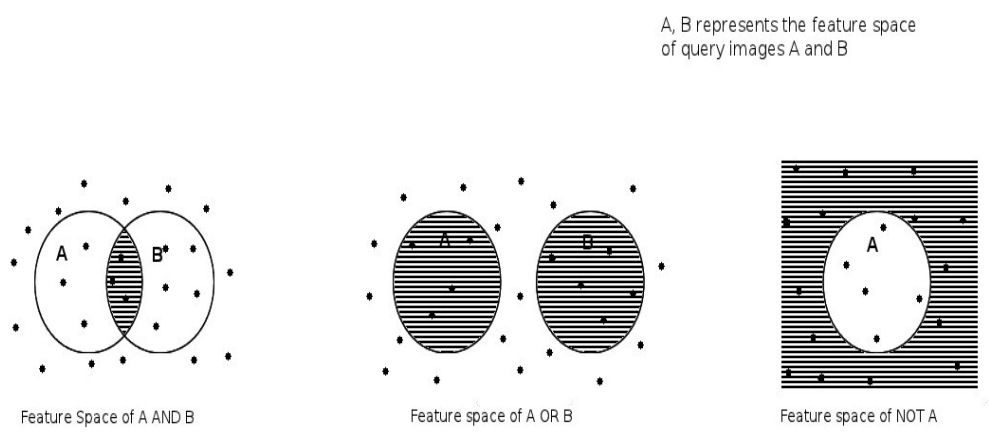

Figure 6.2 Feature Space for AND, OR and NOT operations in multiple image queries

Use of multiple image queries

1. Reduces the gap between machine understanding and user understanding by providing a platform for expressing the user's requirement in a better way.
2. It provides a platform for detailed knowledge representation, by combining more than one image.
3. It helps to see or to compare similar cases in medical diagnosis and provides assistance in medical image interpretation.
4. In the case of mammogram images it helps to learn the extend of malignancy by seeing images in intermediate stages.
5. Helps to reduce diagnostic variability by providing similar images.

6.7 Experimental Set up and Result Analysis

6.7.1 Single Image Queries

Digital Mammogram

This experiment investigates the performance of the proposed technique over a 322 -image mammography dataset taken from MIAS (Mammographic Image Analysis Society) database. The dataset comprises three classes: normal, benign and malignant images with different background tissue and abnormality. Contrast enhancement, background subtraction, pectoral muscle removal and ROI segmentation are applied before extracting features. A 285-dimensional feature vector was computed for each sample, and the features generated are:- Histogram statistics-6, Autocorrelation-1, Spatial Grey-Level-Dependence Matrix Features-6, Grey

Level Difference Statistics-4, Neighbourhood Grey-Tone-Difference Matrix Features-5, SFM-Features-4, Local Binary Patterns-256 and Wavelet Energy Descriptors-3.

The same type of features previously extracted from the reference images in the database is extracted from the query image in a similar manner. The features are input to the database and used to search the similar images, then the results are sorted according to the similarity with the best matches being reported to the user. The key objective of the study is to develop techniques to support medical decisions by efficiently retrieving significant past cases with proven pathology by searching for visually similar cases. When a specialist analyses a new image, he or she can submit the image as a query centre to a CBIR system, which will return the most similar images. Performance is evaluated using different classifiers with entire feature vector and reduced feature vector. The "dimensionality curse" that CBIR systems face when the number of features becomes large is solved by selecting features by applying Principal Component Analysis. As the number of features increases, the relevance of each feature decreases. In addition, some features may work as noise, and increases the computational complexity. This is avoided by PCA. After Principal Component Analysis the size of feature set is reduced to 5 as shown in Fig. 5.9. Fig. 6.3, Fig. 6.4, Fig.6.5 illustrates a CBIR output, from a dataset comprising normal, benign and malignant images. Table 6.1 shows the precision and recall of normal, benign and malignant cases of top 10 and top 20 retrieved images. Table 6.2 shows precision and recall of normal, benign and malignant cases of top 10 and top

20 retrieved images after principal component analysis. Precision and Recall chart for entire feature set and reduced feature set is given in Fig.6.6.

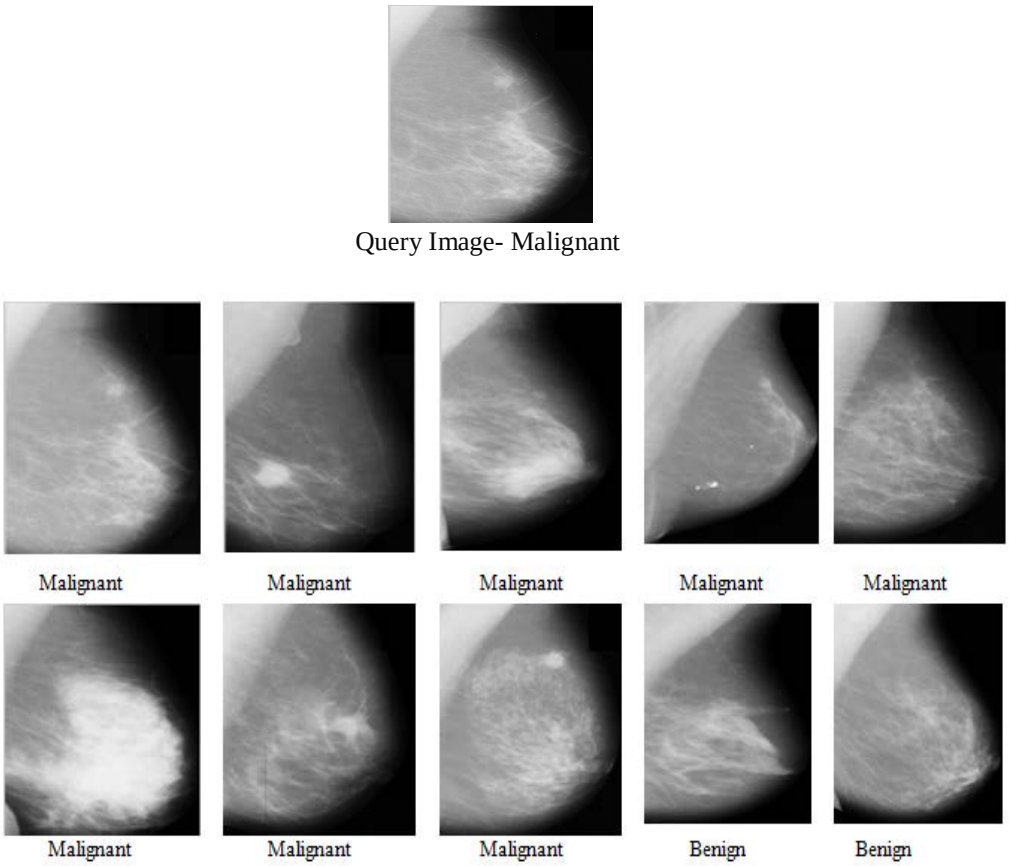

Figure 6.3 Result of single image query- Malignant image

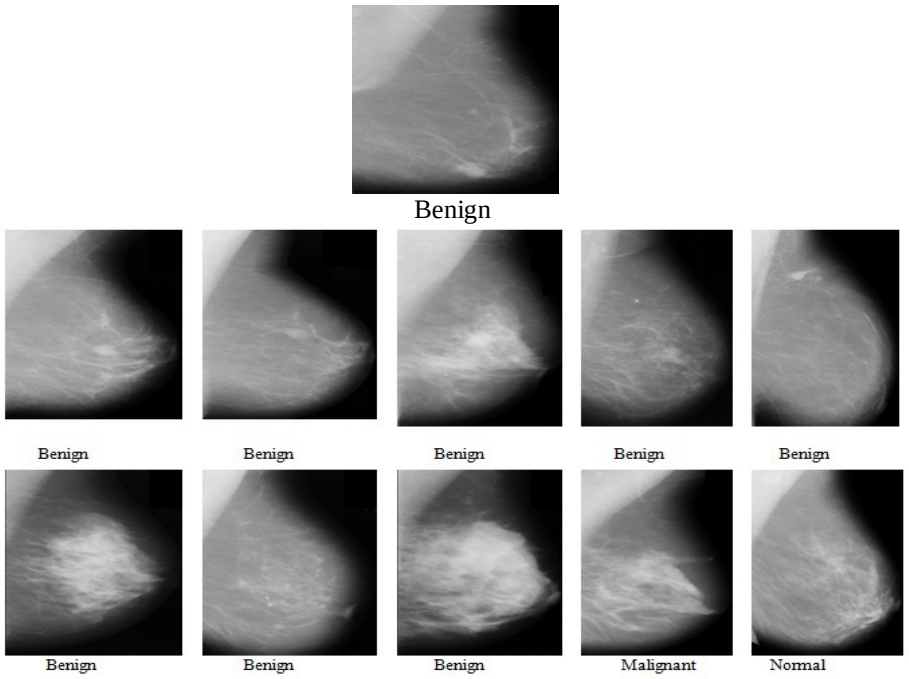

Figure 6.4 Result of single image query- Benign image

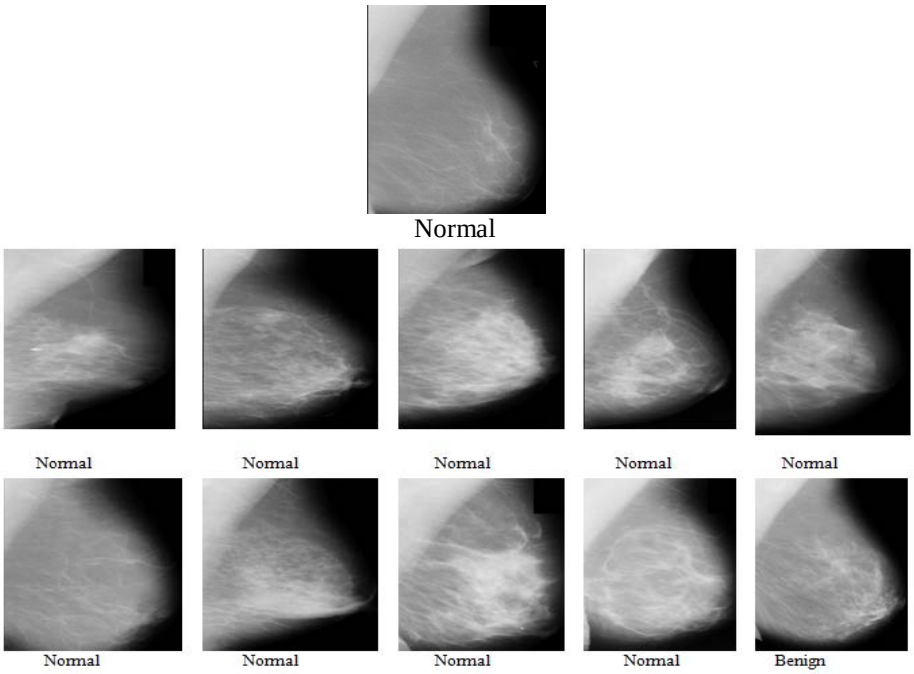

Figure 6.5 Result of single image query- Normal image

Table 6.1 Precision and recall of single image queries - mammogram images

Image Type	Top 10 Retrieval		Top 20 Retrieval	
	Precision	Recall	Precision	Recall
Normal	0.9	0.043	0.85	0.081
Benign	0.88	0.146	0.85	0.283
Malignant	0.96	0.192	0.95	0.38

Table 6.2 Precision and recall of single image queries after PCA- mammogram images

Image Type	Top 10 Retrieval		Top 20 Retrieval	
	Precision	Recall	Precision	Recall
Normal	0.87	0.042	0.83	0.079
Benign	0.86	0.145	0.80	0.271
Malignant	0.93	0.190	0.90	0.367

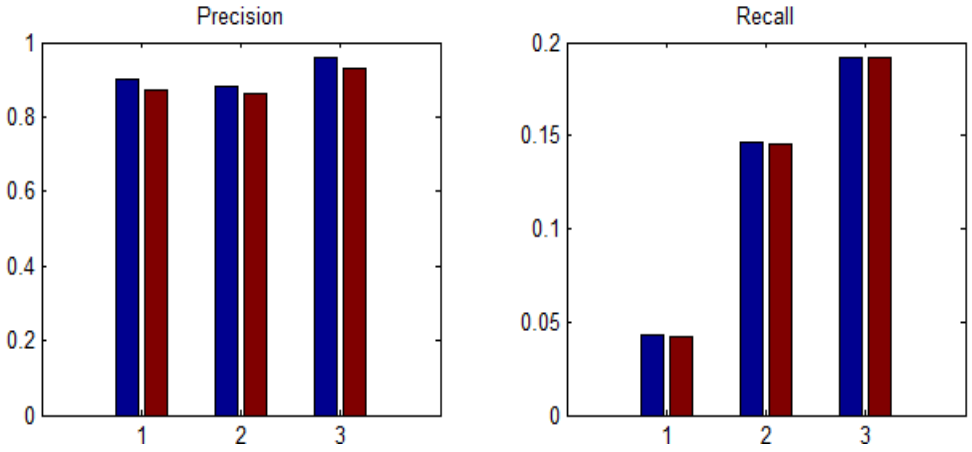

Figure 6.6 Precision and Recall chart for entire feature set and reduced feature set - Mammogram images

Single Image Queries – Placental Sonogram

This experiment also investigates the performance of the proposed technique using placenta images. The dataset includes four classes namely grade 0, grade 1, grade 2 and grade 3. Contrast enhancement, noise reduction and ROI segmentation are applied before extracting features. The feature vector consists of 297 features computed for each sample, namely by

Histogram statistics-6, Autocorrelation-1, Spatial Grey-Level-Dependence Matrix Features-6, Grey Level Difference Statistics-4, Neighbourhood Grey-Tone-Difference Matrix Features-5, SFM-Features-4, Local Binary Patterns-256, Wavelet Energy Descriptors-3, Moment invariants-7 and regional shape descriptors-5 . By inserting the given image into the retrieval system and there by obtaining the top most desired image the radiologist can arrive at conclusion in case of doubtful tissue in hand. Fig. 6.7, Fig. 6.8, Fig.6.9 and Fig.6.10 illustrates a CBIR output, from a dataset comprising grade 0, grade 1, grade 2 and grade3 placenta images. Table 6.3 shows the precision and recall of grade 0, grade1 grade2 and grade 3 cases of top 10 and top 20 retrieved images. Table 6.4 shows precision and recall of grade 0, grade1 grade2 and grade 3 cases of top 10 and top 20 retrieved images after principal component analysis. Precision and Recall chart for entire feature set and reduced feature set is given in Fig.6.11.

Query Image- Grade Zero

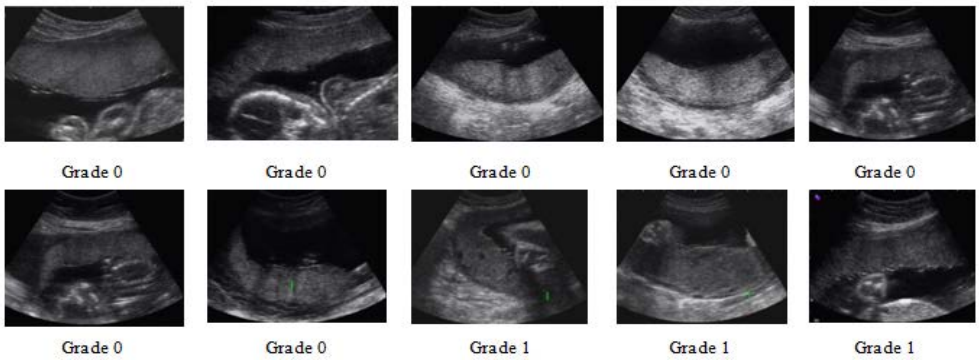

Figure 6.7 Result of single image query- grade 0

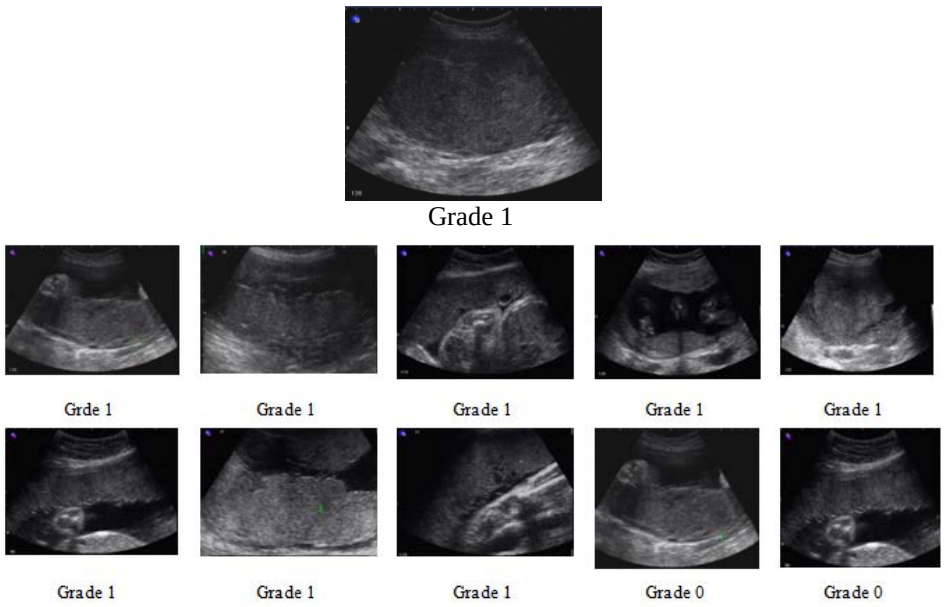

Figure 6.8 Result of single image query- grade 1

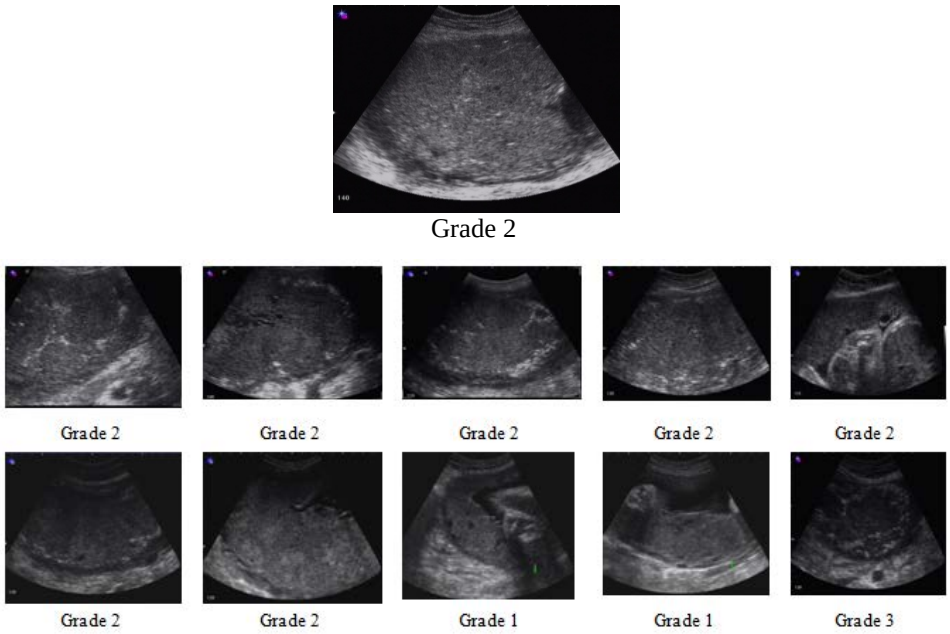

Figure 6.9 Result of single image query- grade 2

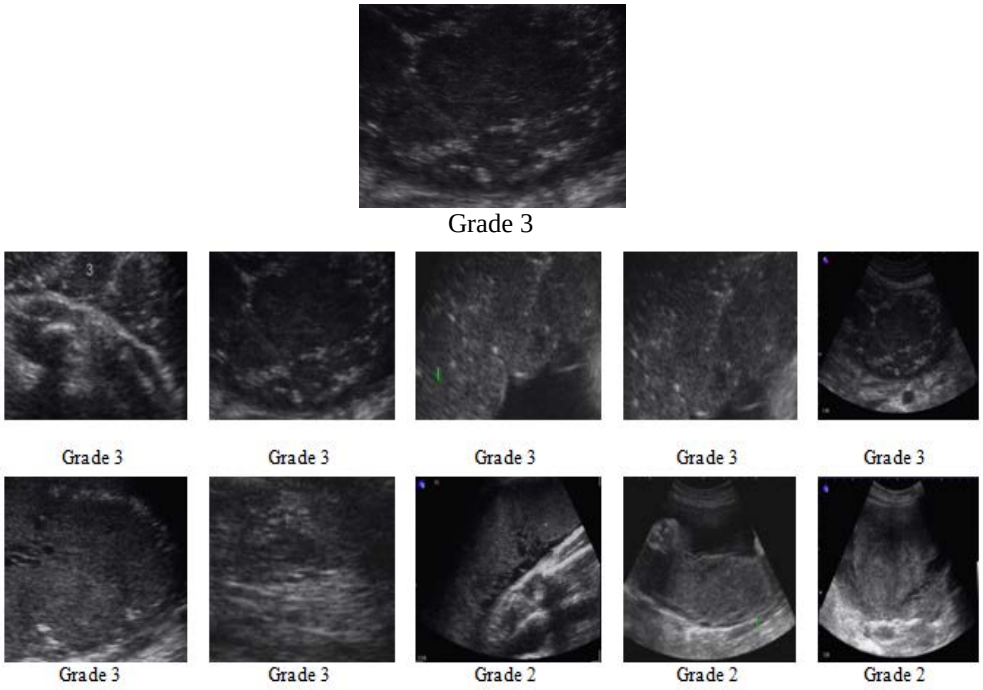

Figure 6.10 Result of single image query- grade 3

Table 6.3 Precision and recall of single image queries-Sonogram images

Image Type	Top 10 Retrieval		Top 20 Retrieval	
	Precision	Recall	Precision	Recall
Grade 0	0.85	0.115	0.80	0.216
Grade 1	0.78	0.083	0.70	0.149
Grade 2	0.79	0.123	0.75	0.234
Grade 3	0.81	0.279	0.75	0.517

Table 6.4 Precision and recall of single image queries after PCA-Sonogram sonogram

Image Type	Top 10 Retrieval		Top 20 Retrieval	
	Precision	Recall	Precision	Recall
Grade 0	0.84	0.114	0.75	0.203
Grade 1	0.77	0.082	0.70	0.149
Grade 2	0.78	0.122	0.70	0.219
Grade 3	0.81	0.279	0.75	0.517

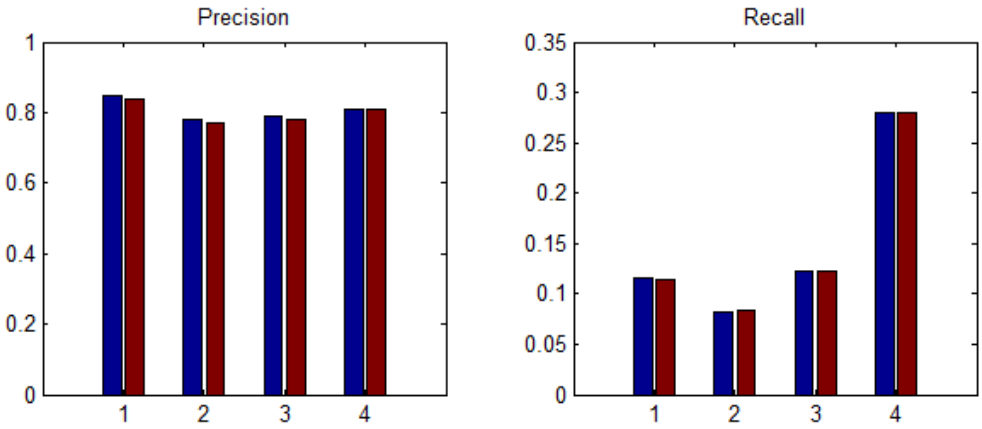

Figure 6.11 Precision and Recall chart for entire feature set and reduced feature set - Sonogram images.

6.7.2 Multiple image queries

The need for image retrieval with AND operation arises when there is a confusion regarding the class of test image. The retrieved images resemble both the query images when the 'AND' operation is used, which makes the classification perfect. Diagnostic variability arises where more than one scanning occurs which can be easily rectified using 'OR' operation. The correct classification is arrived when the retrieved images resemble only to one of the query images. Sample result is shown in Fig.6.12 and Fig 6.13. A 'NOT' operation is used when two images of the same patient taken at two different times show some difference. The result is obtained by considering two operations. The 'label 1 AND NOT label 2' operation retrieves a set of images which belongs to the class 'label 1' and the 'label 2 AND NOT label 1' operation retrieves a set of images which belongs to the class 'label2'. Comparing the ratio of the retrieved images with the total images, classification can be easily arrived at. In such a situation if only a single image is input, the images retrieved are not sufficient to arrive at a correct classification when compared to the images retrieved with 'NOT' operation.

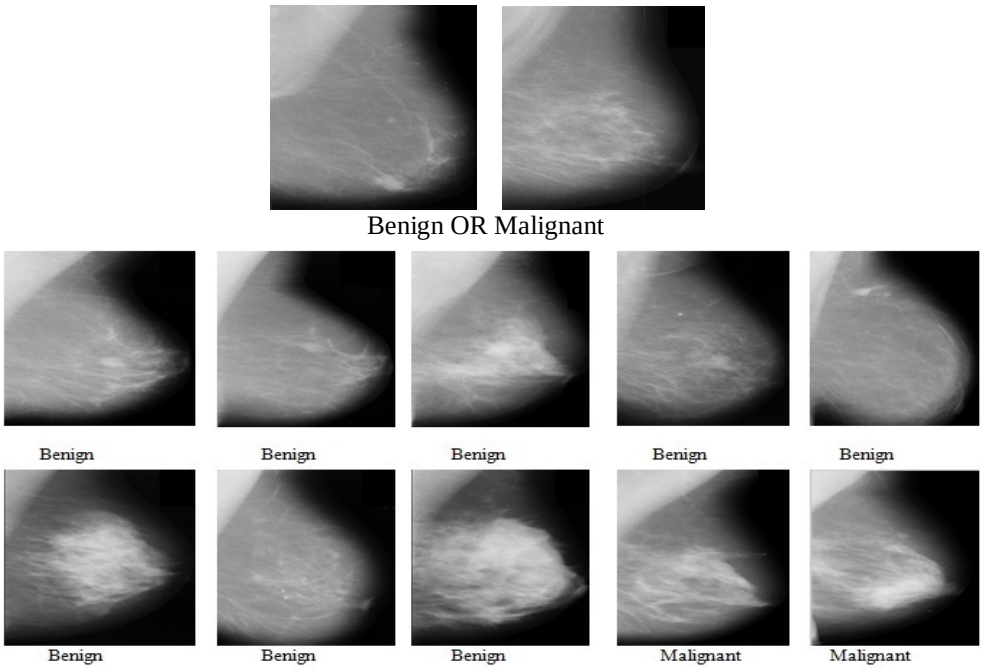

Figure 6.12 Result of OR operation between benign and malignant mammogram images

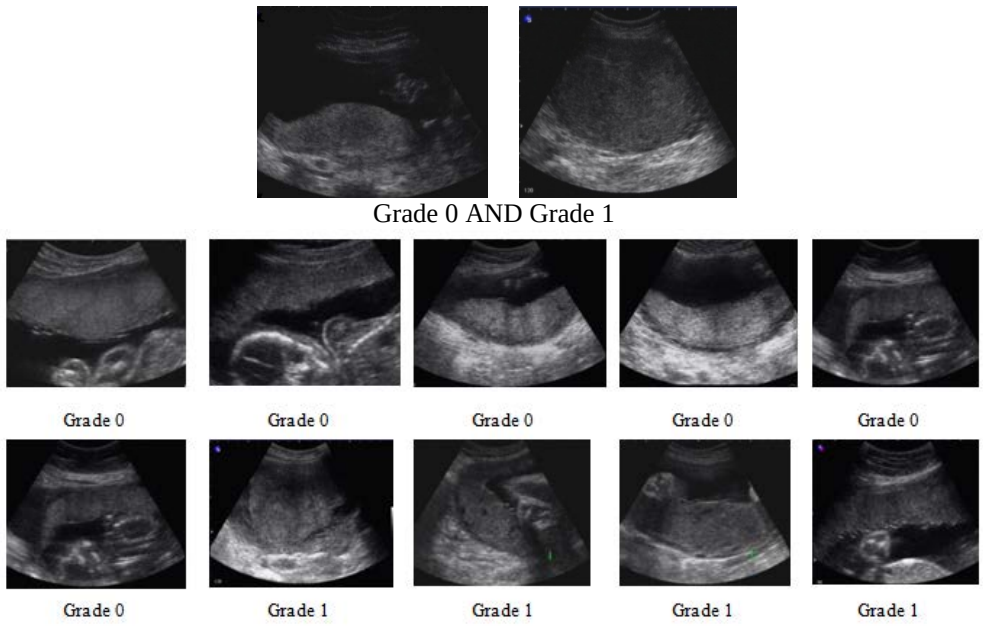

Figure 6.13 Result of AND operation between grade 0 and grade 1 placental images

6.8 Chapter Summary

A general purpose CBIR system is designed and experimented on different applications like character recognition, face recognition and the like. The need and challenges of CBIR in medical domain especially in cancer detection and placental grading directed this work towards medical image retrieval. A major contribution of this chapter is the design of a Content Based Image Retrieval system that supports queries with multiple images. In this system multiple images are combined using relational logical operators such as AND, OR and NOT. Depending on the logical connective used, the system retrieves desired images. The proposed system is tested with mammograms and placenta images. The results are promising.

Chapter 7

CONCLUSION AND FUTURE WORKS

7.1 Conclusion and Major Contributions

The thesis presents an image classification and retrieval system using Machine Learning techniques. It uses Digital Mammograms and Placental Sonograms for analysis. Mammogram Images are classified into normal, benign and malignant. Placental Images are classified into different grades according to the calcification content. The use and development of new algorithms and techniques could overcome many challenges that exist in conventional classification and retrieval systems.

A series of preprocessing operations are conducted on the low contrast high noisy mammogram and sonogram images. Different filters such as Mean, Median, Weiner and Diffusion are applied for removing the noises. Use of a new filter based on Local Binary Patterns gives good result in removing the speckle noise in ultrasound images by preserving the edges and small details in images. To remove the background information and pectoral muscle in mammogram, a two level segmentation is carried out, whereas in placental images the segmentation of region of interest is done manually.

Development and use of appropriate preprocessing operation helps in the extraction of intelligible features which give at most accuracy in classification and retrieval. The proposed work extracts different intensity, texture and shape features which include Histogram statistics, Autocorrelation, Spatial Grey-Level-

Dependence Matrix Features, Grey Level Difference Statistics, Neighbourhood Grey-Tone-Difference Matrix–Features, SFM - Features, Local Binary Patterns, Wavelet Energy Descriptors, Moment Invariants and Regional Shape Descriptors. Identification of the best feature combination for the classification and retrieval of mammogram and placental sonogram images is a major contribution of this work.

In the classification stage, supervised classification using the entire feature set and reduced feature set, which is obtained after Principal Component Analysis are done. Different classifiers such as Multi Layer Perceptrons (MLP), Decision Trees, Support Vector Machines (SVM) and Extreme Learning Machines (ELM) are used. Use of ensemble increases classification accuracy. The novelty in the classification process is the use of ELM for classifying placental images into different grades.

The work also includes the design and use of a CBIR system for retrieving similar images. A general CBIR system is developed and tested with mammograms, sonograms, handwritten Malayalam characters and facial images and thereafter a specific system that can be used for medical applications is designed. The use of CBIR systems with multiple image queries for retrieving desired images is the major contribution here. Multiple images are combined using relational logical operators such as AND, OR and NOT. Most of the existing systems support single image queries or image queries with single ROI. Therefore the use of CBIR system with multiple images is a landmark in the theoretical framework of CBIR.

7.2 Future Suggestions

The proposed work has the potential for further developments because of its simplicity and encouraging results that will motivate its incorporation into real time scanning systems.

- Use of larger database with non visual features attached to the images can also be tried.
- Extraction of more localized features from digital mammograms and placental sonograms.
- Further investigation would be needed in the study of the clinical utility of placental maturity analysis.
- CBIR system should have the ability to track temporal information because most of the diagnosis and treatment process involve a series of follow ups.
- New user interfaces for annotating, browsing and searching based on image content need to be investigated. Research in this area will require usability studies with practitioners.

REFERENCES

[1] T. M. Deserno, *Biomedical image processing*: Springerverlag Berlin Heidelberg, 2011.

[2] C. L. Rock, C. Pande, S. W. Flatt, C. Ying, B. Pakiz, B. A. Parker, *et al.*, "Favorable changes in serum estrogens and other biologic factors after weight loss in breast cancer survivors who are overweight or obese," *Clinical breast cancer*, 2013.

[3] Y. Yao, "Segmentation of breast cancer mass in mammograms and detection using Magnetic Resonance Imaging," *IEEE Image Processing Soc. J. pp*, pp. 561-567, 2004.

[4] R. Rhoades and G. A. Tanner, *Medical physiology*: Little, Brown Boston, 1995.

[5] P. A. Grannum, R. Berkowitz, and J. C. Hobbins, "The ultrasonic changes in the maturing placenta and their relation to fetal pulmonic maturity," *American journal of obstetrics and gynecology*, vol. 133, p. 915, 1979.

[6] R. da Silva Torres and A. X. Falcão, "Content-Based Image Retrieval: Theory and Applications," *RITA*, vol. 13, pp. 161-185, 2006.

[7] A. W. Smeulders, M. Worring, S. Santini, A. Gupta, and R. Jain, "Content-based image retrieval at the end of the early years," *Pattern Analysis and Machine Intelligence, IEEE Transactions on*, vol. 22, pp. 1349-1380, 2000.

[8] K. Thangavel, M. Karnan, R. Sivakumar, and A. K. Mohideen, "Automatic detection of microcalcification in mammograms-a review," *International Journal on Graphics, Vision and Image Processing*, vol. 5, pp. 31-61, 2005.

[9] K. Bhanu Prakash, A. Ramakrishnan, S. Suresh, and T. W. Chow, "Fetal lung maturity analysis using ultrasound image features," *Information Technology in Biomedicine, IEEE Transactions on*, vol. 6, pp. 38-45, 2002.

[10] A. Sau, P. Seed, and K. Langford, "Intraobserver and interobserver variation in the sonographic grading of placental maturity," *Ultrasound in obstetrics & gynecology*, vol. 23, pp. 374-377, 2004.

[11] R. L. Siegle, E. M. Baram, S. R. Reuter, E. A. Clarke, J. L. Lancaster, and C. A. McMahan, "Rates of disagreement in imaging interpretation in a group of community hospitals," *Academic radiology*, vol. 5, pp. 148-154, 1998.

[12] C. A. Almeida and S. A. Barry, *Cancer: basic science and clinical aspects*: Wiley-Blackwell, 2011.

[13] R. Siegel, D. Naishadham, and A. Jemal, "Cancer statistics, 2013," *CA: A Cancer Journal for Clinicians*, vol. 63, pp. 11-30, 2013.

[14] C. DeSantis, R. Siegel, P. Bandi, and A. Jemal, "Breast cancer statistics, 2011," *CA: A Cancer Journal for Clinicians*, vol. 61, pp. 408-418, 2011.

[15] A. Jemal, T. Murray, E. Ward, A. Samuels, R. C. Tiwari, A. Ghafoor, *et al.*, "Cancer statistics, 2005," *CA: a cancer journal for clinicians*, vol. 55, pp. 10-30, 2005.

[16] S. H. Landis, T. Murray, S. Bolden, and P. A. Wingo, "Cancer statistics, 1999," *CA: A cancer Journal for Clinicians*, vol. 49, pp. 8-31, 1999.

[17] http://www.breastcancerindia.net.

[18] K. McPherson, C. Steel, and J. Dixon, "ABC of breast diseases: breast cancer—epidemiology, risk factors, and genetics," *BMJ: British Medical Journal*, vol. 321, p. 624, 2000.

[19] S. J. Nass and I. C. Henderson, *Mammography and beyond: developing technologies for the early detection of breast cancer*: National Academies Press, 2001.

[20] E. Institute, "Top 10 Health Technology Hazards for 2011," *Health Devices*, vol. 39, pp. 404-16, 2010.

[21] L. Tabar, A. Gad, L. Holmberg, U. Ljungquist, C. Fagerberg, L. Baldetorp, *et al.*, "Reduction in mortality from breast cancer after mass screening with mammography: randomised trial from the Breast Cancer Screening Working Group of the Swedish National Board of Health and Welfare," *The Lancet*, vol. 325, pp. 829-832, 1985.

[22] A. C. o. R. B.-R. Committee and A. C. o. Radiology, *Breast imaging reporting and data system*: American College of Radiology, 1998.

[23] K. H. Dow, *Contemporary issues in breast cancer: a nursing perspective*: Jones & Bartlett Learning, 2004.

[24] J. Bozek, M. Mustra, K. Delac, and M. Grgic, "A survey of image processing algorithms in digital mammography," in *Recent Advances in Multimedia Signal Processing and Communications*, ed: Springer, 2009, pp. 631-657.

[25] C. Yarbro, D. Wujcik, and B. H. Gobel, *Cancer nursing: principles and practice*: Jones & Bartlett Learning, 2010.

[26] L. Costaridou, *Medical image analysis methods*: CRC Press, 2005.

[27] G. Dougherty, *Digital image processing for medical applications* vol. 1: Cambridge University Press New York, 2009.

[28] K. Iniewski, *Medical imaging: principles, detectors, and electronics*: Wiley-Interscience, 2009.

[29] J. Pitkin, A. B. Peattie, and B. Magowan, "Obstetrics and gynaecology: an illustrated colour text," 2003.

[30] P. Linares, P. J. McCullagh, N. D. Black, and J. Dornan, "Feature selection for the characterization of ultrasonic images of the placenta using texture classification," in *Biomedical Imaging: Nano to Macro, 2004. IEEE International Symposium on*, 2004, pp. 1147-1150.

[31] C.-Y. Chen, H.-W. Su, S.-H. Pai, C.-W. Hsieh, T.-L. Jong, C.-S. Hsu, *et al.*, "Evaluation of placental maturity by the sonographic textures," *Archives of gynecology and obstetrics*, vol. 284, pp. 13-18, 2011.

[32] H. A. Guimarães Filho, L. L. D. da Costa, E. A. Júnior, L. M. M. Nardozza, P. M. Nowak, A. F. Moron, *et al.*, "Placenta: angiogenesis and vascular assessment through three-dimensional power Doppler ultrasonography," *Archives of gynecology and obstetrics*, vol. 277, pp. 195-200, 2008.

[33] K. Benirschke, P. Kaufmann, and R. N. Baergen, *Pathology of the human placenta* vol. 6: Springer, 2006.

[34] J. Abramowicz and E. Sheiner, "Ultrasound of the placenta: a systematic approach. Part I: imaging," *Placenta*, vol. 29, pp. 225-240, 2008.

[35] C. M. Salafia, V. K. Minior, J. C. Pezzullo, E. J. Popek, T. S. Rosenkrantz, and A. M. Vintzileos, "Intrauterine growth restriction in infants of less than thirty-two weeks' gestation: associated placental pathologic features," *American journal of obstetrics and gynecology*, vol. 173, pp. 1049-1057, 1995.

[36] M. Damodaram, L. Story, E. Eixarch, A. Patel, A. McGuinness, J. Allsop, *et al.*, "Placental MRI in intrauterine fetal growth restriction," *Placenta*, vol. 31, pp. 491-498, 2010.

[37] R. M. Rangayyan, F. J. Ayres, and J. Leo Desautels, "A review of computer-aided diagnosis of breast cancer: Toward the detection of subtle signs," *Journal of the Franklin Institute*, vol. 344, pp. 312-348, 2007.

[38] L. B. Lusted, "Medical electronics," *The New England journal of medicine*, vol. 252, p. 580, 1955.

[39] F. Winsberg, M. Elkin, J. Macy, V. Bordaz, and W. Weymouth, "Detection of radiographic abnormalities in mammograms by means of optical scanning and computer analysis," *Radiology*, vol. 89, pp. 211-215, 1967.

[40] D. J. GETTY, R. M. PICKETT, C. J. D'ORSI, and J. A. SWETS, "Enhanced interpretation of diagnostic images," *Investigative radiology*, vol. 23, pp. 240-252, 1988.

[41] H.-P. Chan, K. Doi, C. J. VYBRONY, R. A. Schmidt, C. E. Metz, K. L. Lam, *et al.*, "Improvement in radiologists' detection of clustered microcalcifications on mammograms: The potential of computer-aided diagnosis," *Investigative radiology*, vol. 25, pp. 1102-1110, 1990.

[42] H. D. Cheng, X. Cai, X. Chen, L. Hu, and X. Lou, "Computer-aided detection and classification of microcalcifications in mammograms: a survey," *Pattern Recognition*, vol. 36, pp. 2967-2991, 12// 2003.

[43] R. Gordon and R. M. Rangayyan, "Feature enhancement of film mammograms using fixed and adaptive neighborhoods," *Applied Optics*, vol. 23, pp. 560-564, 1984.

[44] A. P. Dhawan, G. Buelloni, and R. Gordon, "Enhancement of mammographic features by optimal adaptive neighborhood image processing," *Medical Imaging, IEEE Transactions on*, vol. 5, pp. 8-15, 1986.

[45] J. K. Kim, J. M. Park, K. S. Song, and H. W. Park, "Adaptive mammographic image enhancement using first derivative and local statistics," *Medical Imaging, IEEE Transactions on*, vol. 16, pp. 495-502, 1997.

[46] G. Kom, A. Tiedeu, and M. Kom, "Automated detection of masses in mammograms by local adaptive thresholding," *Computers in Biology and Medicine*, vol. 37, pp. 37-48, 2007.

[47] C. Varela, P. G. Tahoces, A. J. Méndez, M. Souto, and J. J. Vidal, "Computerized detection of breast masses in digitized mammograms," *Computers in Biology and Medicine*, vol. 37, pp. 214-226, 2007.

[48] L. C. Romualdo, M. A. Vieira, H. Schiabel, N. D. Mascarenhas, and L. R. Borges, "Mammographic Image Denoising and Enhancement Using the Anscombe Transformation, Adaptive Wiener Filtering, and the Modulation Transfer Function," *Journal of Digital Imaging*, pp. 1-15.

[49] A. Hassanien, "Fuzzy rough sets hybrid scheme for breast cancer detection," *Image and vision computing*, vol. 25, pp. 172-183, 2007.

[50] H. Cheng and H. Xu, "A novel fuzzy logic approach to mammogram contrast enhancement," *Information Sciences*, vol. 148, pp. 167-184, 2002.

[51] J. Jiang, B. Yao, and A. Wason, "Integration of fuzzy logic and structure tensor towards mammogram contrast enhancement," *Computerized medical imaging and graphics: the official journal of the Computerized Medical Imaging Society*, vol. 29, p. 83, 2005.

[52] P. Gorgel, A. Sertbas, and O. N. Ucan, "A wavelet-based mammographic image denoising and enhancement with homomorphic filtering," *Journal of medical systems*, vol. 34, pp. 993-1002, 2010.

[53] N.-C. Tsai, H.-W. Chen, and S.-L. Hsu, "Computer-aided diagnosis for early-stage breast cancer by using Wavelet Transform," *Computerized Medical Imaging and Graphics*, vol. 35, pp. 1-8, 2011.

[54] S. Mohan and M. Ravishankar, "Optimized Histogram Based Contrast Limited Enhancement for Mammogram Images," 2013.

[55] A. F. Laine, S. Schuler, J. Fan, and W. Huda, "Mammographic feature enhancement by multiscale analysis," *Medical Imaging, IEEE Transactions on*, vol. 13, pp. 725-740, 1994.

[56] J. Scharcanski and C. R. Jung, "Denoising and enhancing digital mammographic images for visual screening," *Computerized Medical Imaging and Graphics*, vol. 30, pp. 243-254, 2006.

[57] A. Mencattini, M. Salmeri, R. Lojacono, M. Frigerio, and F. Caselli, "Mammographic images enhancement and denoising for breast cancer detection using dyadic wavelet processing," *Instrumentation and Measurement, IEEE Transactions on*, vol. 57, pp. 1422-1430, 2008.

[58] M. Bhattacharya and A. Das, "Fuzzy logic based segmentation of microcalcification in breast using digital mammograms considering multiresolution," in *Machine Vision and Image Processing Conference, 2007. IMVIP 2007. International*, 2007, pp. 98-105.

[59] A. Papadopoulos, D. Fotiadis, and L. Costaridou, "Improvement of microcalcification cluster detection in mammography utilizing image enhancement techniques," *Computers in biology and medicine*, vol. 38, pp. 1045-1055, 2008.

[60] R. C. Gonzalez and R. Woods, "Digital image processing (International ed.)," ed: Upper Saddle River, NJ: Prentice Hall, 2008.

[61] D. Brzakovic, X. Luo, and P. Brzakovic, "An approach to automated detection of tumors in mammograms," *Medical Imaging, IEEE Transactions on*, vol. 9, pp. 233-241, 1990.

[62] T. Matsubara, H. Fujita, S. Kasai, M. Goto, Y. Tani, T. Hara, *et al.*, "Development of new schemes for detection and analysis of mammographic masses," in *Intelligent Information Systems, 1997. IIS'97. Proceedings*, 1997, pp. 63-66.

[63] A. Dominguez and A. K. Nandi, "Enhanced multi-level thresholding segmentation and rank based region selection for detection of masses in mammograms," in *Acoustics, Speech and Signal Processing, 2007. ICASSP 2007. IEEE International Conference on*, 2007, pp. I-449-I-452.

[64] M. Kallergi, K. Woods, L. P. Clarke, W. Qian, and R. A. Clark, "Image segmentation in digital mammography: comparison of local thresholding and region growing algorithms," *Computerized medical imaging and graphics*, vol. 16, pp. 323-331, 1992.

[65] L. Sherr, R. M. RangayyarJ, and J. L. Desautels, "Detection and classification of mammographic calcifications," *State of the Art in Digital Mammographic Image Analysis*, vol. 9, p. 198, 1994.

[66] I. N. Bankman, T. Nizialek, I. Simon, O. B. Gatewood, I. N. Weinberg, and W. R. Brody, "Segmentation algorithms for detecting microcalcifications in mammograms," *Information Technology in Biomedicine, IEEE Transactions on,* vol. 1, pp. 141-149, 1997.

[67] A. Rojas Domínguez and A. K. Nandi, "Toward breast cancer diagnosis based on automated segmentation of masses in mammograms," *Pattern Recognition,* vol. 42, pp. 1138-1148, 2009.

[68] T. A. Docusse, A. S. Pereira, and N. Marranghello, "Microcalcification border characterization," *Engineering in Medicine and Biology Magazine, IEEE,* vol. 28, pp. 41-43, 2009.

[69] M. A. Wirth and A. Stapinski, "Segmentation of the breast region in mammograms using active contours," in *Visual Communications and Image Processing 2003*, 2003, pp. 1995-2006.

[70] M. Elter and A. Horsch, "CADx of mammographic masses and clustered microcalcifications: a review," *Medical physics,* vol. 36, p. 2052, 2009.

[71] G. M. Te Brake and N. Karssemeijer, "Segmentation of suspicious densities in digital mammograms," *Medical Physics,* vol. 28, p. 259, 2001.

[72] J. Shi, B. Sahiner, H.-P. Chan, J. Ge, L. Hadjiiski, M. A. Helvie, *et al.*, "Characterization of mammographic masses based on level set segmentation with new image features and patient information," *Medical physics,* vol. 35, p. 280, 2008.

[73] Y. Yuan, M. L. Giger, H. Li, K. Suzuki, and C. Sennett, "A dual-stage method for lesion segmentation on digital mammograms," *Medical physics,* vol. 34, p. 4180, 2007.

[74] W. Qian, M. Kallergi, L. P. Clarke, H.-D. Li, P. Venugopal, D. Song, *et al.*, "Tree structured wavelet transform segmentation of microcalcifications in digital mammography," *Medical physics,* vol. 22, p. 1247, 1995.

[75] R. N. Strickland and H. I. Hahn, "Wavelet transforms for detecting microcalcifications in mammograms," *Medical Imaging, IEEE Transactions on,* vol. 15, pp. 218-229, 1996.

[76] J. J. Heine, S. R. Deans, D. K. Cullers, R. Stauduhar, and L. P. Clarke, "Multiresolution statistical analysis of high-resolution digital mammograms," *Medical Imaging, IEEE Transactions on,* vol. 16, pp. 503-515, 1997.

[77] T. C. Wang and N. B. Karayiannis, "Detection of microcalcifications in digital mammograms using wavelets," *Medical Imaging, IEEE Transactions on,* vol. 17, pp. 498-509, 1998.

[78] E. Regentova, L. Zhang, J. Zheng, and G. Veni, "Microcalcification detection based on wavelet domain hidden markov tree model: study for inclusion to computer aided diagnostic prompting system," *Medical physics,* vol. 34, p. 2206, 2007.

[79] N. Arikidis, A. Karahaliou, S. Skiadopoulos, P. Korfiatis, E. Likaki, G. Panayiotakis, *et al.*, "Size-adapted segmentation of individual mammographic microcalcifications," in *BioInformatics and BioEngineering, 2008. BIBE 2008. 8th IEEE International Conference on*, 2008, pp. 1-5.

[80] D. Zhao, M. Shridhar, and D. Daut, "Morphology on detection of calcifications in mammograms," in *Acoustics, Speech, and Signal Processing, 1992. ICASSP-92., 1992 IEEE International Conference on*, 1992, pp. 129-132.

[81] X. Gao, Y. Wang, X. Li, and D. Tao, "On combining morphological component analysis and concentric morphology model for mammographic mass detection," *Information Technology in Biomedicine, IEEE Transactions on*, vol. 14, pp. 266-273, 2010.

[82] A. Wroblewska, P. Boninski, A. Przelaskowski, and M. Kazubek, "Segmentation and feature extraction for reliable classification of microcalcifications in digital mammograms," *Optoelectronics Review*, pp. 227-236, 2003.

[83] A. Oliver, J. Freixenet, R. Marti, J. Pont, E. Pérez, E. R. Denton, *et al.*, "A novel breast tissue density classification methodology," *Information Technology in Biomedicine, IEEE Transactions on*, vol. 12, pp. 55-65, 2008.

[84] B. Ojeda-Magaña, J. Quintanilla-Domínguez, R. Ruelas, and D. Andina, "Images sub-segmentation with the pfcm clustering algorithm," in *Industrial Informatics, 2009. INDIN 2009. 7th IEEE International Conference on*, 2009, pp. 499-503.

[85] H. Li, K. R. Liu, and S.-C. Lo, "Fractal modeling and segmentation for the enhancement of microcalcifications in digital mammograms," *Medical Imaging, IEEE Transactions on*, vol. 16, pp. 785-798, 1997.

[86] F. Lefebvre, H. Benali, R. Gilles, E. Kahn, and R. Di Paola, "A fractal approach to the segmentation of microcalcifications in digital mammograms," *Medical Physics*, vol. 22, p. 381, 1995.

[87] C. Zhou, L. M. Hadjiiski, C. Paramagul, B. Sahiner, H.-P. Chan, and J. Wei, "Computerized pectoral muscle identification on MLO-view mammograms for CAD applications," in *Medical Imaging*, 2005, pp. 852-857.

[88] S. M. Kwok, R. Chandrasekhar, Y. Attikiouzel, and M. T. Rickard, "Automatic pectoral muscle segmentation on mediolateral oblique view mammograms," *Medical Imaging, IEEE Transactions on*, vol. 23, pp. 1129-1140, 2004.

[89] J. Suckling, D. Dance, E. Moskovic, D. Lewis, and S. Blacker, "Segmentation of mammograms using multiple linked self-organizing neural networks," *Medical Physics*, vol. 22, p. 145, 1995.

[90] M. Masek, R. Chandrasekhar, C. Desilva, and Y. Attikiouzel, "Spatially based application of the minimum cross-entropy thresholding algorithm to segment the pectoral muscle in mammograms," in *Intelligent Information Systems Conference, The Seventh Australian and New Zealand 2001*, 2001, pp. 101-106.

[91] N. Karssemeijer, "Automated classification of parenchymal patterns in mammograms," *Physics in medicine and biology*, vol. 43, p. 365, 1998.

[92] R. Ferrari, R. Rangayyan, J. Desautels, and A. Frere, "Segmentation of mammograms: identification of the skin-air boundary, pectoral muscle, and fibro-glandular disc," in *Proceedings of the 5th international workshop on digital Mammography*, 2000, pp. 573-579.

[93] M. Yam, M. Brady, R. Highnam, C. Behrenbruch, R. English, and Y. Kita, "Three-dimensional reconstruction of microcalcification clusters from two mammographic views," *Medical Imaging, IEEE Transactions on*, vol. 20, pp. 479-489, 2001.

[94] S. Kinoshita, P. Azevedo-Marques, R. Pereira Jr, J. Rodrigues, and R. Rangayyan, "Radon-domain detection of the nipple and the pectoral muscle in mammograms," *Journal of Digital Imaging*, vol. 21, pp. 37-49, 2008.

[95] I. Domingues, J. Cardoso, I. Amaral, I. Moreira, P. Passarinho, J. Santa Comba, *et al.*, "Pectoral muscle detection in mammograms based on the shortest path with endpoints learnt by SVMs," in *Engineering in Medicine and Biology Society (EMBC), 2010 Annual International Conference of the IEEE*, 2010, pp. 3158-3161.

[96] A. Sultana, M. Ciuc, and R. Strungaru, "Detection of pectoral muscle in mammograms using a mean-shift segmentation approach," in *Communications (COMM), 2010 8th International Conference on*, 2010, pp. 165-168.

[97] K. S. Camilus, V. Govindan, and P. Sathidevi, "Computer-aided identification of the pectoral muscle in digitized mammograms," *Journal of digital imaging*, vol. 23, pp. 562-580, 2010.

[98] H. Li, Y. Wang, K. J. R. Liu, S.-C. Lo, and M. T. Freedman, "Computerized radiographic mass detection. I. Lesion site selection by morphological enhancement and contextual segmentation," *Medical Imaging, IEEE Transactions on*, vol. 20, pp. 289-301, 2001.

[99] L. Tarassenko, P. Hayton, N. Cerneaz, and M. Brady, "Novelty detection for the identification of masses in mammograms," in *Artificial Neural Networks, 1995., Fourth International Conference on*, 1995, pp. 442-447.

[100] Z. Huo, M. L. Giger, C. J. Vyborny, D. E. Wolverton, R. A. Schmidt, and K. Doi, "Automated computerized classification of malignant and benign masses on digitized mammograms," *Academic radiology*, vol. 5, pp. 155-168, 1998.

[101] I. Christoyianni, E. Dermatas, and G. Kokkinakis, "Fast detection of masses in computer-aided mammography," *Signal Processing Magazine, IEEE*, vol. 17, pp. 54-64, 2000.

[102] D. Davies and D. Dance, "Automatic computer detection of clustered calcifications in digital mammograms," *Physics in Medicine and Biology,* vol. 35, p. 1111, 1990.

[103] R. M. Nishikawa, Y. Jiang, M. L. Giger, C. Vyborny, and R. Schmidt, "Computer-aided detection of clustered microcalcifications," in *Systems, Man and Cybernetics, 1992., IEEE International Conference on*, 1992, pp. 1375-1378.

[104] K. S. Woods, C. C. DOSS, K. W. BOWYER, J. L. SOLKA, C. E. PRIEBE, and W. P. KEGELMEYER JR, "Comparative evaluation of pattern recognition techniques for detection of microcalcifications in mammography," *International Journal of Pattern Recognition and Artificial Intelligence,* vol. 7, pp. 1417-1436, 1993.

[105] Y. Jiang, R. M. Nishikawa, D. E. Wolverton, C. E. Metz, M. L. Giger, R. A. Schmidt, *et al.*, "Malignant and benign clustered microcalcifications: automated feature analysis and classification," *Radiology,* vol. 198, pp. 671-678, 1996.

[106] B. Zheng, W. Qian, and L. P. Clarke, "Digital mammography: mixed feature neural network with spectral entropy decision for detection of microcalcifications," *Medical Imaging, IEEE Transactions on,* vol. 15, pp. 589-597, 1996.

[107] S. Yu and L. Guan, "A CAD system for the automatic detection of clustered microcalcifications in digitized mammogram films," *Medical Imaging, IEEE Transactions on,* vol. 19, pp. 115-126, 2000.

[108] Z. Huo, M. L. Giger, and C. J. Vyborny, "Computerized analysis of multiple-mammographic views: Potential usefulness of special view mammograms in computer-aided diagnosis," *Medical Imaging, IEEE Transactions on,* vol. 20, pp. 1285-1292, 2001.

[109] N. Petrick, H.-P. Chan, B. Sahiner, and M. A. Helvie, "Combined adaptive enhancement and region-growing segmentation of breast masses on digitized mammograms," *Medical Physics,* vol. 26, p. 1642, 1999.

[110] F. Fauci, S. Bagnasco, R. Bellotti, D. Cascio, S. Cheran, F. De Carlo, *et al.*, "Mammogram segmentation by contour searching and massive lesion classification with neural network," in *Nuclear Science Symposium Conference Record, 2004 IEEE*, 2004, pp. 2695-2699.

[111] N. El-Faramawy, R. Rangayyan, J. Desautels, and O. Alim, "Shape factors for analysis of breast tumors in mammograms," in *Electrical and Computer Engineering, 1996. Canadian Conference on*, 1996, pp. 355-358.

[112] J. S. DaPonte and P. Sherman, "Classification of ultrasonic image texture by statistical discriminant analysis and neural networks," *Computerized medical imaging and graphics,* vol. 15, pp. 3-9, 1991.

[113] A. P. Dhawan, Y. Chitre, and C. Kaiser-Bonasso, "Analysis of mammographic microcalcifications using gray-level image structure features," *Medical Imaging, IEEE Transactions on,* vol. 15, pp. 246-259, 1996.

[114] J. K. Kim and H. W. Park, "Statistical textural features for detection of microcalcifications in digitized mammograms," *Medical Imaging, IEEE Transactions on,* vol. 18, pp. 231-238, 1999.

[115] B. Sahiner, H.-P. Chan, N. Petrick, M. A. Helvie, and M. M. Goodsitt, "Computerized characterization of masses on mammograms: The rubber band straightening transform and texture analysis," *Medical Physics,* vol. 25, p. 516, 1998.

[116] B. Sahiner, H.-P. Chan, N. Petrick, M. A. Helvie, and L. M. Hadjiiski, "Improvement of mammographic mass characterization using spiculation measures and morphological features," *Medical Physics,* vol. 28, p. 1455, 2001.

[117] J. S. Weszka, C. R. Dyer, and A. Rosenfeld, "A comparative study of texture measures for terrain classification," *Systems, Man and Cybernetics, IEEE Transactions on,* pp. 269-285, 1976.

[118] J. G. D. Hardin and P. R. Massopust, "Fractal functions and wavelet expansions based on several scaling functions," *Journal of Approximation Theory,* vol. 78, pp. 373-401, 1994.

[119] B. Sahiner, H.-P. Chan, N. Petrick, D. Wei, M. A. Helvie, D. D. Adler, *et al.*, "Classification of mass and normal breast tissue: a convolution neural network classifier with spatial domain and texture images," *Medical Imaging, IEEE Transactions on,* vol. 15, pp. 598-610, 1996.

[120] B. Sahiner, L. M. Hadjiiski, H.-P. Chan, C. Paramagul, A. Nees, M. Helvie, *et al.*, "Concordance of computer-extracted image features with BI-RADS descriptors for mammographic mass margin," in *Medical Imaging*, 2008, pp. 69151N-69151N-6.

[121] T. Netsch and H.-O. Peitgen, "Scale-space signatures for the detection of clustered microcalcifications in digital mammograms," *Medical Imaging, IEEE Transactions on,* vol. 18, pp. 774-786, 1999.

[122] S. Bothorel, B. Bouchon Meunier, and S. Muller, "A fuzzy logic based approach for semiological analysis of microcalcifications in mammographic images," *International Journal of Intelligent Systems,* vol. 12, pp. 819-848, 1997.

[123] M. Sameti, R. K. Ward, J. Morgan-Parkes, and B. Palcic, "Image feature extraction in the last screening mammograms prior to detection of breast cancer," *Selected Topics in Signal Processing, IEEE Journal of,* vol. 3, pp. 46-52, 2009.

[124] G. Braz Junior, A. Cardoso de Paiva, A. Corrêa Silva, and A. Cesar Muniz de Oliveira, "Classification of breast tissues using Moran's index and Geary's coefficient as texture signatures and SVM," *Computers in Biology and Medicine,* vol. 39, pp. 1063-1072, 2009.

[125] F. Moayedi, Z. Azimifar, R. Boostani, and S. Katebi, "Contourlet-based mammography mass classification using the SVM family," *Computers in Biology and Medicine,* vol. 40, pp. 373-383, 2010.

[126] I. Buciu and A. Gacsadi, "Directional features for automatic tumor classification of mammogram images," *Biomedical Signal Processing and Control*, vol. 6, pp. 370-378, 2011.

[127] L. Nanni, S. Brahnam, and A. Lumini, "A very high performing system to discriminate tissues in mammograms as benign and malignant," *Expert Systems With Applications*, vol. 39, pp. 1968-1971, 2012.

[128] S. K. Biswas and D. P. Mukherjee, "Recognizing architectural distortion in mammogram: a multiscale texture modeling approach with GMM," *Biomedical Engineering, IEEE Transactions on*, vol. 58, pp. 2023-2030, 2011.

[129] C. E. Priebe, J. L. Solka, R. A. Lorey, G. W. Rogers, W. L. Poston, M. Kallergi, *et al.*, "The application of fractal analysis to mammographic tissue classification," *Cancer letters*, vol. 77, pp. 183-189, 1994.

[130] G. D. Tourassi, D. M. Delong, and C. E. Floyd Jr, "A study on the computerized fractal analysis of architectural distortion in screening mammograms," *Physics in medicine and biology*, vol. 51, p. 1299, 2006.

[131] R. M. Rangayyan, S. Prajna, F. J. Ayres, and J. L. Desautels, "Detection of architectural distortion in prior screening mammograms using Gabor filters, phase portraits, fractal dimension, and texture analysis," *International Journal of Computer Assisted Radiology and Surgery*, vol. 2, pp. 347-361, 2008.

[132] Q. Guo, J. Shao, and V. F. Ruiz, "Characterization and classification of tumor lesions using computerized fractal-based texture analysis and support vector machines in digital mammograms," *International journal of computer assisted radiology and surgery*, vol. 4, pp. 11-25, 2009.

[133] H. Liu and L. Yu, "Toward integrating feature selection algorithms for classification and clustering," *Knowledge and Data Engineering, IEEE Transactions on*, vol. 17, pp. 491-502, 2005.

[134] K. Bovis, S. Singh, J. Fieldsend, and C. Pinder, "Identification of masses in digital mammograms with MLP and RBF nets," in *Neural Networks, 2000. IJCNN 2000, Proceedings of the IEEE-INNS-ENNS International Joint Conference on*, 2000, pp. 342-347.

[135] B. Sahiner, H.-P. Chan, D. Wei, N. Petrick, M. A. Helvie, D. D. Adler, *et al.*, "Image feature selection by a genetic algorithm: Application to classification of mass and normal breast tissue," *Medical Physics*, vol. 23, p. 1671, 1996.

[136] B. Verma and P. Zhang, "A novel neural-genetic algorithm to find the most significant combination of features in digital mammograms," *Applied Soft Computing*, vol. 7, pp. 612-625, 2007.

[137] B. Zheng, Y.-H. Chang, X.-H. Wang, and W. F. Good, "Comparison of artificial neural network and Bayesian belief network in a computer-assisted diagnosis scheme for mammography," in *Neural Networks, 1999. IJCNN'99. International Joint Conference on*, 1999, pp. 4181-4185.

[138] H. Cheng, X. Shi, R. Min, L. Hu, X. Cai, and H. Du, "Approaches for automated detection and classification of masses in mammograms," *Pattern recognition*, vol. 39, pp. 646-668, 2006.

[139] A. K. Mohanty, M. R. Senapati, and S. K. Lenka, "A novel image mining technique for classification of mammograms using hybrid feature selection," *Neural Computing and Applications*, pp. 1-11, 2012.

[140] N. R. Pal, B. Bhowmick, S. K. Patel, S. Pal, and J. Das, "A multi-stage neural network aided system for detection of microcalcifications in digitized mammograms," *Neurocomputing*, vol. 71, pp. 2625-2634, 2008.

[141] M. Suganthi and M. Madheswaran, "An improved medical decision support system to identify the breast cancer using mammogram," *Journal of medical systems*, vol. 36, pp. 79-91, 2012.

[142] K. Geetha and K. Thanushkodi, "New particle swarm optimization for feature selection and classification of microcalcifications in mammograms," in *Signal Processing, Communications and Networking, 2008. ICSCN'08. International Conference on*, 2008, pp. 458-463.

[143] K. R. Keerthana and K. Thangavel, "Feature selection in mammogram image using rough set approach," in *Innovations in Emerging Technology (NCOIET), 2011 National Conference on*, 2011, pp. 147-152.

[144] W. Han, J. Dong, Y. Guo, M. Zhang, and J. Wang, "Identification of masses in digital mammogram using an optimal set of features," in *Trust, Security and Privacy in Computing and Communications (TrustCom), 2011 IEEE 10th International Conference on*, 2011, pp. 1763-1768.

[145] J. Ren, D. Wang, and J. Jiang, "Effective recognition of MCCs in mammograms using an improved neural classifier," *Engineering Applications of Artificial Intelligence*, vol. 24, pp. 638-645, 2011.

[146] A. N. Karahaliou, I. S. Boniatis, S. G. Skiadopoulos, F. N. Sakellaropoulos, N. S. Arikidis, E. A. Likaki, *et al.*, "Breast cancer diagnosis: analyzing texture of tissue surrounding microcalcifications," *Information Technology in Biomedicine, IEEE Transactions on*, vol. 12, pp. 731-738, 2008.

[147] J. Dheeba and S. T. Selvi, "A Swarm Optimized Neural Network System for Classification of Microcalcification in Mammograms," *Journal of medical systems*, vol. 36, pp. 3051-3061, 2012.

[148] A. P. Dhawan, Y. S. Chitre, and M. Moskowitz, "Artificial-neural-network-based classification of mammographic microcalcifications using image structure features," in *IS&T/SPIE's Symposium on Electronic Imaging: Science and Technology*, 1993, pp. 820-831.

[149] I. N. Bankman, W. A. Christens-Barry, D. W. Kim, I. N. Weinberg, O. B. Gatewood, and W. R. Brody, "Automated recognition of microcalcification clusters in mammograms," in *IS&T/SPIE's Symposium on Electronic Imaging: Science and Technology*, 1993, pp. 731-738.

[150] D. Kramer and F. Aghdasi, "Classification of microcalcifications in digitised mammograms using multiscale statistical texture analysis," in *Communications and Signal Processing, 1998. COMSIG'98. Proceedings of the 1998 South African Symposium on*, 1998, pp. 121-126.

[151] R. Ferrari, A. de Carvalho, P. Azevedo Marques, and A. Frere, "Computerized classification of breast lesions: shape and texture analysis using an artificial neural network," in *Image Processing and Its Applications, 1999. Seventh International Conference on (Conf. Publ. No. 465)*, 1999, pp. 517-521.

[152] B. Verma and J. Zakos, "A computer-aided diagnosis system for digital mammograms based on fuzzy-neural and feature extraction techniques," *Information Technology in Biomedicine, IEEE Transactions on*, vol. 5, pp. 46-54, 2001.

[153] H. Soltanian-Zadeh, S. Pourabdollah-Nezhad, and F. Rafiee-Rad, "Shape-based and texture-based feature extraction for classification of microcalcifications in mammograms," in *PROC SPIE INT SOC OPT ENG*, 2001, pp. 301-310.

[154] M. P. Sampat, M. K. Markey, and A. C. Bovik, "Computer-aided detection and diagnosis in mammography," *Handbook of image and video processing*, vol. 10, pp. 1195-1217, 2005.

[155] B. Verma, "Novel network architecture and learning algorithm for the classification of mass abnormalities in digitized mammograms," *Artificial Intelligence in Medicine*, vol. 42, pp. 67-79, 2008.

[156] N. Kilic, P. Gorgel, O. N. Ucan, and A. Sertbas, "Mammographic mass detection using wavelets as input to neural networks," *Journal of medical systems*, vol. 34, pp. 1083-1088, 2010.

[157] E. Malar, A. Kandaswamy, D. Chakravarthy, and A. Giri Dharan, "A novel approach for detection and classification of mammographic microcalcifications using wavelet analysis and extreme learning machine," *Computers in Biology and Medicine*, 2012.

[158] T. Subashini, V. Ramalingam, and S. Palanivel, "Automated assessment of breast tissue density in digital mammograms," *Computer Vision and Image Understanding*, vol. 114, pp. 33-43, 2010.

[159] W. Borges Sampaio, E. Moraes Diniz, A. Corrêa Silva, A. Cardoso de Paiva, and M. Gattass, "Detection of masses in mammogram images using CNN, geostatistic functions and SVM," *Computers in biology and medicine*, vol. 41, pp. 653-664, 2011.

[160] Y. Zhang, N. Tomuro, J. Furst, and D. S. Raicu, "Building an ensemble system for diagnosing masses in mammograms," *International journal of computer assisted radiology and surgery*, vol. 7, pp. 323-329, 2012.

[161] S.-T. Luo and B.-W. Cheng, "Diagnosing breast masses in digital mammography using feature selection and ensemble methods," *Journal of medical systems*, vol. 36, pp. 569-577, 2012.

[162] P. M. Leod and B. Verma, "Variable Hidden Neuron Ensemble for Mass Classification in Digital Mammograms [Application Notes]," *Computational Intelligence Magazine, IEEE*, vol. 8, pp. 68-76, 2013.

[163] P. McLeod and B. Verma, "Clustered ensemble neural network for breast mass classification in digital mammography," in *Neural Networks (IJCNN), The 2012 International Joint Conference on*, 2012, pp. 1-6.

[164] D. West, P. Mangiameli, R. Rampal, and V. West, "Ensemble strategies for a medical diagnostic decision support system: A breast cancer diagnosis application," *European Journal of Operational Research*, vol. 162, pp. 532-551, 2005.

[165] B. Sahiner, N. Petrick, H.-P. Chan, L. M. Hadjiiski, C. Paramagul, M. A. Helvie, *et al.*, "Computer-aided characterization of mammographic masses: accuracy of mass segmentation and its effects on characterization," *Medical Imaging, IEEE Transactions on*, vol. 20, pp. 1275-1284, 2001.

[166] H. Li, M. Kallergi, L. Clarke, V. Jain, and R. Clark, "Markov random field for tumor detection in digital mammography," *Medical Imaging, IEEE Transactions on*, vol. 14, pp. 565-576, 1995.

[167] R. Campanini, D. Dongiovanni, E. Iampieri, N. Lanconelli, M. Masotti, G. Palermo, *et al.*, "A novel featureless approach to mass detection in digital mammograms based on support vector machines," *Physics in Medicine and Biology*, vol. 49, p. 961, 2004.

[168] J. Wei, B. Sahiner, L. M. Hadjiiski, H.-P. Chan, N. Petrick, M. A. Helvie, *et al.*, "Computer-aided detection of breast masses on full field digital mammograms," *Medical physics*, vol. 32, p. 2827, 2005.

[169] M. Fraschini, "Mammographic masses classification: novel and simple signal analysis method," *Electronics letters*, vol. 47, pp. 14-15, 2011.

[170] B. Verma, P. McLeod, and A. Klevansky, "A novel soft cluster neural network for the classification of suspicious areas in digital mammograms," *Pattern Recognition*, vol. 42, pp. 1845-1852, 2009.

[171] B. Verma, P. McLeod, and A. Klevansky, "Classification of benign and malignant patterns in digital mammograms for the diagnosis of breast cancer," *Expert Systems with Applications*, vol. 37, pp. 3344-3351, 2010.

[172] J. Ren, "ANN vs. SVM: Which one performs better in classification of MCCs in mammogram imaging," *Knowledge-Based Systems*, vol. 26, pp. 144-153, 2012.

[173] D. Wang, L. Shi, and P. Ann Heng, "Automatic detection of breast cancers in mammograms using structured support vector machines," *Neurocomputing*, vol. 72, pp. 3296-3302, 2009.

[174] S. Yoon and S. Kim, "Mutual information-based SVM-RFE for diagnostic classification of digitized mammograms," *Pattern Recognition Letters*, vol. 30, pp. 1489-1495, 2009.

[175] S. C. Bagui, S. Bagui, K. Pal, and N. R. Pal, "Breast cancer detection using rank nearest neighbor classification rules," *Pattern recognition*, vol. 36, pp. 25-34, 2003.

[176] M. Meselhy Eltoukhy, I. Faye, and B. Belhaouari Samir, "A comparison of wavelet and curvelet for breast cancer diagnosis in digital mammogram," *Computers in Biology and Medicine*, vol. 40, pp. 384-391, 2010.

[177] A. Das and M. Bhattacharya, "GA based neuro fuzzy techniques for breast cancer identification," in *Machine Vision and Image Processing Conference, 2008. IMVIP'08. International*, 2008, pp. 136-141.

[178] A. Keleş, A. Keleş, and U. Yavuz, "Expert system based on neuro-fuzzy rules for diagnosis breast cancer," *Expert Systems with Applications*, vol. 38, pp. 5719-5726, 2011.

[179] S. Shanthi and V. M. Bhaskaran, "Computer aided detection and classification of mammogram using self-adaptive resource allocation network classifier," in *Pattern Recognition, Informatics and Medical Engineering (PRIME), 2012 International Conference on*, 2012, pp. 284-289.

[180] N. Perry, M. Broeders, C. De Wolf, S. Törnberg, R. Holland, and L. Von Karsa, "European guidelines for quality assurance in breast cancer screening and diagnosis. —summary document," *Annals of Oncology*, vol. 19, pp. 614-622, 2008.

[181] F. J. Ayres and R. Rangayvan, "Characterization of architectural distortion in mammograms," *Engineering in Medicine and Biology Magazine, IEEE*, vol. 24, pp. 59-67, 2005.

[182] R. Zwiggelaar, T. C. Parr, J. E. Schumm, I. W. Hutt, C. J. Taylor, S. M. Astley, *et al.*, "Model-based detection of spiculated lesions in mammograms," *Medical Image Analysis*, vol. 3, pp. 39-62, 1999.

[183] T. Matsubara, T. Ichikawa, T. Hara, H. Fujita, S. Kasai, T. Endo, *et al.*, "Automated detection methods for architectural distortions around skinline and within mammary gland on mammograms," in *International Congress Series*, 2003, pp. 950-955.

[184] T. Ichikawa, T. Matsubara, T. Hara, H. Fujita, T. Endo, and T. Iwase, "Automated detection method for architectural distortion areas on mammograms based on morphological processing and surface analysis," in *Medical Imaging 2004*, 2004, pp. 920-925.

[185] P. Miller and S. M. Astley, "Detection of breast asymmetry using anatomical features," in *IS&T/SPIE's Symposium on Electronic Imaging: Science and Technology*, 1993, pp. 433-442.

[186] P. Miller and S. Astley, "Automated detection of breast asymmetry using anatomical features," *State of the Art in Digital Mammographic Image Analysis, Series in Machine Perception and Artificial Intelligence*, vol. 9, pp. 247-261, 1994.

[187] A. C. Bovik, *Handbook of image and video processing*: Access Online via Elsevier, 2010.

[188] P. G. Newman and G. S. Rozycki, "The history of ultrasound," *Surgical clinics of north America*, vol. 78, pp. 179-195, 1998.

[189] I. Donald, J. MacVicar, and T. Brown, "Investigation of abdominal masses by pulsed ultrasound," *The Lancet*, vol. 271, pp. 1188-1195, 1958.

[190] J. Woo, "A short history of the development of ultrasound in obstetrics and gynecology," *See http://www. ob-ultrasound. net/history1. html (last checked 14 May 2011)*, 2002.

[191] S. Campbell, "An improved method of fetal cephalometry by ultrasound," *BJOG: An International Journal of Obstetrics & Gynaecology*, vol. 75, pp. 568-576, 1968.

[192] J. Abramowicz and E. Sheiner, "In utero imaging of the placenta: importance for diseases of pregnancy," *Placenta*, vol. 28, pp. S14-S22, 2007.

[193] W. Lee, J. Kirk, C. Comstock, and R. Romero, "Vasa previa: prenatal detection by three-dimensional ultrasonography," *Ultrasound in obstetrics & gynecology*, vol. 16, pp. 384-387, 2000.

[194] S. Baulies, N. Maiz, A. Munoz, M. Torrents, M. Echevarria, and B. Serra, "Prenatal ultrasound diagnosis of vasa praevia and analysis of risk factors," *Prenatal diagnosis*, vol. 27, pp. 595-599, 2007.

[195] Y. Oyelese and J. C. Smulian, "Placenta previa, placenta accreta, and vasa previa," *Obstetrics & Gynecology*, vol. 107, pp. 927-941, 2006.

[196] C. Glantz and L. Purnell, "Clinical utility of sonography in the diagnosis and treatment of placental abruption," *Journal of ultrasound in medicine*, vol. 21, pp. 837-840, 2002.

[197] D. Gersell, "Chronic villitis, chronic chorioamnionitis, and maternal floor infarction," in *Seminars in diagnostic pathology*, 1993, p. 251.

[198] E. Jauniaux, B. Ramsay, and S. Campbell, "Ultrasonographic investigation of placental morphologic characteristics and size during the second trimester of pregnancy," *Am J Obstct (; necol*, vol. 170, 1994.

[199] P. A. Grannum, R. Berkowitz, and J. C. Hobbins, "The ultrasonic changes in the maturing placenta and their relation to fetal pulmonic maturity," *Am J Obstet Gynecol*, vol. 133, pp. 915-22, 1979.

[200] R. A. Petrucha and L. D. Platt, "Relationship of placental grade to gestational age," *American journal of obstetrics and gynecology*, vol. 144, p. 733, 1982.

[201] D. McKenna, S. Tharmaratnam, S. Mahsud, and J. Dornan, "Ultrasonic evidence of placental calcification at 36 weeks' gestation: maternal and fetal outcomes," *Acta obstetricia et gynecologica Scandinavica*, vol. 84, pp. 7-10, 2005.

[202] M. Ayache, M. Khalil, and F. Tranquart, "DWT to Classify Automatically the Placental Tissues Development: Neural Network Approach," *Journal of Computer Science*, vol. 6, p. 634, 2010.

[203] P. Linares, P. McCullagh, N. Black, and J. Dornan, "Characterization of ultrasonic images of the placenta based on textural features," in *Information Technology Applications in Biomedicine, 2003. 4th International IEEE EMBS Special Topic Conference on*, 2003, pp. 211-214.

[204] Z. Liu, H. Zheng, and S. Lin, "Application of Multi-Classification Support Vector Machine in the B-Placenta Image Classification," in *Computational Intelligence and Software Engineering, 2009. CiSE 2009. International Conference on*, 2009, pp. 1-4.

[205] G. Malathi and V. Shanthi, "Histogram Based Classification of Ultrasound Images of Placenta," in *IJCA*, 2010, pp. 0975-8887.

[206] G. Malathi and V. Shanthi, "Thickness Based Characterization of Ultrasound Placenta Images Using Regression Analysis," *International Journal of Computer Applications*, vol. 3, 2010.

[207] Y. Chen, J. Li, and J. Z. Wang, *Machine learning and statistical modeling approaches to image retrieval* vol. 14: Springer, 2004.

[208] W. C. Seng and S. H. Mirisaee, "Evaluation of a content-based retrieval system for blood cell images with automated methods," *Journal of medical systems*, vol. 35, pp. 571-578, 2011.

[209] R. Datta, D. Joshi, J. Li, and J. Z. Wang, "Image retrieval: Ideas, influences, and trends of the new age," *ACM Computing Surveys (CSUR)*, vol. 40, p. 5, 2008.

[210] X. S. Zhou, S. Zillner, M. Moeller, M. Sintek, Y. Zhan, A. Krishnan, *et al.*, "Semantics and CBIR: a medical imaging perspective," in *Proceedings of the 2008 international conference on Content-based image and video retrieval*, 2008, pp. 571-580.

[211] M. J. Swain and D. H. Ballard, "Color indexing," *International journal of computer vision*, vol. 7, pp. 11-32, 1991.

[212] M. Flickner, H. Sawhney, W. Niblack, J. Ashley, Q. Huang, B. Dom, *et al.*, "Query by image and video content: The QBIC system," *Computer*, vol. 28, pp. 23-32, 1995.

[213] J. R. Smith and S.-F. Chang, "VisualSEEk: a fully automated content-based image query system," in *Proceedings of the fourth ACM international conference on Multimedia*, 1997, pp. 87-98.

[214] T. Gevers and A. W. Smeulders, "Pictoseek: Combining color and shape invariant features for image retrieval," *Image Processing, IEEE Transactions on*, vol. 9, pp. 102-119, 2000.

[215] J. Huang, S. R. Kumar, M. Mitra, W.-J. Zhu, and R. Zabih, "Spatial color indexing and applications," *International Journal of Computer Vision*, vol. 35, pp. 245-268, 1999.

[216] H. Tamura, S. Mori, and T. Yamawaki, "Textural features corresponding to visual perception," *Systems, Man and Cybernetics, IEEE Transactions on*, vol. 8, pp. 460-473, 1978.

[217] F. Liu and R. W. Picard, "Periodicity, directionality, and randomness: Wold features for image modeling and retrieval," *Pattern Analysis and Machine Intelligence, IEEE Transactions on*, vol. 18, pp. 722-733, 1996.

[218] C. Schmid and R. Mohr, "Local grayvalue invariants for image retrieval," *Pattern Analysis and Machine Intelligence, IEEE Transactions on*, vol. 19, pp. 530-535, 1997.

[219] T. Tuytelaars and L. Van Gool, "Content-based image retrieval based on local affinely invariant regions," in *Visual Information and Information Systems*, 1999, pp. 493-500.

[220] B. S. Manjunath and W.-Y. Ma, "Texture features for browsing and retrieval of image data," *Pattern Analysis and Machine Intelligence, IEEE Transactions on*, vol. 18, pp. 837-842, 1996.

[221] J. Z. Wang, G. Wiederhold, O. Firschein, and S. X. Wei, "Content-based image indexing and searching using Daubechies' wavelets," *International Journal on Digital Libraries*, vol. 1, pp. 311-328, 1998.

[222] A. Del Bimbo, "Visual information retrieval," 1999.

[223] R. C. Wilson and E. R. Hancock, "Structural matching by discrete relaxation," *Pattern Analysis and Machine Intelligence, IEEE Transactions on*, vol. 19, pp. 634-648, 1997.

[224] H. J. Wolfson and I. Rigoutsos, "Geometric hashing: An overview," *Computational Science & Engineering, IEEE*, vol. 4, pp. 10-21, 1997.

[225] R. Fagin, "Combining fuzzy information from multiple systems," in *Proceedings of the fifteenth ACM SIGACT-SIGMOD-SIGART symposium on Principles of database systems*, 1996, pp. 216-226.

[226] M. Weber, M. Welling, and P. Perona, *Unsupervised learning of models for recognition*: Springer, 2000.

[227] I. J. Cox, M. L. Miller, S. M. Omohundro, and P. N. Yianilos, "Target testing and the PicHunter Bayesian multimedia retrieval system," in *Research and Technology Advances in Digital Libraries, 1996. ADL'96., Proceedings of the Third Forum on*, 1996, pp. 66-75.

[228] W.-Y. Ma and B. S. Manjunath, "Netra: A toolbox for navigating large image databases," *Multimedia systems*, vol. 7, pp. 184-198, 1999.

[229] S. Mukherjea, K. Hirata, and Y. Hara, "Amore: A world wide web image retrieval engine," *World Wide Web*, vol. 2, pp. 115-132, 1999.

[230] F. Jing, M. Li, L. Zhang, H.-J. Zhang, and B. Zhang, "Learning in region-based image retrieval," in *Image and Video Retrieval*, ed: Springer, 2003, pp. 206-215.

[231] C. Town and D. Sinclair, "Content based image retrieval using semantic visual categories," *TR2000-14, AT&T Labs Cambridge*, 2000.

[232] J. Yue, Z. Li, L. Liu, and Z. Fu, "Content-based image retrieval using color and texture fused features," *Mathematical and Computer Modelling*, vol. 54, pp. 1121-1127, 2011.

[233] S. Tong and E. Chang, "Support vector machine active learning for image retrieval," in *Proceedings of the ninth ACM international conference on Multimedia*, 2001, pp. 107-118.

[234] S. Das and D. Rudrapal, "Analysis of Color Moment as a Low Level Feature in Improvement of Content Based Image Retrieval," in *Proceedings of the Fourth International Conference on Signal and Image Processing 2012 (ICSIP 2012)*, 2013, pp. 387-397.

[235] X. Zheng, D. Cai, X. He, W.-Y. Ma, and X. Lin, "Locality preserving clustering for image database," in *Proceedings of the 12th annual ACM international conference on Multimedia*, 2004, pp. 885-891.

[236] K.-W. Park, J.-W. Jeong, and D.-H. Lee, "OLYBIA: ontology-based automatic image annotation system using semantic inference rules," in *Advances in databases: concepts, systems and applications*, ed: Springer, 2007, pp. 485-496.

[237] Y. Liu, D. Zhang, and G. Lu, "Region-based image retrieval with high-level semantics using decision tree learning," *Pattern Recognition*, vol. 41, pp. 2554-2570, 2008.

[238] C.-H. Lin, R.-T. Chen, and Y.-K. Chan, "A smart content-based image retrieval system based on color and texture feature," *Image and Vision Computing,* vol. 27, pp. 658-665, 2009.

[239] E. Rashedi, H. Nezamabadi-Pour, and S. Saryazdi, "A simultaneous feature adaptation and feature selection method for content-based image retrieval systems," *Knowledge-Based Systems,* vol. 39, pp. 85-94, 2013.

[240] G.-H. Liu and J.-Y. Yang, "Content-based image retrieval using color difference histogram," *Pattern Recognition,* vol. 46, pp. 188-198, 2013.

[241] J. Z. Wang, J. Li, and G. Wiederhold, "SIMPLIcity: Semantics-sensitive integrated matching for picture libraries," *Pattern Analysis and Machine Intelligence, IEEE Transactions on,* vol. 23, pp. 947-963, 2001.

[242] P. Salembier, T. Sikora, and B. Manjunath, *Introduction to MPEG-7: multimedia content description interface*: John Wiley & Sons, Inc., 2002.

[243] X. Qi and Y. Han, "Incorporating multiple SVMs for automatic image annotation," *Pattern Recognition,* vol. 40, pp. 728-741, 2007.

[244] M. Subrahmanyam, R. Maheshwari, and R. Balasubramanian, "Local maximum edge binary patterns: A new descriptor for image retrieval and object tracking," *Signal Processing,* vol. 92, pp. 1467-1479, 2012.

[245] V. Mezaris, I. Kompatsiaris, and M. G. Strintzis, "An ontology approach to object-based image retrieval," in *Image Processing, 2003. ICIP 2003. Proceedings. 2003 International Conference on*, 2003, pp. II-511-14 vol. 3.

[246] X.-Y. Wang, Y.-J. Yu, and H.-Y. Yang, "An effective image retrieval scheme using color, texture and shape features," *Computer Standards & Interfaces,* vol. 33, pp. 59-68, 2011.

[247] S. Lee, "Symmetry-driven shape description for image retrieval," *Image and Vision Computing,* 2013.

[248] D. Androutsos, K. Plataniotiss, and A. N. Venetsanopoulos, "Distance measures for color image retrieval," in *Image Processing, 1998. ICIP 98. Proceedings. 1998 International Conference on*, 1998, pp. 770-774.

[249] Z. Chen and B. Zhu, "Some formal analysis of Rocchio's similarity-based relevance feedback algorithm," in *Algorithms and Computation*, ed: Springer, 2000, pp. 108-119.

[250] Y. Rubner, C. Tomasi, and L. J. Guibas, "A metric for distributions with applications to image databases," in *Computer Vision, 1998. Sixth International Conference on*, 1998, pp. 59-66.

[251] J. Wang, J. Li, D. Chan, and G. Wiederhold, "Semantics-sensitive retrieval for digital picture libraries," *D-Lib Magazine,* vol. 5, 1999.

[252] B. Li, E. Chang, and C.-T. Wu, "DPF-a perceptual distance function for image retrieval," in *Image Processing. 2002. Proceedings. 2002 International Conference on*, 2002, pp. II-597-II-600 vol. 2.

[253] N. Vasconcelos and A. Lippman, "A multiresolution manifold distance for invariant image similarity," *Multimedia, IEEE Transactions on*, vol. 7, pp. 127-142, 2005.

[254] Y. Chen, J. Z. Wang, and R. Krovetz, "Clue: Cluster-based retrieval of images by unsupervised learning," *Image Processing, IEEE Transactions on*, vol. 14, pp. 1187-1201, 2005.

[255] E. Yildizer, A. M. Balci, M. Hassan, and R. Alhajj, "Efficient content-based image retrieval using multiple support vector machines ensemble," *Expert Systems with Applications*, vol. 39, pp. 2385-2396, 2012.

[256] J. Wu, H. Shen, Y.-D. Li, Z.-B. Xiao, M.-Y. Lu, and C.-L. Wang, "Learning a Hybrid Similarity Measure for Image Retrieval," *Pattern Recognition*, 2013.

[257] G. Salton, "Automatic text processing," *Science*, vol. 168, pp. 335-343, 1970.

[258] Y. Rui, T. S. Huang, M. Ortega, and S. Mehrotra, "Relevance feedback: a power tool for interactive content-based image retrieval," *Circuits and Systems for Video Technology, IEEE Transactions on*, vol. 8, pp. 644-655, 1998.

[259] Y. Rui and T. Huang, "Optimizing learning in image retrieval," in *Computer Vision and Pattern Recognition, 2000. Proceedings. IEEE Conference on*, 2000, pp. 236-243.

[260] X. S. Zhou and T. S. Huang, "Relevance feedback in image retrieval: A comprehensive review," *Multimedia systems*, vol. 8, pp. 536-544, 2003.

[261] I. J. Cox, M. L. Miller, T. P. Minka, and P. N. Yianilos, "An optimized interaction strategy for bayesian relevance feedback," in *Computer Vision and Pattern Recognition, 1998. Proceedings. 1998 IEEE Computer Society Conference on*, 1998, pp. 553-558.

[262] X. S. Zhou and T. S. Huang, "Small sample learning during multimedia retrieval using biasmap," in *Computer Vision and Pattern Recognition, 2001. CVPR 2001. Proceedings of the 2001 IEEE Computer Society Conference on*, 2001, pp. I-11-I-17 vol. 1.

[263] K. Tieu and P. Viola, "Boosting image retrieval," *International Journal of Computer Vision*, vol. 56, pp. 17-36, 2004.

[264] D. Angluin, "Queries and concept learning," *Machine learning*, vol. 2, pp. 319-342, 1988.

[265] Y. Freund, H. S. Seung, E. Shamir, and N. Tishby, "Selective sampling using the query by committee algorithm," *Machine learning*, vol. 28, pp. 133-168, 1997.

[266] C. Meilhac and C. Nastar, "Relevance feedback and category search in image databases," in *Multimedia Computing and Systems, 1999. IEEE International Conference on*, 1999, pp. 512-517.

[267] Y. Chen, X. S. Zhou, and T. S. Huang, "One-class SVM for learning in image retrieval," in *Image Processing, 2001. Proceedings. 2001 International Conference on*, 2001, pp. 34-37.

[268] S. Tong and D. Koller, "Support vector machine active learning with applications to text classification," *The Journal of Machine Learning Research*, vol. 2, pp. 45-66, 2002.

[269] N. Vasconcelos and A. Lippman, "Bayesian relevance feedback for content-based image retrieval," in *Content-based Access of Image and Video Libraries, 2000. Proceedings. IEEE Workshop on*, 2000, pp. 63-67.

[270] J. Laaksonen, M. Koskela, S. Laakso, and E. Oja, "PicSOM–content-based image retrieval with self-organizing maps," *Pattern Recognition Letters*, vol. 21, pp. 1199-1207, 2000.

[271] L. Wang, *Support Vector Machines: theory and applications* vol. 177: Springer, 2005.

[272] D. Gebara and R. Alhajj, "Waveq: Combining wavelet analysis and clustering for effective image retrieval," in *Advanced Information Networking and Applications Workshops, 2007, AINAW'07. 21st International Conference on*, 2007, pp. 289-294.

[273] C. Zhang and X. Chen, "OCRS: an interactive object-based image clustering and retrieval system," *Multimedia Tools and Applications*, vol. 35, pp. 71-89, 2007.

[274] D. J. Foran, L. Yang, W. Chen, J. Hu, L. A. Goodell, M. Reiss, *et al.*, "ImageMiner: a software system for comparative analysis of tissue microarrays using content-based image retrieval, high-performance computing, and grid technology," *Journal of the American Medical Informatics Association*, vol. 18, pp. 403-415, 2011.

[275] T. M. Deserno, T. Aach, K. Amunts, W. Hillen, T. Kuhlen, and I. Scholl, "Advances in medical image processing," *Computer Science-Research and Development*, vol. 26, pp. 1-3, 2011.

[276] E. H. Shortliffe and J. J. Cimino, *Medical informatics: computer applications in health care and biomedicine*: Springer, 2006.

[277] C. B. Akgül, D. L. Rubin, S. Napel, C. F. Beaulieu, H. Greenspan, and B. Acar, "Content-based image retrieval in radiology: current status and future directions," *Journal of Digital Imaging*, vol. 24, pp. 208-222, 2011.

[278] H. D. Tagare, C. C. Jaffe, and J. Duncan, "Medical image databases a content-based retrieval approach," *Journal of the American Medical Informatics Association*, vol. 4, pp. 184-198, 1997.

[279] H. J. Lowe, I. Antipov, W. Hersh, and C. A. Smith, "Towards knowledge-based retrieval of medical images. The role of semantic indexing, image content representation and knowledge-based retrieval," in *Proceedings of the AMIA Symposium*, 1998, p. 882.

[280] H. Müller, N. Michoux, D. Bandon, and A. Geissbuhler, "A review of content-based image retrieval systems in medical applications—clinical benefits and future directions," *International journal of medical informatics*, vol. 73, pp. 1-23, 2004.

[281] W. Hsu, S. Antani, L. R. Long, L. Neve, and G. R. Thoma, "SPIRS: a Web-based image retrieval system for large biomedical databases," *International Journal of Medical Informatics*, vol. 78, pp. S13-S24, 2009.

[282] W. Wan Ahmad and M. F. A. Fauzi, "Comparison of different feature extraction techniques in content-based image retrieval for CT brain images," in *Multimedia Signal Processing, 2008 IEEE 10th Workshop on*, 2008, pp. 503-508.

[283] G. Quellec, M. Lamard, G. Cazuguel, B. Cochener, and C. Roux, "Wavelet optimization for content-based image retrieval in medical databases," *Medical image analysis*, vol. 14, pp. 227-241, 2010.

[284] K. Yuan, Z. Tian, J. Zou, Y. Bai, and Q. You, "Brain CT image database building for computer-aided diagnosis using content-based image retrieval," *Information Processing & Management*, vol. 47, pp. 176-185, 2011.

[285] A. Oberoi, V. Bakshi, R. Sharma, and M. Singh, "A Framework for Medical Image Retrieval Using Local Tetra Patterns," *International Journal of Engineering and Technology*, vol. 5, 2013.

[286] J. Xu, J. Faruque, C. F. Beaulieu, D. Rubin, and S. Napel, "A comprehensive descriptor of shape: method and application to content-based retrieval of similar appearing lesions in medical images," *Journal of Digital Imaging*, vol. 25, pp. 121-128, 2012.

[287] D. Comaniciu, P. Meer, and D. J. Foran, "Image-guided decision support system for pathology," *Machine Vision and Applications*, vol. 11, pp. 213-224, 1999.

[288] D. M. KWAK, B. S. KIM, O. K. YOON, C. H. PARK, J. U. WON, and K. H. PARK, "Content-Based Ultrasound Image Retrieval Using a Coarse to Fine Approach," *Annals of the New York Academy of Sciences*, vol. 980, pp. 212-224, 2002.

[289] J.-H. Lim and J.-P. Chevallet, "Vismed: a visual vocabulary approach for medical image indexing and retrieval," in *Information Retrieval Technology*, ed: Springer, 2005, pp. 84-96.

[290] M. Gletsos, S. G. Mougiakakou, G. K. Matsopoulos, K. S. Nikita, A. S. Nikita, and D. Kelekis, "A computer-aided diagnostic system to characterize CT focal liver lesions: design and optimization of a neural network classifier," *Information Technology in Biomedicine, IEEE Transactions on*, vol. 7, pp. 153-162, 2003.

[291] M. M. Rahman, P. Bhattacharya, and B. C. Desai, "A framework for medical image retrieval using machine learning and statistical similarity matching techniques with relevance feedback," *Information Technology in Biomedicine, IEEE Transactions on*, vol. 11, pp. 58-69, 2007.

[292] J.-M. Cauvin, C. Le Guillou, B. Solaiman, M. Robaszkiewicz, P. Le Beux, and C. Roux, "Computer-assisted diagnosis system in digestive endoscopy," *Information Technology in Biomedicine, IEEE Transactions on*, vol. 7, pp. 256-262, 2003.

[293] K. Lubbers, A. P. de Vries, T. Huibers, and P. van der Vet, "A probabilistic approach to medical image retrieval," in *Multilingual Information Access for Text, Speech and Images*, ed: Springer, 2005, pp. 761-772.

[294] B. Ramamurthy, K. Chandran, V. Meenakshi, and V. Shilpa, "CBMIR: Content Based Medical Image Retrieval System Using Texture and Intensity for Dental Images," in *Eco-friendly Computing and Communication Systems*, ed: Springer, 2012, pp. 125-134.

[295] C.-R. Shyu, C. E. Brodley, A. C. Kak, A. Kosaka, A. M. Aisen, and L. S. Broderick, "ASSERT: a physician-in-the-loop content-based retrieval system for HRCT image databases," *Computer Vision and Image Understanding*, vol. 75, pp. 111-132, 1999.

[296] H. Alto, R. M. Rangayyan, and J. L. Desautels, "Content-based retrieval and analysis of mammographic masses," *Journal of Electronic Imaging*, vol. 14, pp. 023016-023016-17, 2005.

[297] D. A. Chandy, J. S. Johnson, and S. E. Selvan, "Texture feature extraction using gray level statistical matrix for content-based mammogram retrieval," *Multimedia Tools and Applications*, pp. 1-14, 2013.

[298] X. Qian and H. D. Tagare, "Optimal embedding for shape indexing in medical image databases," in *Medical Image Computing and Computer-Assisted Intervention–MICCAI 2005*, ed: Springer, 2005, pp. 377-384.

[299] S. Antani, D. Lee, L. R. Long, and G. R. Thoma, "Evaluation of shape similarity measurement methods for spine X-ray images," *Journal of Visual Communication and Image Representation*, vol. 15, pp. 285-302, 2004.

[300] E. Balmashnova, B. Platel, L. Florack, and B. ter Haar Romeny, "Content-based image retrieval by means of scale-space top-points and differential invariants," in *Proceedings of the MICCAI Workshop on Medical Content-Based Image Retrieval for Biomedical Image Archives: Achievements, Problems, and Prospects (Brisbane, Australia*, 2007, pp. 83-92.

[301] P. Golland, W. E. L. Grimson, M. E. Shenton, and R. Kikinis, "Detection and analysis of statistical differences in anatomical shape," *Medical image analysis*, vol. 9, pp. 69-86, 2005.

[302] S. Doyle, M. Hwang, S. Naik, M. Feldman, J. Tomaszeweski, and A. Madabhushi, "Using manifold learning for content-based image retrieval of prostate histopathology," in *MICCAI 2007 Workshop on Content-based Image Retrieval for Biomedical Image Archives: Achievements, Problems, and Prospects*, 2007, pp. 53-62.

[303] R. Bansal, L. H. Staib, D. Xu, H. Zhu, and B. S. Peterson, "Statistical analyses of brain surfaces using Gaussian random fields on 2-D manifolds," *Medical Imaging, IEEE Transactions on*, vol. 26, pp. 46-57, 2007.

[304] J. Z. Wang, "Pathfinder: multiresolution region-based searching of pathology images using IRM," in *Proceedings of the AMIA Symposium*, 2000, p. 883.

[305] D. Pokrajac, V. Megalooikonomou, A. Lazarevic, D. Kontos, and Z. Obradovic, "Applying spatial distribution analysis techniques to classification of 3D medical images," *Artificial Intelligence in Medicine*, vol. 33, pp. 261-280, 2005.

[306] M. Toews and T. Arbel, "A statistical parts-based model of anatomical variability," *Medical Imaging, IEEE Transactions on*, vol. 26, pp. 497-508, 2007.

[307] H. R. Marsiglia, F. Pigatto, A. Basilicata, M. Gargiulo, J. Pulley, and F. S. Sasso, "A visual query-by-example image database for chest CT images: potential role as a decision and educational support tool for radiologists," *Journal of Digital Imaging*, vol. 18, pp. 78-84, 2005.

[308] E. G. M. Petrakis, C. Faloutsos, and K.-I. Lin, "ImageMap: An image indexing method based on spatial similarity," *Knowledge and Data Engineering, IEEE Transactions on*, vol. 14, pp. 979-987, 2002.

[309] S. F. Da Silva, M. X. Ribeiro, J. d. E. Batista Neto, C. Traina-Jr, and A. J. Traina, "Improving the ranking quality of medical image retrieval using a genetic feature selection method," *Decision Support Systems*, vol. 51, pp. 810-820, 2011.

[310] W. Jiang, G. Er, Q. Dai, and J. Gu, "Similarity-based online feature selection in content-based image retrieval," *Image Processing, IEEE Transactions on*, vol. 15, pp. 702-712, 2006.

[311] S. V. Aschkenasy, C. Jansen, R. Osterwalder, A. Linka, M. Unser, S. Marsch, *et al.*, "Unsupervised image classification of medical ultrasound data by multiresolution elastic registration," *Ultrasound in medicine & biology*, vol. 32, pp. 1047-1054, 2006.

[312] J. Amores and P. Radeva, "Registration and retrieval of highly elastic bodies using contextual information," *Pattern recognition letters*, vol. 26, pp. 1720-1731, 2005.

[313] J. Glaunès, A. Qiu, M. I. Miller, and L. Younes, "Large deformation diffeomorphic metric curve mapping," *International journal of computer vision*, vol. 80, pp. 317-336, 2008.

[314] M. I. Miller and L. Younes, "Group actions, homeomorphisms, and matching: A general framework," *International Journal of Computer Vision*, vol. 41, pp. 61-84, 2001.

[315] R. C. Veltkamp, "Shape matching: Similarity measures and algorithms," in *Shape Modeling and Applications, SMI 2001 International Conference on.*, 2001, pp. 188-197.

[316] D. Tao, X. Tang, X. Li, and X. Wu, "Asymmetric bagging and random subspace for support vector machines-based relevance feedback in image retrieval," *Pattern Analysis and Machine Intelligence, IEEE Transactions on*, vol. 28, pp. 1088-1099, 2006.

[317] D. K. Iakovidis, N. Pelekis, E. E. Kotsifakos, I. Kopanakis, H. Karanikas, and Y. Theodoridis, "A pattern similarity scheme for medical image retrieval," *Information Technology in Biomedicine, IEEE Transactions on*, vol. 13, pp. 442-450, 2009.

[318] L. H. Tang, R. Hanka, H. H. Ip, and R. Lam, "Extraction of semantic features of histological images for content-based retrieval of images," in *Proceedings of SPIE Medical Imaging*, 2000, pp. 360-368.

[319] S. Antani, L. R. Long, and G. R. Thoma, "A Biomedical Information System for Combined Content-Based Retrieval of Spine X-Ray Images, Associated Text Information," in *ICVGIP*, 2002.

[320] D. Keysers, H. Ney, B. B. Wein, and T. M. Lehmann, "Statistical framework for model-based image retrieval in medical applications," *Journal of Electronic Imaging*, vol. 12, pp. 59-68, 2003.

[321] A. Mueen, R. Zainuddin, and M. S. Baba, "MIARS: A medical image retrieval system," *Journal of medical systems*, vol. 34, pp. 859-864, 2010.

[322] Y. Liu and F. Dellaert, "A classification based similarity metric for 3D image retrieval," in *Computer Vision and Pattern Recognition, 1998. Proceedings. 1998 IEEE Computer Society Conference on*, 1998, pp. 800-805.

[323] R. Chbeir, Y. Amghar, and A. Flory, "MIMS: A Prototype for medical image retrieval," in *RIAO*, 2000, pp. 846-861.

[324] A. Mojsilovic and J. Gomes, "Semantic based categorization, browsing and retrieval in medical image databases," in *Image Processing. 2002. Proceedings. 2002 International Conference on*, 2002, pp. III-145-III-148 vol. 3.

[325] W.-J. Kuo, R.-F. Chang, C. C. Lee, W. K. Moon, and D.-R. Chen, "Retrieval technique for the diagnosis of solid breast tumors on sonogram," *Ultrasound in medicine & biology*, vol. 28, pp. 903-909, 2002.

[326] T. Glatard, J. Montagnat, and I. E. Magnin, "Texture based medical image indexing and retrieval: application to cardiac imaging," in *Proceedings of the 6th ACM SIGMM international workshop on Multimedia information retrieval*, 2004, pp. 135-142.

[327] I. El-Naqa, Y. Yang, N. P. Galatsanos, R. M. Nishikawa, and M. N. Wernick, "A similarity learning approach to content-based image retrieval: application to digital mammography," *Medical Imaging, IEEE Transactions on,* vol. 23, pp. 1233-1244, 2004.

[328] M.-R. Siadat, H. Soltanian-Zadeh, F. Fotouhi, and K. Elisevich, "Content-based image database system for epilepsy," *Computer Methods and Programs in Biomedicine,* vol. 79, pp. 209-226, 2005.

[329] J. Kim, W. Cai, D. Feng, and H. Wu, "A new way for multidimensional medical data management: volume of interest (VOI)-based retrieval of medical images with visual and functional features," *Information Technology in Biomedicine, IEEE Transactions on,* vol. 10, pp. 598-607, 2006.

[330] B. Bai, P. Kantor, A. Shokoufandeh, and D. Silver, "fMRI brain image retrieval based on ICA components," in *Current Trends in Computer Science, 2007. ENC 2007. Eighth Mexican International Conference on,* 2007, pp. 10-17.

[331] E. A. Sickles, "Mammographic features of 300 consecutive nonpalpable breast cancers," *American Journal of Roentgenology,* vol. 146, pp. 661-663, 1986.

[332] J. G. Elmore, C. K. Wells, C. H. Lee, D. H. Howard, and A. R. Feinstein, "Variability in radiologists' interpretations of mammograms," *New England Journal of Medicine,* vol. 331, pp. 1493-1499, 1994.

[333] J. C. Felipe, M. X. Ribeiro, E. P. Sousa, A. J. Traina, and C. Traina Jr, "Effective shape-based retrieval and classification of mammograms," in *Proceedings of the 2006 ACM symposium on Applied computing,* 2006, pp. 250-255.

[334] S. K. Kinoshita, P. M. de Azevedo-Marques, R. R. Pereira Jr, J. A. H. Rodrigues, and R. M. Rangayyan, "Content-based retrieval of mammograms using visual features related to breast density patterns," *Journal of Digital Imaging,* vol. 20, pp. 172-190, 2007.

[335] X.-H. Wang, S. C. Park, and B. Zheng, "Improving performance of content-based image retrieval schemes in searching for similar breast mass regions: an assessment," *Physics in medicine and biology,* vol. 54, p. 949, 2009.

[336] J. H. Oh, I. El Naqa, and Y. Yang, "Online learning of relevance feedback from expert readers for mammogram retrieval," in *Signals, Systems and Computers, 2009 Conference Record of the Forty-Third Asilomar Conference on,* 2009, pp. 17-21.

[337] J. E. De Oliveira, A. Machado, G. C. Chavez, A. P. B. Lopes, T. M. Deserno, and A. d. A. Araújo, "MammoSys: A content-based image retrieval system using breast density patterns," *computer methods and programs in biomedicine,* vol. 99, pp. 289-297, 2010.

[338] C.-H. Wei, Y. Li, and P. J. Huang, "Mammogram retrieval through machine learning within BI-RADS standards," *Journal of Biomedical Informatics*, vol. 44, pp. 607-614, 2011.

[339] J. Suckling et al., "The Mammographic Image Analysis Society Digital Mammogram Database Exerpta Medica", *International Congress Series* 1069,pp.375-378.

[340] S. M. Pizer, E. P. Amburn, J. D. Austin, R. Cromartie, A. Geselowitz, T. Greer, *et al.*, "Adaptive histogram equalization and its variations," *Computer vision, graphics, and image processing*, vol. 39, pp. 355-368, 1987.

[341] K. Zuiderveld, "Contrast limited adaptive histogram equalization," in *Graphics gems IV*, 1994, pp. 474-485.

[342] O. V. Michailovich and A. Tannenbaum, "Despeckling of medical ultrasound images," *Ultrasonics, Ferroelectrics and Frequency Control, IEEE Transactions on*, vol. 53, pp. 64-78, 2006.

[343] C. Chinrungrueng and A. Suvichakorn, "Fast edge-preserving noise reduction for ultrasound images," in *Nuclear Science Symposium Conference Record, 2000 IEEE*, 2000, pp. 18/99-18103.

[344] A. Suvichakorn and C. Chinrungrueng, "Speckle noise reduction based on least squares approximation," in *Circuits and Systems, 2000. IEEE APCCAS 2000. The 2000 IEEE Asia-Pacific Conference on*, 2000, pp. 430-433.

[345] S. Roomi and R. Rajee, "Speckle noise removal in ultrasound images using Particle Swarm Optimization technique," in *Recent Trends in Information Technology (ICRTIT), 2011 International Conference on*, 2011, pp. 926-931.

[346] T. Loupas, W. McDicken, and P. Allan, "An adaptive weighted median filter for speckle suppression in medical ultrasonic images," *Circuits and Systems, IEEE Transactions on*, vol. 36, pp. 129-135, 1989.

[347] R. Sivakumar, M. Gayathri, and D. Nedumaran, "Speckle filtering of ultrasound B-Scan Images-a comparative study between spatial and diffusion filters," in *Open Systems (ICOS), 2010 IEEE Conference on*, 2010, pp. 80-85.

[348] R. G. Dantas and E. T. Costa, "Ultrasound speckle reduction using modified Gabor filters," *Ultrasonics, Ferroelectrics and Frequency Control, IEEE Transactions on*, vol. 54, pp. 530-538, 2007.

[349] G. Gavriloaia and R. Gavriloaia, "Improving quality of medical ultrasound images by filtering of frames sequences," in *E-Health and Bioengineering Conference (EHB), 2011*, 2011, pp. 1-4.

[350] X. Hao, S. Gao, and X. Gao, "A novel multiscale nonlinear thresholding method for ultrasonic speckle suppressing," *Medical Imaging, IEEE Transactions on*, vol. 18, pp. 787-794, 1999.

[351] A. Achim, A. Bezerianos, and P. Tsakalides, "Novel Bayesian multiscale method for speckle removal in medical ultrasound images," *Medical Imaging, IEEE Transactions on*, vol. 20, pp. 772-783, 2001.

[352] H. Rabbani, M. Vafadust, P. Abolmaesumi, and S. Gazor, "Speckle noise reduction of medical ultrasound images in complex wavelet domain using mixture priors," *Biomedical Engineering, IEEE Transactions on*, vol. 55, pp. 2152-2160, 2008.

[353] A. Pizurica, W. Philips, I. Lemahieu, and M. Acheroy, "A versatile wavelet domain noise filtration technique for medical imaging," *Medical Imaging, IEEE Transactions on*, vol. 22, pp. 323-331, 2003.

[354] Y. Yu and J. Yadegar, "Regularized speckle reducing anisotropic diffusion for feature characterization," in *Image Processing, 2006 IEEE International Conference on*, 2006, pp. 1577-1580.

[355] H.-Y. Yang, X.-Y. Wang, T.-X. Qu, and Z.-K. Fu, "Image denoising using bilateral filter and Gaussian scale mixtures in shiftable complex directional pyramid domain," *Computers & Electrical Engineering*, vol. 37, pp. 656-668, 2011.

[356] H. Bhadauria and M. Dewal, "Medical image denoising using adaptive fusion of curvelet transform and total variation," *Computers & Electrical Engineering*, 2012.

[357] C. P. Loizou and C. S. Pattichis, "Despeckle filtering algorithms and software for ultrasound imaging," *Synthesis Lectures on Algorithms and Software in Engineering*, vol. 1, pp. 1-166, 2008.

[358] K. D. Toennies, *Guide to medical image analysis*: Springer, 2012.

[359] N. Wiener, *Extrapolation, interpolation, and smoothing of stationary time series: with engineering applications*: Technology Press of the Massachusetts Institute of Technology, 1950.

[360] L. Yaroslavsky, *Digital Holography and Digital Image Processing:: Principles, Methods, Algorithms*: Kluwer Academic Pub, 2004.

[361] P. Perona and J. Malik, "Scale-space and edge detection using anisotropic diffusion," *Pattern Analysis and Machine Intelligence, IEEE Transactions on*, vol. 12, pp. 629-639, 1990.

[362] T. Ojala, M. Pietikainen, and T. Maenpaa, "Multiresolution gray-scale and rotation invariant texture classification with local binary patterns," *Pattern Analysis and Machine Intelligence, IEEE Transactions on*, vol. 24, pp. 971-987, 2002.

[363] T. Ahonen, A. Hadid, and M. Pietikainen, "Face description with local binary patterns: Application to face recognition," *Pattern Analysis and Machine Intelligence, IEEE Transactions on*, vol. 28, pp. 2037-2041, 2006.

[364] A. Hadid and M. Pietikäinen, "Combining appearance and motion for face and gender recognition from videos," *Pattern Recognition*, vol. 42, pp. 2818-2827, 2009.

[365] B. Li and M.-H. Meng, "Tumor recognition in wireless capsule endoscopy images using textural features and SVM-based feature selection," *Information Technology in Biomedicine, IEEE Transactions on*, vol. 16, pp. 323-329, 2012.

[366] S. Malathi and C. Meena, "An efficient method for partial fingerprint recognition based on Local Binary Pattern," in *Communication Control and Computing Technologies (ICCCCT), 2010 IEEE International Conference on*, 2010, pp. 569-572.

[367] M. Hanmandlu, A. Gureja, and A. Jain, "Palm print recognition using Local Binary Pattern operator and support vector machines," in *Signal and Image Processing (ICSIP), 2010 International Conference on*, 2010, pp. 158-162.

[368] Z. Seyed Mohsen, P. Hamid Reza, and B. Touka, "Vessel Extraction of Conjunctival Images Using LBPs and ANFIS," *ISRN Machine Vision*, vol. 2012, 2011.

[369] A. Varghese, R. R. Varghese, K. Balakrishnan, and J. Paul, "Level identification of brain MR images using histogram of a LBP variant," in *Computational Intelligence & Computing Research (ICCIC), 2012 IEEE International Conference on*, 2012, pp. 1-4.

[370] M. Topi, O. Timo, P. Matti, and S. Maricor, "Robust texture classification by subsets of local binary patterns," in *Pattern Recognition, 2000. Proceedings. 15th International Conference on*, 2000, pp. 935-938.

[371] S. Liao, M. W. Law, and A. C. Chung, "Dominant local binary patterns for texture classification," *Image Processing, IEEE Transactions on*, vol. 18, pp. 1107-1118, 2009.

[372] X. Tan and B. Triggs, "Fusing Gabor and LBP feature sets for kernel-based face recognition," in *Analysis and Modeling of Faces and Gestures*, ed: Springer, 2007, pp. 235-249.

[373] M. Heikkila and M. Pietikainen, "A texture-based method for modeling the background and detecting moving objects," *Pattern Analysis and Machine Intelligence, IEEE Transactions on*, vol. 28, pp. 657-662, 2006.

[374] M. Amadasun and R. King, "Textural features corresponding to textural properties," *Systems, Man and Cybernetics, IEEE Transactions on*, vol. 19, pp. 1264-1274, 1989.

[375] G. Srinivasan and G. Shobha, "Statistical texture analysis," *proceedings of world academy of science, engg & tech*, vol. 36, 2008.

[376] S. Lee, *Genetic Learning for Adaptative Image Segmentation* vol. 287: Springer, 1994.

[377] M. Sonka, V. Hlavac, and R. Boyle, "Digital Image processing and Computer Vision," *Cengage India Learning Private limited, New Delhi*, 2007.

[378] R. M. Haralick, "Statistical and structural approaches to texture," *Proceedings of the IEEE,* vol. 67, pp. 786-804, 1979.

[379] C.-M. Wu and Y.-C. Chen, "Statistical feature matrix for texture analysis," *CVGIP: Graphical Models and Image Processing,* vol. 54, pp. 407-419, 1992.

[380] M.-K. Hu, "Visual pattern recognition by moment invariants," *Information Theory, IRE Transactions on,* vol. 8, pp. 179-187, 1962.

[381] M. S. Nixon and A. S. Aguado, *Feature Extraction and Image Processing for Computer Vision*: Academic Press, 2012.

[382] K. J. Cios, *Data mining: a knowledge discovery approach*: Springer, 2007.

[383] B. Liu, *Web data mining: exploring hyperlinks, contents, and usage data*: Springer, 2007.

[384] J. Han, M. Kamber, and J. Pei, *Data mining: concepts and techniques*: Morgan kaufmann, 2006.

[385] W. S. McCulloch and W. Pitts, "A logical calculus of the ideas immanent in nervous activity," *The Bulletin of Mathematical Biophysics,* vol. 5, pp. 115-133, 1943.

[386] F. Rosenblatt, "The perceptron: a probabilistic model for information storage and organization in the brain," *Psychological review,* vol. 65, p. 386, 1958.

[387] B. Widrow and M. A. Lehr, "30 years of adaptive neural networks: perceptron, madaline, and backpropagation," *Proceedings of the IEEE,* vol. 78, pp. 1415-1442, 1990.

[388] M. T. Hagan, H. B. Demuth, and M. H. Beale, *Neural network design*: Pws Pub. Boston, 1996.

[389] M. F. Møller, "A scaled conjugate gradient algorithm for fast supervised learning," *Neural networks,* vol. 6, pp. 525-533, 1993.

[390] J. R. Quinlan, *C4. 5: programs for machine learning* vol. 1: Morgan kaufmann, 1993.

[391] J. R. Quinlan, "Induction of decision trees," *Machine learning,* vol. 1, pp. 81-106, 1986.

[392] I. H. Witten and E. Frank, *Data Mining: Practical machine learning tools and techniques*: Morgan Kaufmann, 2005.

[393] C. Cortes and V. Vapnik, "Support-vector networks," *Machine learning,* vol. 20, pp. 273-297, 1995.

[394] V. N. Vapnik, "Statistical learning theory," 1998.

[395] M. Roffilli, "Advanced machine learning techniques for digital mammography," *TechnicalReport, Department of Computer Science University of Bologna, Italy*, 2006.

[396] B. E. Boser, I. M. Guyon, and V. N. Vapnik, "A training algorithm for optimal margin classifiers," in *Proceedings of the fifth annual workshop on Computational learning theory*, 1992, pp. 144-152.

[397] G.-B. Huang, Q.-Y. Zhu, and C.-K. Siew, "Extreme learning machine: a new learning scheme of feedforward neural networks," in *Neural Networks, 2004. Proceedings. 2004 IEEE International Joint Conference on*, 2004, pp. 985-990.

[398] G.-B. Huang, D. H. Wang, and Y. Lan, "Extreme learning machines: a survey," *International Journal of Machine Learning and Cybernetics*, vol. 2, pp. 107-122, 2011.

[399] M.-B. Li, G.-B. Huang, P. Saratchandran, and N. Sundararajan, "Fully complex extreme learning machine," *Neurocomputing*, vol. 68, pp. 306-314, 2005.

[400] G.-B. Huang, L. Chen, and C.-K. Siew, "Universal approximation using incremental constructive feedforward networks with random hidden nodes," *Neural Networks, IEEE Transactions on*, vol. 17, pp. 879-892, 2006.

[401] N.-Y. Liang, G.-B. Huang, P. Saratchandran, and N. Sundararajan, "A fast and accurate online sequential learning algorithm for feedforward networks," *Neural Networks, IEEE Transactions on*, vol. 17, pp. 1411-1423, 2006.

[402] N.-Y. Liang, P. Saratchandran, G.-B. Huang, and N. Sundararajan, "Classification of mental tasks from EEG signals using extreme learning machine," *International Journal of Neural Systems*, vol. 16, pp. 29-38, 2006.

[403] S. Ramaswamy, P. Tamayo, R. Rifkin, S. Mukherjee, C.-H. Yeang, M. Angelo, *et al.*, "Multiclass cancer diagnosis using tumor gene expression signatures," *Proceedings of the National Academy of Sciences*, vol. 98, pp. 15149-15154, 2001.

[404] G.-B. Huang and H. A. Babri, "Upper bounds on the number of hidden neurons in feedforward networks with arbitrary bounded nonlinear activation functions," *Neural Networks, IEEE Transactions on*, vol. 9, pp. 224-229, 1998.

[405] G.-B. Huang, Q.-Y. Zhu, and C.-K. Siew, "Extreme learning machine: theory and applications," *Neurocomputing*, vol. 70, pp. 489-501, 2006.

[406] C. R. Rao and S. K. Mitra, *Generalized inverse of matrices and its applications* vol. 7: Wiley New York, 1971.

[407] P. Bühlmann and B. Yu, "Boosting with the L 2 loss: regression and classification," *Journal of the American Statistical Association*, vol. 98, pp. 324-339, 2003.

[408] L. K. Hansen and P. Salamon, "Neural network ensembles," *Pattern Analysis and Machine Intelligence, IEEE Transactions on*, vol. 12, pp. 993-1001, 1990.

[409] R. E. Schapire, "The strength of weak learnability," *Machine learning*, vol. 5, pp. 197-227, 1990.

[410] Z.-H. Zhou, *Ensemble methods: foundations and algorithms*: CRC Press, 2012.

[411] K. Pearson, "LIII. On lines and planes of closest fit to systems of points in space," *The London, Edinburgh, and Dublin Philosophical Magazine and Journal of Science*, vol. 2, pp. 559-572, 1901.

[412] H. Hotelling, "Analysis of a complex of statistical variables into principal components," *Journal of educational psychology*, vol. 24, p. 417, 1933.

[413] C. M. Bishop and N. M. Nasrabadi, *Pattern recognition and machine learning* vol. 1: springer New York, 2006.

[414] J. L. Fleiss, J. Cohen, and B. Everitt, "Large sample standard errors of kappa and weighted kappa," *Psychological Bulletin*, vol. 72, p. 323, 1969.

[415] S. Joseph and K. Balakrishnan, "Multi-Query Content Based Image Retrieval System using Local Binary Patterns," *International Journal of Computer Applications*, vol. 17, pp. 1-5, 2011.

[416] S. Joseph, J. John, K. Balakrishnan, and P. K. Vijayaraghavan, "Content based image retrieval system for Malayalam handwritten characters," in *Electronics Computer Technology (ICECT), 2011 3rd International Conference on*, 2011, pp. 386-390.

[417] R. A. Greenes and J. F. Brinkley, "Imaging systems," *Medical Informatics: Computer Applications in Healthcare (2nd edition), Springer, New York*, pp. 485-538, 2000.

[418] J. Tang and S. Acton, "An image retrieval algorithm using multiple query images," in *Signal Processing and Its Applications, 2003. Proceedings. Seventh International Symposium on*, 2003, pp. 193-196.

[419] S. M. Tahaghoghi, J. A. Thom, and H. E. Williams, "Multiple example queries in content-based image retrieval," in *String Processing and Information Retrieval*, 2002, pp. 227-241.

[420] Q. Iqbal and J. Aggarwal, "Feature integration, multi-image queries and relevance feedback in image retrieval," in *Invited Paper, 6th International Conference on Visual Information Systems (VISUAL 2003), Miami, Florida*, 2003, pp. 467-474.

[421] H. C. Akakin and M. N. Gurcan, "Content-based microscopic image retrieval system for multi-image queries," *Information Technology in Biomedicine, IEEE Transactions on*, vol. 16, pp. 758-769, 2012.